QUANTIFICATION OF STREAM SEDIMENT INPUTS FROM STEEP

FORESTED MOUNTAINS

by

Erkan Istanbulluoglu

A dissertation submitted in partial fulfillment
of the requirements for the degree

of

DOCTOR OF PHILOSOPHY
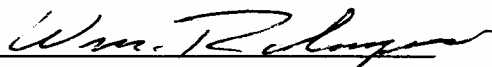
in

Civil and Environmental Engineering

Approved:

_____
Dr. David G. Tarboton
Major Professor

_____
Dr. William J. Rahmeyer
Committee Member

_____
Dr. Joel L. Pederson
Committee Member

_____
Dr. Robert T. Pack
Committee Member

_____
Dr. John C. Schmidt
Committee Member

_____
Dr. Thomas L. Kent
Dean of Graduate Studies

UTAH STATE UNIVERSITY
Logan, Utah

2003

ABSTRACT

Quantification of Stream Sediment Inputs

from Steep Forested Mountains

by

Erkan Istanbulluoglu, Doctor of Philosophy

Utah State University, 2002

Major Professor: Dr. David G. Tarboton
Department: Civil and Environmental Engineering

Mountain environments are regions of high erosion rates due to steep slopes and

extreme weather and climate forcing. In steep, soil-mantled forested mountains, long-

term sediment yield is often dominated by rare catastrophic erosion events. Some of these

catastrophic erosion events are linked to natural and anthropogenic watershed

disturbances. They may cause significant property damage and life loss. Episodic

sediment delivery to streams disturbs the ecologic environment and aquatic habitats. The

frequency and magnitude of mountain sediment yields is a complex function of

topography, climate, and vegetation cover. This dissertation focuses on understanding of

the erosion processes on steep slopes and the factors controlling catastrophic erosion

events from a theoretical and empirical perspective based on field data analysis.

The dissertation is a collection of three papers. Field information used in the

papers is compiled from study watersheds in the Idaho batholith. The first paper presents

a probabilistic approach for channel initiation due to overland flow and shows the application of the theory using channel head data from two watersheds. The probability distribution of area-slope thresholds (aS^α) derived from the probabilistic theory is compared to and found to match well with the observed area-slope thresholds at channel head locations in the field. The second paper reports field observations of soil loss volumes due to gully formation during a single thunderstorm event. The paper theoretically relates sediment transport capacity to runoff rate, slope and drainage area, then uses the soil loss observations to calibrate the nonlinear relationship between sediment transport and drainage area and slope. The paper also shows that the concavity index of the gully profiles obtained from the area and slope exponents of the calibrated sediment transport function using field data agrees well with the observed profile concavity of the gullies. Finally, the last paper describes a numerical framework for modeling the frequency and magnitude of sediment yields in the Idaho batholith. Simulation results show good correspondence with field observations of event sediment yields and long-term averages of soil loss over time scales up to 10,000 years. The model underscores the influence of forest vegetation and vegetation disturbances on erosion. The findings of the papers contribute to the understanding of how mountain ranges erode and have applicability in modeling the erosion response to land use and climate changes.

(214 pages)

ACKNOWLEDGMENTS

I thank my major professor, Dr. David Tarboton, for providing me guidance, excitement, and inspiration during my studies. I discovered and developed myself as a researcher while working with him. I would like to thank Dr. Robert T. Pack for stimulating my curiosity and developing my understanding of geomorphology in the field. I also thank him for the financial support he provided during my studies. I thank Dr. Charles H. Luce for updating me with the literature and exciting discussions. I would like to thank the other members of my committee, Drs. Jack Schmidt, Joel Pederson and William Rahmeyer. The classes I took from them provided invaluable contributions to my education.

Further thanks go to Lee Benda, Dan Miller, Jim Clayton, and Tom Black for their valuable inputs and their support in the field work. I also would like to thank David Montgomery for his review and suggestions on Chapter 2 and Gary Parker for interesting discussions and his motivation on Chapter 3. My thanks go to Kathleen Geier-Hayes for providing field information on the wildfire probabilities used in Chapter 4.

I thank my fellow graduate students in the hydrology lab and especially Craig Goodwin for interesting discussions and their warm friendship.

Finally my thanks go to my wife, Zeynep, for her love, support, and patience.

Erkan Istanbulluoglu

CONTENTS

LIST OF TABLES

LIST OF FIGURES

CHAPTER 1

INTRODUCTION

In this dissertation we concentrate on erosion processes and the influence of vegetation and disturbances on the frequency and magnitude of sediment yields in humid, soil-mantled forested mountainous basins. Hillslope processes that are continuously active year-around form an approximate equilibrium between soil production by weathering and removal by erosion in soil-mantled and vegetated hillslopes [*Selby*, 1993]. During this time of equilibrium, established vegetation imposes an upper limit to the extent of the channel network by providing a significant threshold for runoff erosion and mass movements [*Dietrich and Dunne*, 1993; *Tucker and Slingerland*, 1997]. Channels then transport the sediment delivered by soil creep from the surrounding hillslopes. This period of equilibrium is interrupted by extreme events or other natural disturbances such as fires that destroy the vegetation cover, evacuate the sediment stored in hollows over millennial time scales and deliver large pulses of sediment to the valley floor and disturb the aquatic habitats [*Benda and Dunne*, 1997; *Benda et al.*, 1998]. Natural disturbances and the spatial heterogeneity created by the geomorphic response to watershed disturbances form a mosaic of non-equilibrium habitats of various ages that allow a large number of species to coexists [*Pollock*, 1998]. On the other hand anthropogenic disturbances such as dam building, forest clearing and timber harvests modify the type, frequency and magnitude of natural disturbances and threaten the naturally evolved ecologic and aquatic habitats [*Li et al.*, 1987; *Hobbs and Huenneke*, 1992; *Reeves et al.*, 1998]. For example one of the most important consequences of the alteration of natural

disturbance regimes in the Pacific Northwest has been the widespread decline of anadromous salmonids [*Reeves et al.*, 1998]. Mountain erosion is episodic, and the interactions between episodic disturbances and the recovery of ecologic and aquatic habitats are complex and yet not fully explored. Therefore comparing the consequences of anthropogenic disturbances to the natural is inherently difficult.

The major motivation for this dissertation was two related questions: 1) Do forest management activities alter the frequency and magnitude of sediment yields compared to the natural sediment delivery regime of mountainous forested basins? 2) How can we quantify the effects of forest disturbances due to natural wildfires and management on the geomorphic response? First we study two important problems in geomorphology, channel initiation and fluvial sediment transport on steep mountainous watersheds, using field observations and theory. Then we implement the physical understanding learned from field observations in a more comprehensive numerical modeling structure of mountain erosion.

Field information used in the dissertation is compiled from steep soil-mantled mountains of the Idaho batholith. In the study watershed valleys are typically narrow and V shaped with steep slopes. Slope range from 10 % up to approximately 100 % with an average of 50% on hillslopes. The colluvium is grussy, clay-poor and was produced due to the disintegration of Idaho batholith rocks [*Meyer et al.*, 2001]. It shows little or no cohesion and is subject to runoff erosion and mass wasting especially following vegetation disturbances [*Gray and Megahan*, 1981].

The dissertation is organized into five chapters including this introduction and the summary. The three primary chapters are individual papers. The first paper is in press, the second in review and the third will be submitted for journal publication.

Chapter 2 presents a probabilistic approach to channel initiation. The channel head, the upstream limit of observable erosion and concentration of flow within definable banks, represents an important transition point form hillslope to channel processes. *Gilbert* [1877, 1909] argued that hillslope erosion is controlled by slope dependent diffusive sediment transport processes that form convex slopes, whereas valley development is due to incisive sediment transport function of both discharge and slope [*Montgomery*, 1991]. Consistent with the Gilbert hypothesis several workers related the transition from diffusive to incisive sediment transport processes to the location of channel and valley heads [*Smith and Bretherton*, 1972; *Kirkby*, 1987; *Tarboton et al.*, 1992; *Kirkby and Bull*, 2000] based on the idea that above the channel head diffusional sediment transport infills the fluvial incisions, whereas below the channel head fluvial sediment transport overwhelms the diffusional transport and valleys form. This hypothesis is relevant for valley development and maintenance over geologic time scales of several thousands to million years [*Montgomery and Dietrich*, 1994]. *Horton* [1945] hypothesized that an unchanneled hillslope represents a "belt of no erosion" and proposed that erosion and rill initiation occurs where shear stress imposed by overland flow exceeds a threshold necessary to entrain soil particles over a critical distance from the watershed divide. Horton's hypothesis is more relevant to shorter time scales, especially when the temporal variation in discharge and erosion thresholds is considered. Since the

diffusive infilling is not recognized, channels may incise even at diffusion dominated hillslope locations according to Horton's hypothesis. *Montgomery and Dietrich* [1988, 1989, 1994], *Dietrich et al.* [1993], and *Montgomery and Dietrich* [1994] presented field data on channel head locations that support Horton's theory and discussed the existence of a slope dependent contributing area threshold required to support a channel head. *Montgomery and Dietrich* [1992] and *Dietrich et al.* [1993] showed that data from channel heads observed in their Tennessee valley field site fit an inverse relationship between the specific catchment area (upslope contributing area per unit contour width), "a" and local slope, "S" of the form,

$$aS^{\alpha} = C \tag{1}$$

where α is an exponent that varies between 1 and 2 and C is a constant. They found that with $\alpha=2$, the majority of the channel heads observed are captured between two topographic threshold lines with C values of 25m and 200m. This reveals a factor of eight variation in the contributing area sizes required for channel initiation for a given slope in the field.

In chapter 2 we developed the logical next step of formalizing the description of the observed variability by interpreting the threshold C as a random variable derived physically from the random variability of quantities involved in the channel initiation process. This chapter also compares the simulated probability distributions of channel initiation thresholds to the observed area-slope thresholds at channel head locations in the Idaho batholith and to the Tennesse Valley data set reported by *Montgomery and Dietrich*

[1989]. The theory can be used to map the probability of channel initiation to evaluate the erosional consequences of land use changes and extreme storm events.

Despite the extensive use of sediment transport laws in modeling hillslope erosion [*Foster*, 1982; *Woolhiser et al.*, 1990] and landscape evolution [*Willgoose et al.*, 1991; *Howard*, 1999] no field studies show evidence for the form and calibration of such laws on scales relevant to the sediment transport phenomena in self formed channels [*Dietrich et al.*, 2001].

A standard assumption in landscape evolution models is to characterize the sediment transport capacity, Q_s, as a non-linear function of flow discharge Q, or contributing area, A, used as a surrogate for discharge and local slope, S,

$$Q_s = \chi_{Q_s} A^M S^N \qquad (2)$$

where, χ_{Q_s} is a parameter that is usually a function of runoff rate and a sediment transport constant and M and N are exponents. In theory the sediment transport law imposes a power law relationship between local slope and upslope area under the assumption of dynamic equilibrium. For transport limited catchments this relationship is [*Tarboton et al.*, 1992]

$$S \propto A^{\theta_c}, \qquad \theta_c = \frac{M-1}{N} \qquad (3)$$

where, θ_c is the concavity index. In modeling studies the selection of M and N is not based on direct determination of field measurements but from the observed concavity index of river profiles [*Hancock et al.*, 2001] and even without knowing that the observed

profile is evolved over the long term under transport limited conditions [*Dietrich et al.*, 2001].

Chapter 3 reports field observations of soil loss volumes due to gully formation during a single thunderstorm event in the Idaho batholith. The paper first theoretically relates sediment transport capacity to runoff rate, slope and drainage area, second uses the soil loss observations to calibrate the M and N exponents of (2) and then compares the concavity index derived from erosion volume observations with the field observations of the concavity of gully profiles. It also uses the probabilistic approach for channel initiation described in chapter 2 to map the expected sediment transport capacity.

Chapter 4 describes a numerical model for predicting the frequency and magnitude of sediment yields in forested basins in the Idaho batholith. The model runs on Digital Elevation Models (DEMs) and simulates hillslope soil development based on continuous hillslope processes, soil removal by gully erosion, shallow landsliding and debris flows. The model is similar in spirit to the ones developed by *Benda and Dunne* [1997] and *Lancaster et al.* [2001] but differs in the implementation of gully erosion, vegetation dynamics of understory vegetation cover and runoff generation. The model predicts the stabilizing effects of vegetation by relating the overland flow roughness produced by vegetation inversely to the ratio used to partition total flow shear stress between that acting on soil particles and that acting on vegetation. The stabilizing effect of vegetation on slope stability through root cohesion is also modeled. In the model wildfires kill the vegetation and reduce the root cohesion and vegetation roughness. Vegetation is allowed to regrow in the time between disturbances. We also model the

occurrence of fire related soil hydrophobicity and relate it to runoff generation process. An inverse relationship between vegetation cover density and soil hydrophobicty is hypothesized and modeled. The paper examines the implications of forest vegetation cover conditions and disturbances by wildfires and timber harvest on sediment yields in a sample basin in the Idaho batholith.

The theories developed and tested in chapters 2, 3 and 4 use field information collected in a steep soil-mantled basin in the Idaho batholith. The models described in this dissertation are calibrated with and currently relevant for small steep soil-mantled watersheds with cohesionless soils where sediment yield is dominated by episodic sediment delivery.

The erosion model presented in chapter 4 simulates spatially uniform forest fire occurrences and precipitation forcing and is not applicable to large basins where spatial patterns are observed in these model components. The model is not also applicable to areas where day-to-day sediment transport dominates the annual sediment yield unless the hydrology component of the model is reformulated to account for the rates and durations of individual precipitation events and interstorm periods.

Soil cohesion may have significant influence on erosion and landslide initiation and sediment transport by providing additional shear strength and increasing erosion thresholds. Therefore in order for the model to be applicable for cohesive soils possible effects of soil cohesion on erosion dynamics should be considered in the theory and further tested against field observations.

One other limitation in the model developed in chapter 4 is that the dynamics of wood transport and sediment and wood storage in the basin is not modeled. Sometimes woody debris flow deposits form debris dams on the main channel that may alter the frequency and magnitude of sediment yield at the watershed outlet [*Lancaster et al.*, 2001]. The priority in the model was to address the influence of vegetation and disturbances on the frequency and magnitude of sediment input to the network. Therefore, processes for sediment routing and storage in the channel network are not model in this dissertation.

References

Benda, L., and T. Dunne, Stochastic forcing of sediment supply to channel networks from landsliding and debris flow, *Water Resour. Res.*, 33(12), 2849-2863, 1997.

Benda, L., D. J. Miller, T. Dunne, and G. H. Reeves, Dynamic landscape systems, in *River Ecology and Management: Lessons from the Pacific Coastal Ecoregion*, edited by R. J. Naiman and R. E. Bilby, pp. 261-288, Springer-Verlag, New York, 1998.

Dietrich, W. E., D. Bellugi, A. M. Heimsath, J. J. Roering, L. S. Sklar, and J. D. Stock, Geomorphic transport laws for predicting landscape form and dynamics, in *A MARGINS Education and Planning Workshop Developing a Community Sediment Model*, available at; http://instaar.colorado.edu/deltaforce/workshop/csm.html. 2001.

Dietrich, W. E., and T. Dunne, The channel head, in *Channel Network Hydrology*, edited by K. Beven and M. J. Kirkby, pp. 175-219, John Wiley, New York, 1993.

Dietrich, W. E., C. J. Wilson, D. R. Montgomery and J. McKean, Analysis of erosion thresholds, channel networks, and landscape morphology using a digital terrain model, *J. Geol.*, 101, 259-278, 1993.

Foster, G. R., Modeling the erosion process, in *Hydrologic Modeling of Small Watersheds*, edited by C. T. Haan, ASAE Monograph No. 5., pp. 295-380, Am. Soc. Agric. Eng, St. Joseph, MI., 1982.

Gilbert, G. K., Geology of the Henry Mountains, in *U.S. Geog. Geol. Surv.*, p. 160, 1877.

Gilbert, G. K., The convexity of hill tops, *J. of Geol.*, 17, 344-350, 1909.

Gray, D. H., and W. F. Megahan, Forest vegetation removal and slope stability in the Idaho Batholith., *USDA For. Serv. Res. Pap. INT-271*, p. 23. Intermt. For. and Range. Exp. Stn., Ogden, Utah, 1981.

Hancock, G. R., G. R. Willgoose, and K. G. Evans, Testing the Siberia landscape evolution model using the Tin Camp creek, northern territory, Australia, field catchment, *Earth Surf. Processes and Landforms*, 27(2), 125-143, 2001.

Hobbs, R. J., and L. F. Huenneke, Distrubance, diversity, and invasion: Implications for conservation, *Conservation Biology*, 6, 324-337, 1992.

Horton, R. E., Erosional development of streams and their drainage basins: hydrophysical approach to quantitative morphology, *Geol. Soc. Amer. Bull.*, 56, 275-370, 1945.

Howard, A., Simulation of gully erosion and bistable landforms, in *Incised Rriver Channels Processes,Forms, Engineering and Management*, edited by S. E. Darby and A. Simon, pp. 277-299, John Wiley, New York, 1999.

Kirkby, M. J., Modelling some influences of soil erosion, landslides and valley gradient on drainage density and hollow development, in *Geomorphological Models,Theoretical and Empirical Aspects*, edited by F. Ahnert, Catena, Supplement 10, pp. 1-14, 1987.

Kirkby, M. J., and L. Bull, Some factors controlling gully growth in fine-grained sediments: a model applied in southeast Spain, *Catena*, 40, 127-146, 2000.

Lancaster, S. T., S. K. Hayes, and G. E. Grant, Modeling sediment and wood storage dynamics in small mountainous watersheds, in *AGU Volume on Geomorphic Processes and Riverine Habitat*, edited by B. P. J. Dorava, F. Fitzpatrick, and D. Montgomery, 2001.

Li, H. W., C. B. Schreck, C. E. Bond, and E. Rexstad, Factors influencing changes in fish assemblages of Pacific streams, in *Community and Evolutionary Ecology in North American Stream Fishes*, edited by W. J. Matthews and D. C. Heins, Universtiy of Oklahoma Press, Norman, Oklahoma, USA, pp. 193-202, 1987.

Meyer, G. A., J. L. Pierce, S. H. Wood and A. J. T. Jull, Fire, storms and erosional events in the Idaho batholith, *Hydrol. Processes*, 15, 3025-3038. 2001.

Montgomery, D. R., *Channel Initiation and Landscape Evolution*, PhD Thesis, University of California at Berkeley, 1991.

Montgomery, D. R., and W. E. Dietrich, Where do channels begin, *Nature*, 336, 232-234, 1988.

Montgomery, D. R., and W. E. Dietrich, Source areas, drainage density and channel initiation, *Water Resour. Res.*, 25(8), 1907-1918, 1989.

Montgomery, D. R., and W. E. Dietrich, Channel initiation and the problem of landscape scale, *Science*, 255, 826-830, 1992.

Montgomery, D. R., and W. E. Dietrich, Landscape dissection and drainage area-slope thresholds, in *Process Models and Theoretical Geomorphology*, edited by M. J. Kirkby, pp. 221-246, John Wiley, 1994.

Pollock, M. M., Biodiversity, in *River Ecology and Management: Lessons from the Pacific Coastal Ecoregion*, edited by R. J. Naiman and R. E. Bilby, pp. 430-452, Springer-Verlag, New York, 1998.

Reeves, G. H., P. A. Bisson, and J. M. Dambacher, Fish communities, in *River Ecology and Management: Lessons from the Pacific Coastal Ecoregion*, edited by R. J. Naiman and R. E. Bilby, pp. 200-234, Springer-Verlag, New York, 1998.

Selby, M. J., *Hillslope materials and processes*, Oxford University Press Inc., New York, 451 pp., 1993.

Smith, T. R., and F. P. Bretherton, Stability and the conservation of mass in drainage basin evolution, *Water Resour. Res.*, 8(6), 1506-1529, 1972.

Tarboton, D. G., R. L. Bras, and I. Rodriguez-Iturbe, A physical basis for drainage density, *Geomorphol.*, 5(1/2), 59-76, 1992.

Tucker, G. E., and R. Slingerland, Drainage basin responses to climate change, *Water Resour. Res.*, 33(8), 2031-2047, 1997.

Willgoose, G., R. L. Bras, and I. Rodriguez-Iturbe, A coupled channel network growth and hillslope evolution model 1. Theory, *Water Resour. Res.*, 27(7), 1671-1684, 1991.

Woolhiser, D. A., R. E. Smith and D. C. Goodrich, *KINEROS, a kinematic runoff and erosion model; documentation and user manual*, ARS-77, 130 pp., Agric. Res. Serv., U.S. Dep. of Agric., Tuscon, Ariz., 1990.

CHAPTER 2

A PROBABILISTIC APPROACH FOR CHANNEL INITIATION[1]

Abstract. The channel head represents an important transition point from hillslope to fluvial processes. There is a nonlinear threshold transition across the channel head with sediment transport much larger in channels than on hillslopes. Deterministic specific catchment area, a, thresholds for channel initiation, sometimes dependent on slope, S, in the form of $aS^\alpha \geq C$, have been suggested. In this paper the channel initiation problem is viewed probabilistically with a spatially variable probability of channel initiation that depends on slope, specific catchment area and the probability distributions of median grain size, surface roughness and excess rainfall rate. The channel initiation threshold C is cast as a random variable to characterize the variability of aS^α at channel heads. Using field measurements from the Idaho Batholith, we show that median grain size measurements at each channel head explain a significant part of the observed variability of aS^α. We then characterize the variability of model inputs (median grain size, roughness and excess rainfall) using probability distributions and show that the probability distribution of area-slope threshold derived from these inputs matches the probability distribution of area-slope thresholds measured at field channel head locations. A gamma probability distribution provides a reasonable match to the distributions of area-slope

threshold measured and modeled at channel heads in our study area and in other published channel head data set.

1. Introduction

Substantial amounts of sediment are transported from hillslopes to streams due to flow concentration and the incision of channels. The upslope boundary of concentrated water flow and sediment transport between definable banks is called a stream channel head [*Dietrich and Dunne*, 1993]. The channel head has been either regarded as a point of transition in the sediment transport process where incisive wash processes begin to dominate over diffusive processes [*Smith and Bretherton*, 1972], or as a point where incision starts with the exceedence of an erosional threshold [e.g., *Horton*, 1945; *Montgomery and Dietrich*, 1988; *Willgoose et al.*, 1991; *Dietrich et al.*, 1993].

Laboratory, field and theoretical studies of sediment transport mechanics have concluded that fluvial transport of sediment grains does not occur until a critical shear stress is exceeded [*Shields*, 1936; *Yalin and Karahan*, 1979]. *Horton* [1945] proposed that an erosion threshold controls the location of channel heads. He suggested that the critical distance below the topographic divide required for sheet flow erosion is the same as that required for channel incision. According to Horton's theory, channels as erosion features may expand rapidly upslope in response to changed climate and land use conditions and can even form during individual storm events. Field experiments under rainfall simulation demonstrated that sheet flow is inherently unstable and can easily separate into streams, incise channels, and integrate into a network [*Dunne and Aubry*,

1986]. However, such a tendency can be reversed by raindrop impact, soil creep, and other diffusive processes [*Dunne and Aubry*, 1986]. This has also been shown theoretically by *Smith and Bretherton* [1972].

Based on field evidence and theory, *Montgomery and Dietrich* [1988, 1989, 1994], *Dietrich et al.* [1993] and *Montgomery* [1994, 1999] discussed the existence of a slope dependent contributing area threshold required to support a channel head. This threshold is similar to Horton's critical distance description for channelization but accounts for channel initiation by saturation overland flow and pore-pressure induced landsliding. *Montgomery and Dietrich* [1992] and *Dietrich et al.* [1993] showed that data from channel heads observed in their Tennessee valley field site fit an inverse relationship between the specific catchment area (upslope contributing area per unit contour width), "a" and local slope, "S" of the form,

$$aS^\alpha = C \tag{1}$$

where α is an exponent that varies between 1 and 2 and C is a constant. They found that with $\alpha=2$, all the channel heads observed are captured between two topographic threshold lines with C values of 25m and 200m. This reveals a factor of eight variation in the contributing area sizes required for channel initiation for a given slope in the field. *Montgomery and Dietrich* [1992] explained this observation as: "This scatter probably arises from both spatial and temporal variation in the hydrologic and erosional processes governing channel initiation and should introduce considerable variation into channel and valley development, thus contributing a random aspect to the appearance of many

landscapes." The model was thus generally successful at delineating slope-area bounds for channel head locations but acknowledged scatter due to spatial variations in hydrologic and erosional processes [*Dietrich et al.*, 1993; *Prosser and Dietrich*, 1995; *Prosser and Abernety*, 1996].

The lack of a distinct topographic threshold at channel heads in the form suggested in the literature was also reported in case of intense gullying due to land use pattern changes [*Prosser and Soufi*, 1998; *Desmet and Govers*, 1997]. *Desmet et al.* [1999] experimented with different area exponents in equation (1) to see how they could best match grid cells observed to be gullied in the field to grid cells predicted to be gullied, while setting the threshold C to keep the fraction of area mapped as gullies roughly constant. Their best results classified 70 to 80% of grid cells correctly, although this success does depend on their threshold C and does not consider the number of grid cells in excess of the threshold not considered to be gullied.

Erosion is highly nonlinear with threshold functionality or dependence upon the occurrence of channelization. A model that uses a single channel initiation threshold based on average or central tendency parameters will predict significant erosion only in locations where channelization is predicted on a long-term basis. The work cited above has indicated the presence of variability in the channel initiation threshold and the need for a model that explicitly recognizes this variability. Here we take the logical next step of formalizing the description of this variability by interpreting the threshold C as a random variable, with probability distribution derived physically from the random variability of quantities involved in the erosion process. This description of channel

initiation incorporates higher frequency temporary excursions of channelization into terrain that is on the average not channeled over longer time scales. Estimating sediment transport rates from hillslopes is important during extreme rainfall events, when ephemeral rills and gullies are formed. In this study the question of how to parameterize the variability of relevant hydraulic and hydrologic hillslope properties used deterministically in the previous models has been studied and a probabilistic approach to channel initiation has been developed. Our probabilistic model, recognizing the uncertainty and spatial as well as temporal variability in its parameters, predicts a contribution to erosion (represented probabilistically) due to channelization even at locations that do not meet the central tendency channelization threshold. It is our premise in this paper that this new approach provides further insights into the role of uncertainty in the prediction of erosion for soil management purposes.

In what follows we first develop a theory of channel initiation that expresses the probability of channel initiation in terms of the randomness of channel initiation threshold C derived from primary random inputs of sediment size, additional roughness (roughness due to vegetation and obstructions) and excess precipitation rate and show its contribution to probabilistic representation of erosion and sediment transport. This theory assumes the initiation of channels where shear stress exceeds a critical value [*Dietrich and Dunne*, 1993] and develops the probability distribution for this occurrence. The theory can be used to map the probability of channel initiation both for a single channel forming runoff event and integrating over a range of events in time as long as appropriate probability distributions are used to characterize the model inputs. The single

event approach, which emphasizes spatial variability, is used in this paper to test the

concept through comparison to observed gully initiation from a single storm. The

integrated approach that incorporates both spatial and temporal variability is most

appropriate for practical management applications, but is less easily tested directly, so we

suggest justification of the integrated approach based upon the results from single event

tests.

We then describe our field area where the channel heads were mapped and

median sediment size, d_{50}, was measured at each channel head. We test the theoretical

relationship between d_{50} and channel initiation threshold. Finally we select reasonable

probability distributions for the other random inputs to C and compare the probability

distributions of derived C to the probability distributions of observed aS^{α} at channel

heads. We show that the distribution of derived C is well approximated by a gamma

distribution, and that a similar gamma distribution matches the distribution of area slope

observations in other published channel head data.

2. Probabilistic Approach for Channel Initiation

The total shear stress associated with overland flow is

$$\tau_t = \rho_w gyS \tag{2}$$

where, ρ_w is the density of water, g gravitational acceleration, y is the flow depth and S is

the sine of the slope angle. Effective shear stress acting on the bare soil surface is a

portion of τ_t due to shear stress partitioning between vegetation, soil and other roughness

elements such as obstructions and surface irregularities [*Foster et al.*, 1989]. The

effective shear stress, τ_f acting on the bare soil surface can be approximated by

[*Tiscareno-Lopez et al.*, 1994],

$$\tau_f = \tau_t (\frac{n_b}{n_a + n_b})^{1.5} \tag{3}$$

where, n_b is Manning's roughness coefficient for bare soil and n_a is additional roughness

due to vegetation, obstructions and surface irregularities [*Arcement and Schneider*, 1984].

Bare soil roughness can be explicitly related to median sediment diameter, d_{50}. Many

empirical relationships presented for n_b have a general form [*Yen*, 1992],

$$n_b = kd_{50}^p \tag{4}$$

where k is a constant and p=1/6. We used k=0.0474, the value proposed by Strickler for

sand. In this relationship d_{50} is expressed in m. This equation has been used for overland

flow [*Julien and Simons*, 1985]. With the d_{50} values we observed in the field this

relationship gives values for n_b in the range 0.01 to 0.03 consistent with the range of n_b

values for sand and gravel suggested for overland flow routing by *Woolhiser et al.* [1990]

and *Engman et al.* [1986].

Using laboratory and field data and some data from the literature *Rouhipour et al.*

[1999] showed that Manning's equation gives more accurate estimates of overland flow

velocity than the Darcy-Weisbach and Chezy equations. Assuming uniform overland

flow, the depth y in (2) from Manning's equation is,

$$y = [(n_b + n_a)q_o / S^{1/2}]^{3/5} \tag{5}$$

where, q_o is the overland flow per unit contour width. Substituting (5) into (2) and (3), the effective shear stress can be written as,

$$\tau_f = \beta_1 q_o^{m_1} S^{n_1} \tag{6}$$

where, m_1=0.6, n_1=0.7 and $\beta_1 = \rho_w g n_b^{1.5} (n_b + n_a)^{-0.9}$. If we assume that overland flow incises a channel when τ_f exceeds a critical channel initiation shear stress threshold, τ_c, then a channelization threshold would be,

$$\beta_1 q_o^{m_1} S^{n_1} \geq \tau_c. \tag{7}$$

We consider two models for runoff generation to estimate q_o in equations (6) and (7). The first model assumes that q_o is proportional to the specific catchment area, a, as,

$$q_o = ra \tag{8}$$

where r is the net water input rate (rainfall or snowmelt minus evaporation and infiltration). This we term "infiltration excess" because r is the precipitation in excess of infiltration independent of topography. Substituting (8) into (7) and rearranging gives,

$$aS^\alpha \geq C \tag{9}$$

where $\alpha = n_1/m_1 = 1.167$ and C is an area-slope threshold for channel initiation similar to the form suggested previously [*Willgoose*, 1989; *Dietrich et al.*, 1993] given by

$$C = \left(\frac{\tau_c}{\rho_w g n_b^{1.5} (n_b + n_a)^{-0.9} r^{m_1}} \right)^{1/m_1}. \tag{10}$$

With the positive value for α, equation (9) predicts a negative relationship between slope and drainage area for constant C at channel heads.

The second model for runoff generation assumes a limited lateral transport capacity in the soil profile equal to slope times transmissivity, TS. Overland flow is assumed to occur when this capacity is exceeded, and is equal to the surface water input in excess of the lateral transport capacity.

$$q_o = ra - TS = r(a - a_s), \quad a > a_s \tag{11a}$$

where

$$a_s = ST/r \tag{11b}$$

is the specific catchment area required for saturation under steady-state conditions, and T is the transmissivity of soil profile. This is a saturation excess model for runoff generation similar to TOPMODEL [*Beven and Kirkby*, 1979]. Runoff occurs only for locations where the wetness index a/S exceeds a threshold, here equal to T/r.

Using the relationships in (7) and (11) the threshold for channel initiation for saturation excess overland flow can be written as,

$$(a - a_s) S^\alpha \geq C. \tag{12}$$

With this model the drainage area required to support runoff increases with slope. This

can lead to a positive area-slope relationship for constant C at channel heads

[*Montgomery and Dietrich*, 1994; *Montgomery*, 1999].

Our model assumes channel initiation when the shear stress required to initiate

sediment transport (incipient motion or detachment) from the bare soil surface is

exceeded. This, through equation (10) gives the channelization threshold, C. The critical

shear stress, τ_c, that goes into equation (10) is estimated from Shield's [1936] equation as,

$$\tau_c = \tau^* g (\rho_s - \rho_w) d_{50} \tag{13}$$

where τ^* is the dimensionless critical shear stress for incipient motion or detachment of

particles with the median grain size, d_{50}, and ρ_s is the sediment density. For rough

turbulent flows an average value of $\tau^* \cong 0.045\text{-}0.046$ [*Gessler*, 1971; *Miller et al.*, 1977;

Yalin and Karahan, 1979]. τ^* may also be obtained from the Shields diagram using the

shear Reynolds number,

$$R^* = u^* \frac{d_{50}}{\nu} = \sqrt{\tau_t / \rho_w} \frac{d_{50}}{\nu} = \sqrt{gyS} \frac{d_{50}}{\nu} \tag{14}$$

where ν is the kinematic viscosity and equation (2) has been used to obtain the right hand

expression. When τ^* is evaluated using this approach it depends on r and topographic

variables a and S. However this dependence is weak. We simulated a range of a, S and r

values representative of the terrain and effective rainfall in our field site and found that τ^*

ranged narrowly between 0.04 and 0.046, so selected $\tau^* = 0.043$ for the remainder of this

work. This has the advantage of keeping the channel initiation threshold C independent of topographic variables making for more meaningful comparisons with aS^{α} at channel heads. There may in fact be a wider range in τ^* values for rough turbulent flows [*Buffington and Montgomery,* 1997] that will likely contribute to the variability of channel heads observed in the field. However $\tau^* = 0.043$ is consistent with the τ^* values reported by [*Buffington and Montgomery,* 1997] for coarse sand and fine gravel observed in our field areas.

The left hand sides of (9) and (12) include topographic variables which can be derived from digital elevation models (DEMs) using algorithms to evaluate local slopes and specific catchment areas such as from *Tarboton* [1997]. The C parameter on the right hand side of (9) and (12) absorbs all the other hydrologic and geomorphic parameters. Obtaining proper values for C may require field studies and experiments as well as remote sensing analysis. However even under a fixed land use condition or geological setting the parameters absorbed by C may show significant variability in space and time, particularly in the case of r. To account for this we assume spatially homogenous probability distributions for d_{50}, n_a and r, which are used to calculate C in (10). To simplify matters we ignore variability of r within the area contributing to each point and thus assume that (8) and (11) hold for each specific realization of random r. This assumption lets us characterize both spatial and temporal variations of the area-slope threshold C. The scheme to derive a probability distribution for C and to calculate probability of channel initiation over the terrain is shown in Figure 2-1. This Figure depicts the terrain inputs S and a, which are combined to aS^{α} and random inputs d_{50}, r and

n_a. We selected d_{50} as a random variable, because it can be used to estimate both n_b and τ_c from equations (4) and (13) respectively and it can be measured in the field. Once n_b is estimated from d_{50}, then possible ranges of additional Manning's roughness, n_a can be obtained from tables of total Manning's roughness (n_b+n_a) coefficients for overland flow based on land use conditions [e.g., *Engman*, 1986; *Woolhiser et al.*, 1990]. The quantities τ_c, n_b, n_a and r are combined through equation (10) to obtain C. This Figure amounts to a Bayes net for estimating the probability distribution of C given uncertainty in the inputs d_{50}, r and n_a, characterized by probability distributions. For the infiltration excess overland flow model, the spatial probability of channel initiation (PCI) of a given location can be described by the probability of channel initiation threshold C being less than or equal to aS^α calculated from the terrain, formalized as,

$$PCI^{ie} = P(C \le aS^\alpha) = \int_0^{aS^\alpha} f_C(C)dC \qquad (15)$$

where $f_C(C)$ is the probability density function of C. Evaluating the probability of channel initiation for saturation overland flow is more complex than that of infiltration excess because it involves the parameter as T/r, which should also vary randomly because of the randomness in r, and perhaps also T. First we write (12) in the form of (9) as,

$$aS^\alpha \ge B + C \qquad (16)$$

where B= $S^{\alpha+1}$T/r. Here we have the addition of two related random numbers. Let $C' = B + C$, then the probability density function for C', $f_{C'}(C')$ can be evaluated at

each location and integrated to give the probability of channel initiation due to saturation

excess overland flow,

$$PCI^{se} = P(C' \le aS^{\alpha}) = \int_0^{aS^{\alpha}} f_{C'}(C') dC' . \qquad (17)$$

Barling et al, [1994] indicated that the steady-state assumption originating in

TOPMODEL and expressed here in equations (8) and (11) has some limitations. They

calculated specific catchment area as a function of rainfall duration (partial contributing

area). This idea may be implemented by using a partial contributing area in equation (15)

and (17). In general we expect that the partial contributing area should be a function of

water input duration, D, and so would use $a(D)S^{\alpha}$ as the upper limit in the integral of

equations (15) and (17).

We have not derived functional forms for the probability distributions of PCI

given by equations (15) and (17). Instead we use Monte Carlo simulation to generate

samples of C for the numerical evaluation of PCI. We show numerically that the results

from this Monte Carlo simulation can be approximated using a gamma distribution.

Equations (15) and (17) express the probability of channel initiation at each point

conditional on probability distributions of the inputs, namely sediment size, additional

roughness and runoff rate. The sediment size and additional roughness are spatial
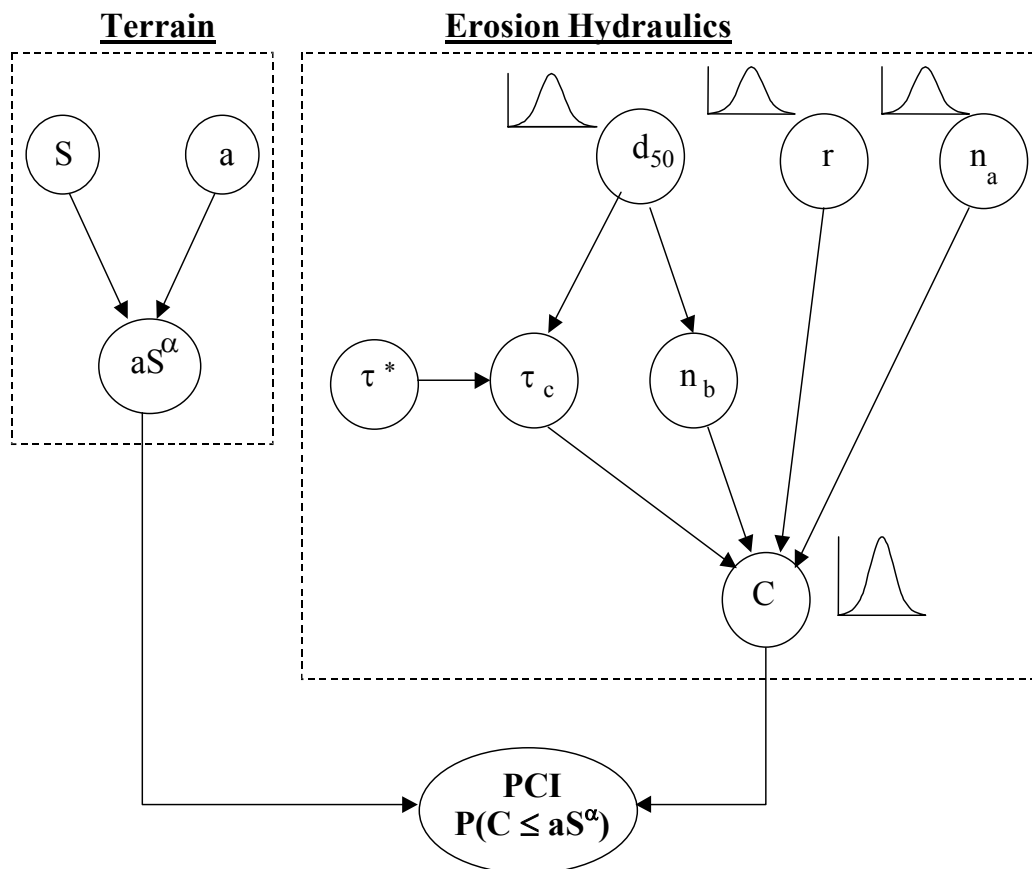
Figure 2-1. Information flow network used to derive a probability distribution for channel initiation threshold C, and to calculate the probability of channel initiation (PCI) over the terrain.

probability distributions. Only one realization of these will actually exist in any given landscape. However the specific spatial pattern of sediment size and additional roughness is practically unobservable so the probability distributions quantify the uncertainty in knowing this information. Additional roughness, in part due to vegetation may also be affected by land management activities. Effective runoff on the other hand is both spatially and temporally variable, and for practical applications should be quantified using a probability distribution for representative extreme events over a design period.

The PCI concept can then, when coupled with local detachment (erosion) and the sediment transport models, and integrated spatially express the aggregate expected value of erosion. This integrated estimate may be non zero as long as the PCI is greater than zero somewhere in the area, even though a threshold erosion model may have predicted no erosion due to channel incision because the single average or central tendency erosion threshold was not exceeded.

3. Field Study

3.1..Setting

The above-described methodology has been applied in the Idaho Batholith and its ability to characterize the probability distributions of observed C at channel head locations has been tested. This area consists of an extensive mass of granitic rock (16,000 mi^2) that covers a large portion of Idaho and some parts of Montana. It is almost entirely mountainous and forested. Extremely erodible coarse textured soils are found on steep gradients that often exceed 70% [*Megahan*, 1974]. Average precipitation is approximately 1000 mm. Localized high intensity rainstorms of short duration are common during summer. At other times of the year low intensity storms with longer durations occur, often in conjunction with snowmelt. Following soil disturbance, the combination of steep topography, high-soil erodibility, and high-climate stress often results in accelerated surface erosion [*Megahan and Kidd*, 1972]. The specific study areas selected are Trapper and Robert E. Lee Creeks within the North Fork of the Boise River in southwestern Idaho (see Figure 2-2). Trapper Creek was intensely burned by a wildfire

in 1994 and extreme gullying was initiated by a convective summer storm in 1995, possibly due to water repellent conditions of the surface soil. The gullies generated by this storm are probably ephemeral channels, but nevertheless resulted in considerable erosion. Robert E. Lee (REL) Creek was partially burned to a light to moderate degree. Although REL Creek is adjacent to Trapper Creek intense gullying did not occur in REL Creek, presumably due to either higher infiltration capacity from less water repellency or lower localized rainfall intensities, or a combination of both these effects.

3.2. Field Observations

A limited data set of channel head locations was collected using the definition of the channel head as the upstream limit of observable erosion and concentration of flow within definable banks [*Montgomery and Dietrich*, 1989]. Channel heads in Trapper Creek have headcuts of 0.3m to 1m in width and an average of 0.5 m depth. Some headcuts were even observed at the ridge crest. Local slopes (over a length of 10 to 20 m) at the channel heads were measured in the field using a Suunto inclinometer and a GPS was used to record locations. Sediment size samples were collected just above the headcuts to approximate the sediment size in transport when the incisions occurred. These samples were sieved and the median size of each sample was determined.

Contributing areas were derived from the 30m DEM of the study site using the D∞ algorithm [*Tarboton*, 1997]. Contributing area was also checked in a few channel head locations by hiking perpendicular to what was judged to be the elevation contours,
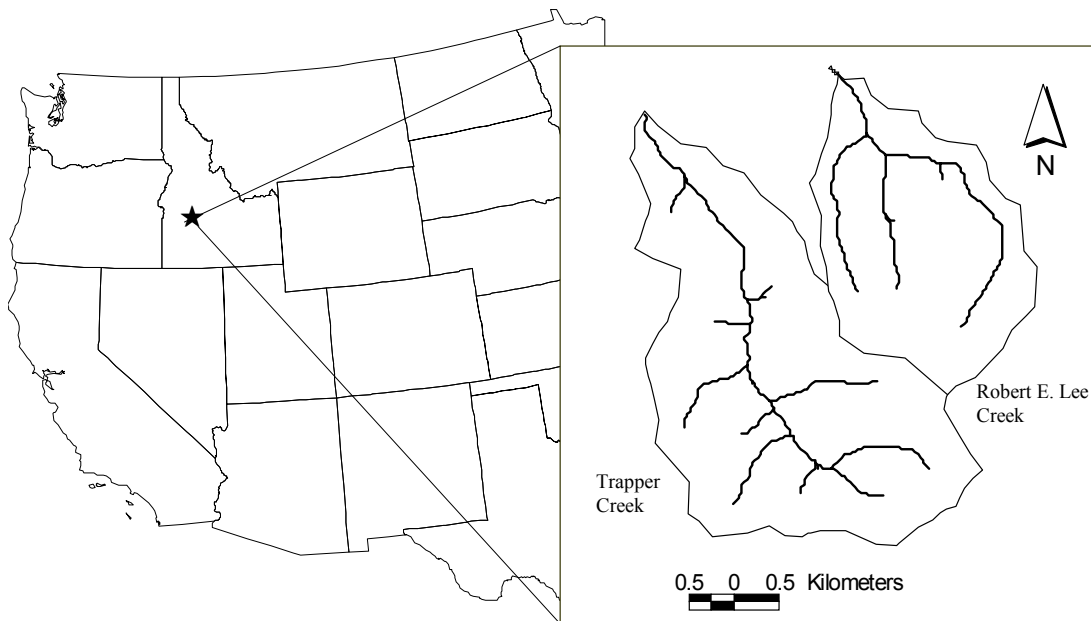
Figure 2-2. Location map of the field sites.

from both sides of the channel heads. This data for Trapper Creek is presented in Table 2-1.

Channels in Trapper Creek were usually discontinuous and faded out downstream from the most upstream limit of erosion within definable banks, with sequential headcuts occurring downslope. In these cases we also recorded the locations of the most downslope headcut, which we term the head of the continuous channel. Starting from the heads of the continuous channels, slopes were measured in the field at intervals from 20 to 40 m for distances ranging between 150 m and 500 m downslope. GPS was used to record the slope measurement locations and contributing areas were again derived from the 30m DEM of the study site using the D∞ algorithm [*Tarboton*, 1997].

We do not know the rainfall rate of the storm that incised the channels in Trapper Creek. However some forest service personnel were exposed to that storm and they estimated that more than an inch of rain fell in less than half an hour. It is conceivable that this kind of a convective storm event could result in local intensities of between 50 mm/h and 100 mm/h.

Two distinct types of channel heads were observed in REL Creek. We observed channel incisions due to saturation excess overland flow (SEOF) where fire effects were insignificant. The vegetation mat was broken mostly by seepage forces and sediment entrained by saturation overland flow. These channel heads support gravel-bed streams with definable banks stabilized by vegetation. Infiltration excess overland flow (IEOF) channel incisions were observed where there is disturbance by light to moderate fire or forest harvest or there is bedrock exposure and coarse materials such as cobbles and rock fragments on the surface. There was not significant vegetation cover around IEOF channel heads in REL Creek and channels were ephemeral discontinuous small gullies. The channel heads located on hillslopes where there is coarse surface material, rock fragments or exposed bedrock were separated in the model analysis because the percentage of rock was not quantified in our field measurements limiting our ability to use methods that account for rock percentage [*Abrahams and Parsons*, 1991; *Nearing et al.*, 1999].

Table 2-1. Observed Specific Catchment Area, Slope, and Median Grain Size at Channel Head Locations in Trapper Creek and Calculated Parameters Required to Estimate Channel Initiation Threshold, C, and Calculated C values at Each Location

Observed			Calculated				
Specific catchment area (m)	Slope m/m	d_{50} (mm)	aS^{α} (m)	n_b	n_t	τ_c (Pa)	C
100	0.42	1.700	33.1	0.0164	0.0684	1.17	15.48
30	0.32	1.700	7.5	0.0164	0.0684	1.17	15.48
30	0.23	*	5.2	*	*	*	
46	0.40	2.000	14.5	0.0168	0.0688	1.38	19.15
125	0.72	*	66.8	*	*	*	
30	0.31	1.300	7.3	0.0157	0.0677	0.89	10.90
40	0.25	1.330	7.7	0.0157	0.0677	0.91	11.23
61	0.45	*	21.6	*	*	*	
67	0.45	*	23.7	*	*	*	
123	0.45	2.200	43.5	0.0171	0.0691	1.51	21.71
56	0.30	1.630	13.1	0.0163	0.0683	1.12	14.65
53	0.39	2.000	16.3	0.0168	0.0688	1.38	19.15
72.7	0.42	*	24.0	*	*	*	
30	0.23	1.600	5.2	0.0162	0.0682	1.10	14.30
68	0.41	2.380	21.9	0.0173	0.0693	1.64	24.06
45	0.32	2.250	11.3	0.0172	0.0692	1.55	22.35
30	0.31	*	7.3	*	*	*	
68	0.60	2.200	31.3	0.0171	0.0691	1.51	21.71
57	0.46	1.750	20.6	0.0165	0.0685	1.20	16.08
59	0.53	2.730	24.3	0.0177	0.0697	1.88	28.81
40	0.30	1.700	9.3	0.0164	0.0684	1.17	15.48
32	0.40	2.100	10.1	0.0170	0.0690	1.44	20.42
60	0.49	*	23.0	*	*	*	
139	0.67	*	70.2	*	*	*	
103	0.53	2.900	42.5	0.0179	0.0699	1.99	31.19
70	0.35	1.600	19.2	0.0162	0.0682	1.10	14.30
88	0.40	2.900	27.7	0.0179	0.0699	1.99	31.19

*: No sediment size distribution data is available for those channel heads.

4. Results

4.1. Point-wise Comparison of the Observed
aS^α and Calculated C at Channel Heads

The theory developed above suggested that variations in d_{50}, n_a and r are

responsible for the variation in aS^α at channel heads. Here the measured values of d_{50} in

Trapper Creek are used to test the contribution of d_{50} to this variability. We set $\alpha=1.167$

following equation (9). We also set r = 35 mm/h in the infiltration excess runoff model

assuming about 50% infiltration due to the water repellency remaining a year after the

wildfire and rainfall around 70 mm/h in the range 50 to 100 mm/h reported for the

channel forming storm. We adjusted n_a to optimize the fit of C values to aS^α, and

obtained $n_a = 0.052$. This is within the range from 0.04 to 0.12 reported by *Woolhiser et

al.* [1990] and *ASCE* [1996] for sparse vegetation and surface litter.

Table 2-1 includes values of aS^α calculated at each observed channel head and τ_c

estimated from d_{50} using equation (13). This τ_c is used with equation (10) to evaluate C.

Figure 2-3 plots C versus observed aS^α. The regression R^2 and Nash-Sutcliff error

measure [e.g., *Gupta et al.*, 1998]

$$NS = 1 - \frac{\sum_{i=1}^{n}\left(C_i - aS^\alpha_{\ i}\right)^2}{\sum_{i=1}^{n}\left(aS^\alpha_{\ i} - \overline{aS^\alpha}\right)^2} \tag{18}$$

indicate that about 40% of the variability in observed aS^α may be attributed to d_{50}. A similar fit can be obtained for different r values by adjusting n_a with both r and n_a still being within the range of their uncertainty.

4.2. Comparison of Channel Initiation Probability Distributions

The point-wise comparison shown in Figure 2-3 revealed uncertainties associated not only with d_{50}, but also r and n_a. Here we employed the scheme given in Figure 2-1 to derive a probability distribution for C by Monte Carlo Simulation and compare the derived distribution with the aS^α distribution observed at channel heads in the field.
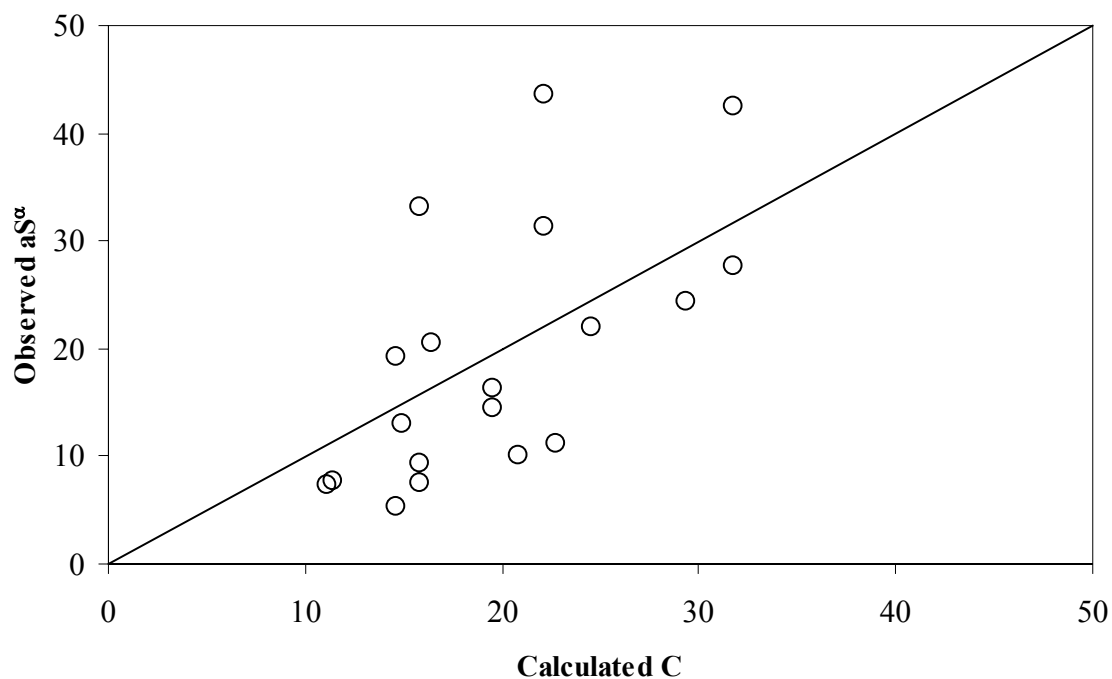
Figure 2-3. Plot of calculated C versus the observed aS^α for channel heads in Trapper Creek. Straight line is the 1:1 line. R^2=0.387 and NS=0.377.

This is a single event test of the PCI concept with probability distributions of the inputs chosen as estimates of the single 1995 event responsible for initiation of the channels mapped.

We found that the d_{50} data from Trapper Creek presented in table 2-1 was well described by a log-normal distribution with mean $d_{50} = 2$ mm and standard deviation of 0.48 mm (Figure 2-4). Uniform distributions were used for the other two input variables, with r between bounds of 15 and 55 mm/h and n_a between bounds of 0.015 and 0.1. These distributions quantify the uncertainty associated with this single event in a simple way. In management applications that integrate over time, other distributions may be more appropriate, specifically for r. 1500 random values for d_{50}, r and n_a were generated. Figure 2-5 compares the cumulative distribution of the simulated C to the cumulative distribution of the observed aS^{α} for channel heads observed in Trapper Creek. The bounds in the probability distributions for r and n_a have been adjusted by trial and error to achieve this fit, but are well within the range that is plausible. The field observed channel head aS^{α} have an average, standard deviation and skewness of 26 m 18.4 m and 1.13. The same statistics obtained for C from the Monte Carlo simulation scheme are; 26 m, 18.5 m and 1.56 respectively. Both the simulation statistics and the cumulative distribution of the simulated C show good correspondence with the observed aS^{α} variability in the field.
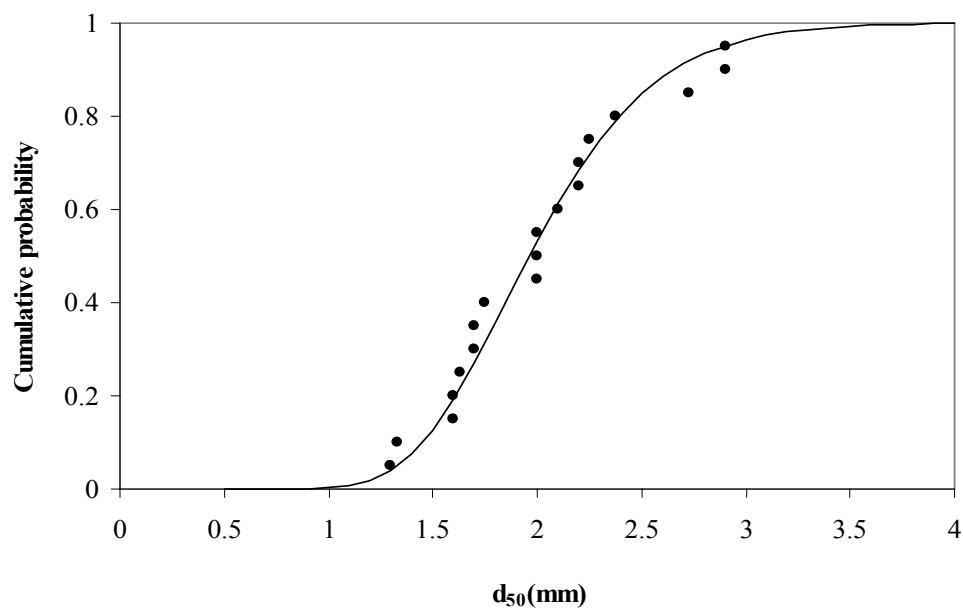
Figure 2-4. Log-normal distribution (solid line) fitted to the cumulative distribution of the median sediment size, d_{50}, measurements from Trapper Creek at channel heads estimated by using the Weibull plotting position.
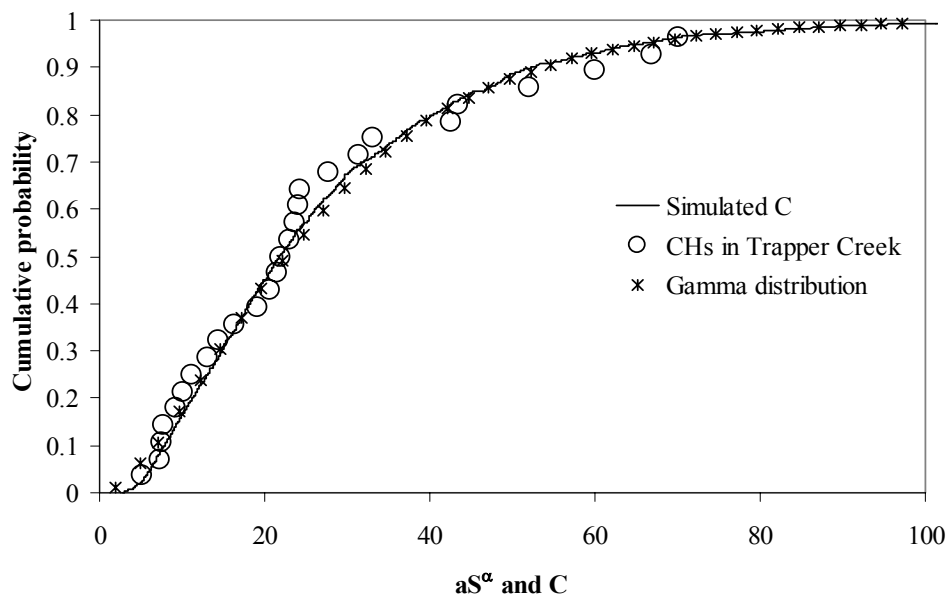
Figure 2-5. Comparison of the cumulative distribution from the simulations of C to the cumulative distribution of observed aS^{α} at channel heads in Trapper Creek and gamma distribution fitted to the observed aS^{α} CDF's by Weibull plotting position.
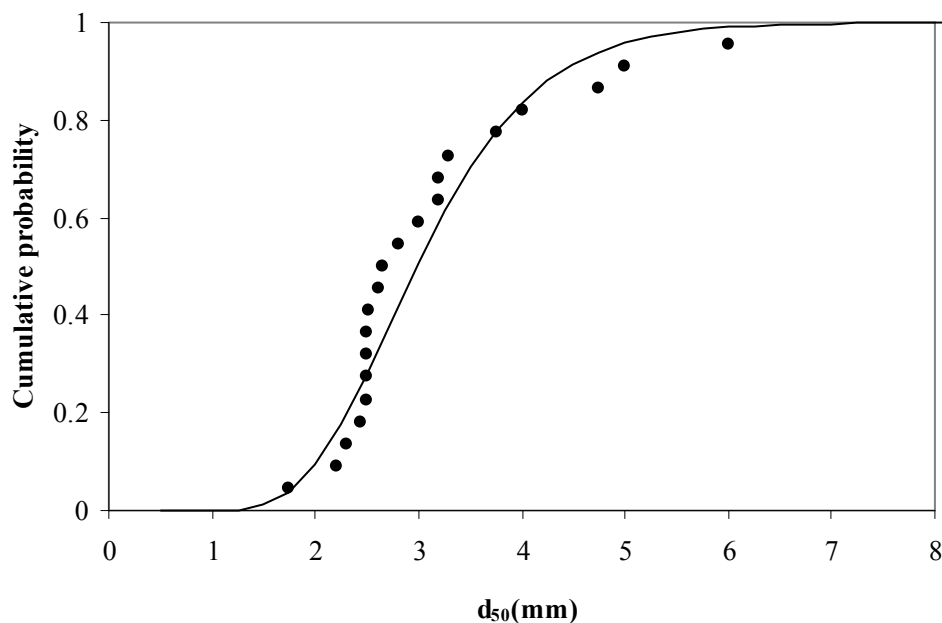
Figure 2-6. Log-normal distribution (solid line) fitted to the cumulative distribution of the median sediment size, d_{50}, measurements from REL Creek estimated by using the Weibull plotting position.

Two distinct channel initiation processes, IEOF and SEOF were observed in REL Creek. We found that the d_{50} data set collected from REL Creek at sites where the channel heads were observed can be fit by a log-normal distribution (Figure 2-6). The measured d_{50} data has a mean and standard deviation of 3.12 mm and 1.05 mm respectively. These numbers are larger than for Trapper Creek. REL Creek soils were generally coarser than Trapper Creek. The log-normal distribution (Figure 2-6) is used for both IEOF and SEOF channel initiation processes in REL Creek to characterize the d_{50} variability. Uniform distributions were used for the other two inputs r and n_a. We used r between bounds of 20 and 30 mm/h and n_a between 0.043 and 0.1 to estimate the PCI for IEOF channel heads. Comparison of the cumulative distributions of the simulated

C and the observed aS^α for IEOF channel heads in REL Creek is given in Figure 2-7a. The average, standard deviation and the skewness of the field observed aS^α of the IEOF incisions in REL Creek were 70 m, 33 m and 1.5 respectively. The same statistics obtained from the model are 73 m, 39 m and 1.7. Since the locations in the REL Creek where IEOF channel heads were observed were lightly burned compared to Trapper Creek, our calibrations of r and n_a are consistent with lower runoff rates (higher infiltration or less intense rainfall) and slightly higher additional roughness values (more vegetation) in those sites.

The IEOF channel heads shown in Figure 2-7a (as circles) do not include those where coarse surface material, rock fragments and bedrock exposure was observed. Instead the probability distribution of these is shown separately (as triangles) in Figure 2-7a. Apart from two points at the high end of the distribution all these channel heads with coarse material, rock fragments and exposed bedrock lie to the right of the aS^α distribution from the other more sandy locations, consistent with the idea that there is a higher critical shear stress threshold at these locations.

At most of the locations of SEOF channel heads saturation and exfiltration was observed in the field without any significant sediment detachment around the channel heads. Equation (11b) gives the specific catchment area required for SEOF. In this equation a value of T/r = 900m defines a zone of saturation that just includes all the SEOF channel head locations that we mapped. This provides an upper bound on T/r because a finite increment of flow is required to initiate sediment detachment around the channel heads.
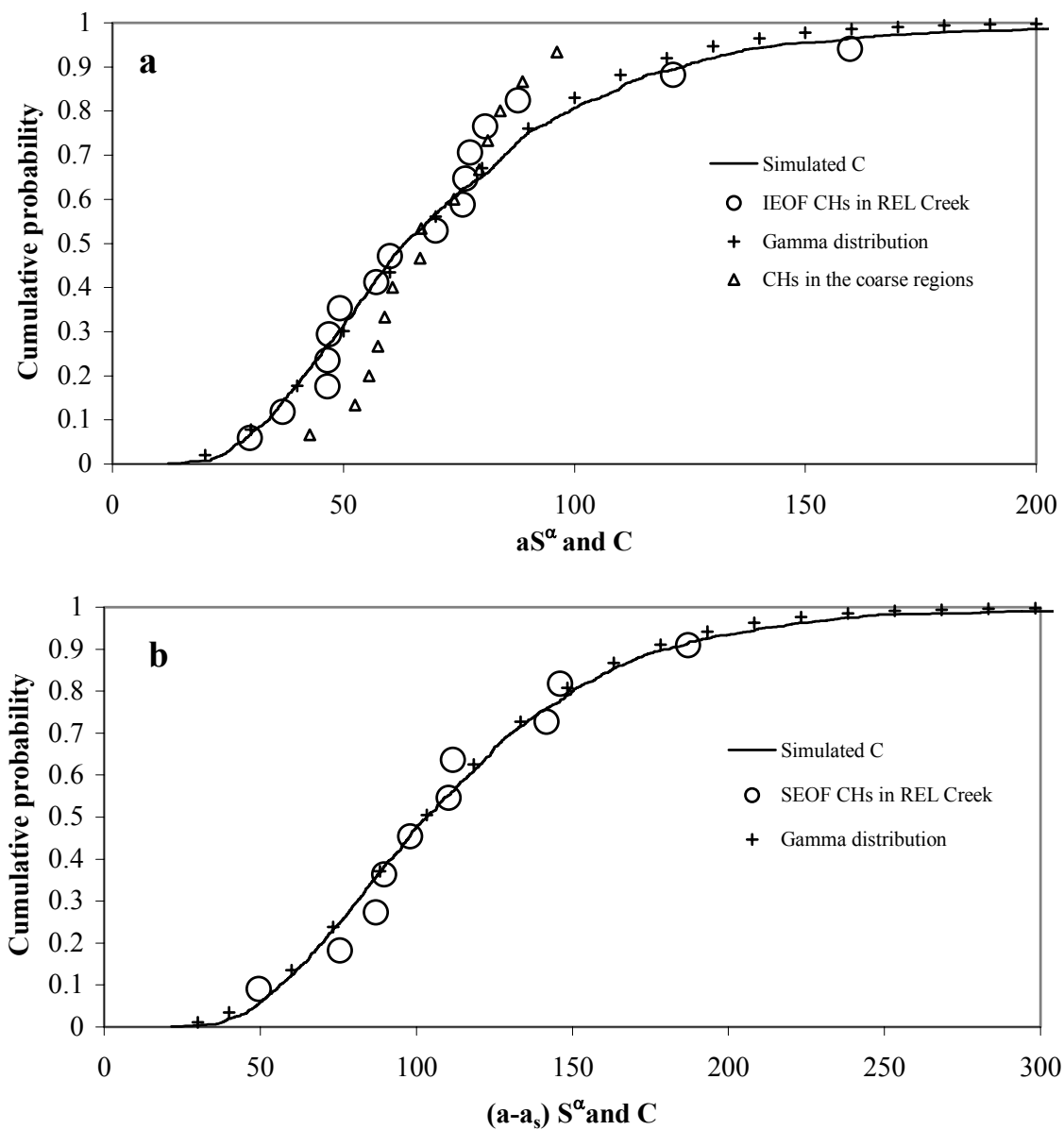
Figure 2-7. Comparison of the cumulative distribution from the simulations of C to the cumulative distribution of observed aS$^\alpha$ at channel heads in REL Creek and gamma distribution fitted to the observed aS$^\alpha$. Figure (7a) for infiltration excess overland flow (IEOF) channel heads (CH) and figure (7b) for saturation excess overland flow (SEOF) channel heads. CDF's by Weibull plotting position.

We modeled the saturation excess channel initiation process assuming a constant T/r of 600 m in (11) and (12). From DEM analysis we saw that this value saturates the axis of the major hollows in the watershed and leaves out most of the IEOF channels where no signs of recent sediment transport was observed. Various combinations of T and r can produce a T/r saturation threshold value of 600 m. For example a T of 40 m^2/day requires a steady-state precipitation rate of approximately 0.066 m/day. We analyzed 69 years of available precipitation records in the region and found that a daily rainfall of 0.066 m (66 mm) has a return period of about 80 years. The presence of snow can enhance the surface water input due to snowmelt by the rain on snow effect being added to rainfall inputs. However there is also leakage from the shallow soil into bedrock fractures common in the area. *Megahan and Clayton* [1986] presented 58 bed-rock saturated hydraulic conductivity tests ranging from 0 to 1.7 m/day with a mean and a median value of 0.175 m/day and 0.02 m/day.

We used a constant r of 0.066 m/day (2.75 mm/h) with T = 40 m^2/day to characterize the rainfall plus possible snowmelt minus deep percolation losses and evapotranspiration for the SEOF channel initiation analysis. For comparison *Montgomery* [1994] used T = 65 m^2/day in the Oregon coast range and *Dietrich et al.* [1993] used T = 17 m^2 in their Tennessee Valley California study area. We used the same log-normal probability distribution for d_{50} from field observations in REL Creek (Figure 2-6) as was used for the IEOF channel initiation analysis. We selected 0.0135 and 0.006 for the lower and upper bound of the uniform distribution for n_a through calibration. Here the effect of additional roughness (n_a) is minor because the vegetation

mat was broken by seepage forces in most sites. Figure 7b compares the cumulative

probability distributions of the observed $(a-a_s)S^\alpha$ and the simulated C at SEOF channel

heads. Since the calibrated additional roughness values are very low, and r and T were

held constant, this Figure shows how the random variation of median sediment sizes can

produce significant variation of channel head locations on the terrain.

In the PCI theory, equations (15) and (17) require the probability density function

of C. Several parametric probability distributions such as exponential, normal, log-

normal and gamma were fitted using the mean and variance of the aS^α observed. Among

those we found that gamma distribution gave the best correspondence with the observed

aS^α and simulated C distributions (Figures 2-5 and 2-7). The gamma probability density

function is given by,

$$f_C(C) = \frac{\lambda(\lambda C)^{k-1} e^{-\lambda C}}{\Gamma(k)} \tag{19}$$

where, C is the threshold for channel initiation and λ and k are the distribution parameters

which can be estimated from the mean, μ_C, and variance, σ_C^2, of the observations using

$\mu_C = k/\lambda$ and $\sigma_C^2 = k/\lambda^2$. $\Gamma(\ )$ is the gamma function.

4.3. Sensitivity Analysis

Figure 2-8 shows the sensitivity of the cumulative distribution of C to the

distributions used for d_{50}, r and n_a. In Figure 2-8a cumulative distributions for C were

generated holding d_{50} at its minimum observed, mean and maximum observed values but

generating n_a and r from their random distributions. Figure 2-8b shows the cumulative

distributions obtained holding r fixed at its lower bound, mean and upper bound values

while generating n_a and d_{50} from their random distributions. Figure 2-8c shows the

cumulative distributions obtained holding n_a fixed at its lower bound, mean and upper

bound values while generating r and d_{50} from their random distributions.

Montgomery and Dietrich [1989] tabulated source areas and slopes at 63 channel

heads in their Tennessee Valley California study area. Figure 2-9 plots the cumulative

distribution of AS^α for this data and shows that it is also well approximated by a gamma

distribution. Note that in this comparison contributing area A in m^2 is used rather than

specific catchment area because the colluvial fill width given in the Montgomery and
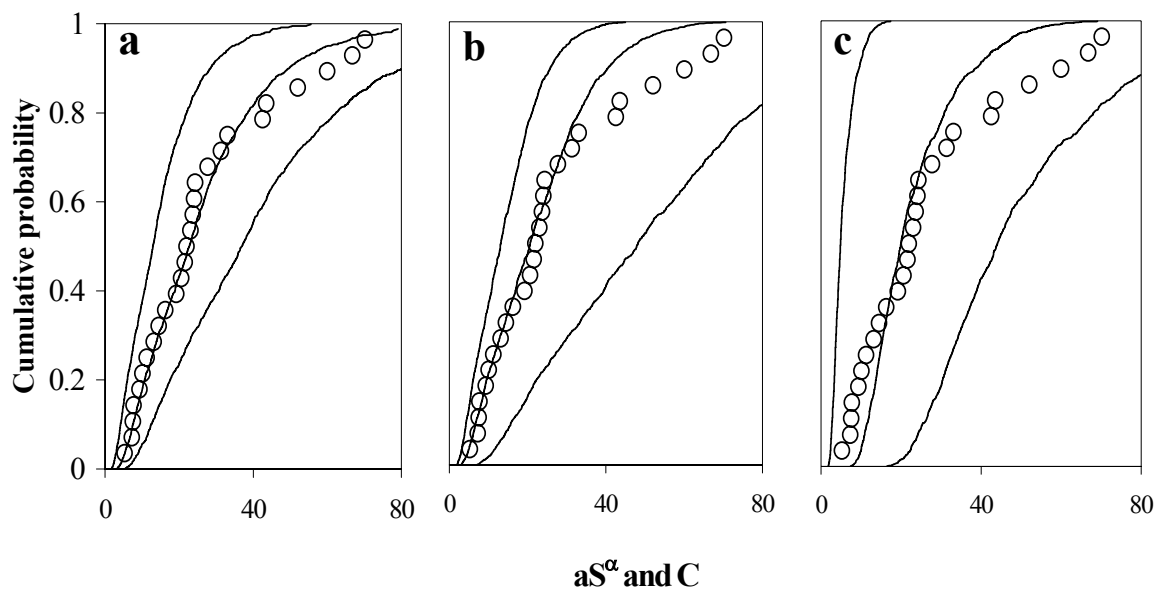
Figure 2-8. Sensitivity of the cumulative distribution of C to the distributions used for d_{50}, r, and n_a. In the figures curves from left to right are; (8a); d_{50}=1.3 mm, d_{50}=2 mm, d_{50}=2.9 mm; (8b) r=55 mm/h, r=35 mm/h and r=15 mm/h; (8c), n_a=0.01, n_a=0.052, n_a=0.1. Circles are the Trapper Creek channel head data.
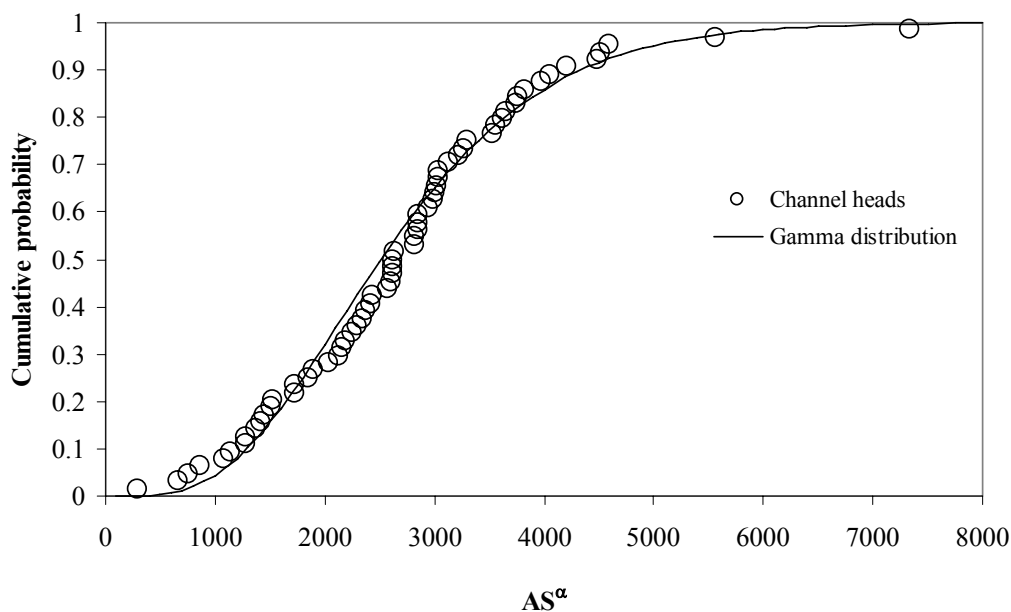
Figure 2-9. Gamma distribution (solid line) fitted to Tennessee Valley channel head data set [*Montgomery and Dietrich*, 1989].

Dietrich paper is not the same as contour width in the definition of specific catchment area. We have not attempted to fit parameters to the distributions for r, n_a and d_{50} for this area because we have insufficient information to do so. Nevertheless we present this data as third party data illustrative of variability of channel initiation threshold of the same form as predicted by our theory.

Since the gamma distribution fits the data well we used it in equation (15) to derive a map of PCI over the study watersheds (Figure 2-10). aS^{α} is evaluated at each point from the DEM. PCI is then mapped at each location as the cumulative probability from the incomplete gamma function associated with the aS^{α} value and fitted gamma distribution parameters. The maps show the topographic expression of PCI. Channel head

locations towards the upper ends of high PCI zones are consistent with the theory. The

PCI values mapped in Trapper Creek correspond to the gamma distribution fitted to

observed channel heads (all IEOF) in Figure 2-5. The PCI values mapped in REL Creek

correspond to the gamma distribution fitted to the observed IEOF channel heads in figure

7a. The different gamma distributions lead to different PCI values for these watersheds,

which reflect the effects of the more intense fire in Trapper and increased PCI following

the fire.
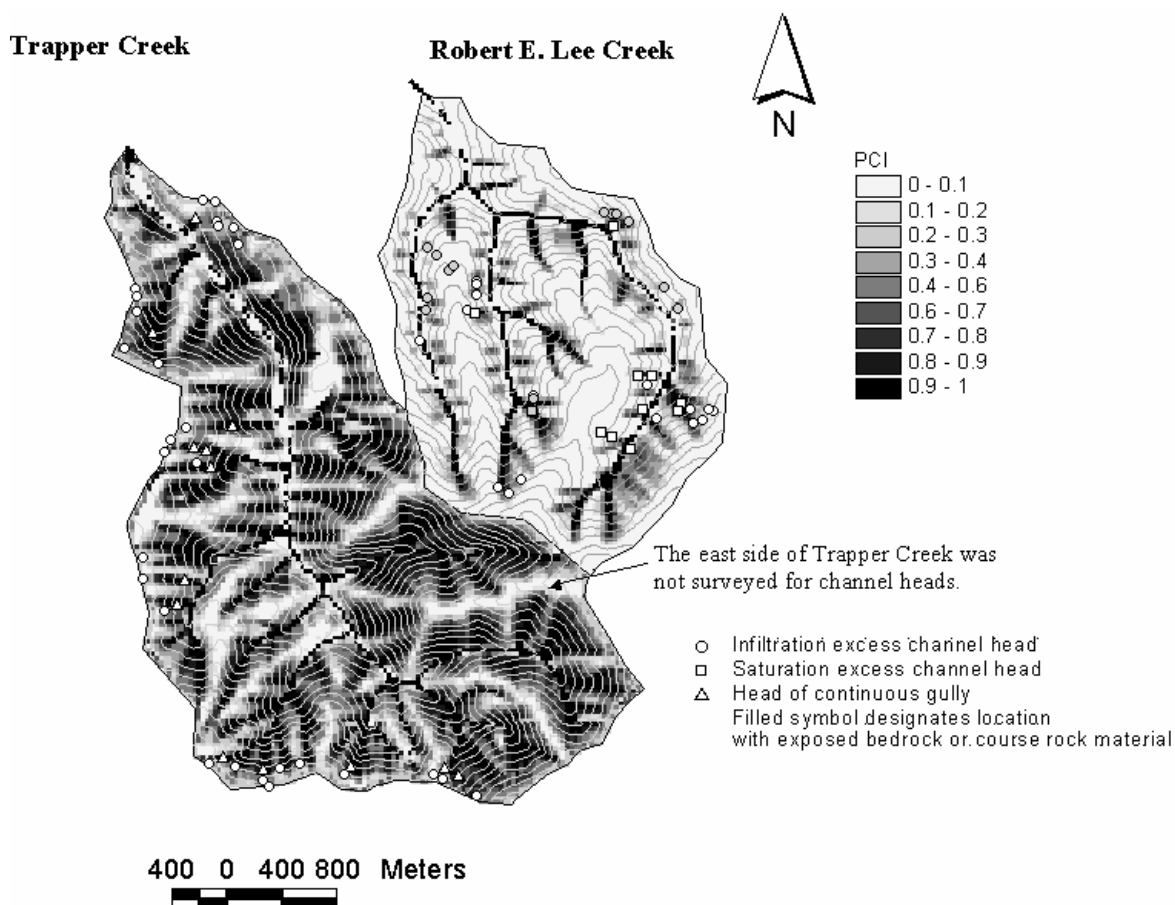
Figure 2-10. Probability of channel initiation (PCI) maps of the study areas derived using the Gamma distribution and mapped channel head locations. Contour interval is 30 m in both watersheds

4.4. Analyzing Hillslope to Channel Transition
   ### Using PCI In Slope-Area Diagrams

Slope versus contributing area diagrams are often used to unravel geomorphic

processes from DEMs and field observations [*Montgomery and Dietrich*, 1992; *Tarboton*

et al., 1992; *Ijjasz-Vasquez and Bras*, 1995]. In order to show the use of PCI for

evaluating the channelization process on slope-area diagrams, Figures 2-11 and 2-12

show the slope-area representation of the PCI theory using contours of equal PCI for our

study watersheds. The probabilistic approach generates a specific PCI as a function of

slope and specific catchment area. The probability of channel initiation increases with

the increase of either slope or specific catchment area. In Trapper Creek where the heads

of continuous channels were mapped separately we see that heads of observed continuous

channels tend to occur in zones with high PCI (the triangles on Figure 2-11 that occur

where PCI > 0.7) while channel heads not associated with continuous channels occur

where PCI is lower (circles on Figure 2-11).

In section 4 we used a T/r=600 m with equation (11b) to model saturation excess.

The line separating saturated from unsaturated areas is shown on Figure 2-12 (the dashed

saturation line) according to this relationship. This separates naturally in slope-area

space the channel heads where saturation was observed (SEOF channel heads) from those

where saturation was not observed (IEOF channel heads).

5.   Discussions and Conclusions

Erosion threshold theories for channel initiation [e.g., *Montgomery and Dietrich*,

1988, 1989; *Dietrich et al.,* 1993; *Montgomery and Foufoula-Georgiou*, 1993] have often

Figure 2-11. Specific catchment area versus local slope plot for channel heads, heads of continuous gullies, and gullies observed in Trapper Creek. Dashed lines are the PCI curves from left to right, as labeled.

attributed the observed inverse relationship between the drainage area to support a channel head and the local slope at channel heads to the analytical form of erosion threshold functions such as equation (9). A positive relationship between drainage area and local slope at channel heads can be explained (referring to equations 11 and 12) in terms of the increase in drainage area required to support runoff with increasing slope, in a saturation threshold runoff model [*Montgomery and Dietrich*, 1994]. Both of these effects are seen in Figure 2-12 where the IEOF constant PCI contours have a negative slope-area relationship and the saturation line and constant PCI contours for SEOF where slope is large have a positive slope-area relationship. We observed (Figure 2-11) a positive relationship between area and slope at channel head locations in Trapper Creek,

but an inverse relationship similar to the previous studies in IEOF channel heads in REL

Creek (Figure 2-12) and a somewhat constant slope with varying specific catchment area

in SEOF channel heads in REL Creek. *Prosser and Soufi* [1998] found no clear slope

dependency on the drainage area required to support gully heads in intensely gullied

hillslopes following land use change.

In interpreting these results we feel that the observed slope-area relationships

derived from the topography of landforms and the functional relationship between area

and slope derived from the excess-shear stress model with constant threshold are two
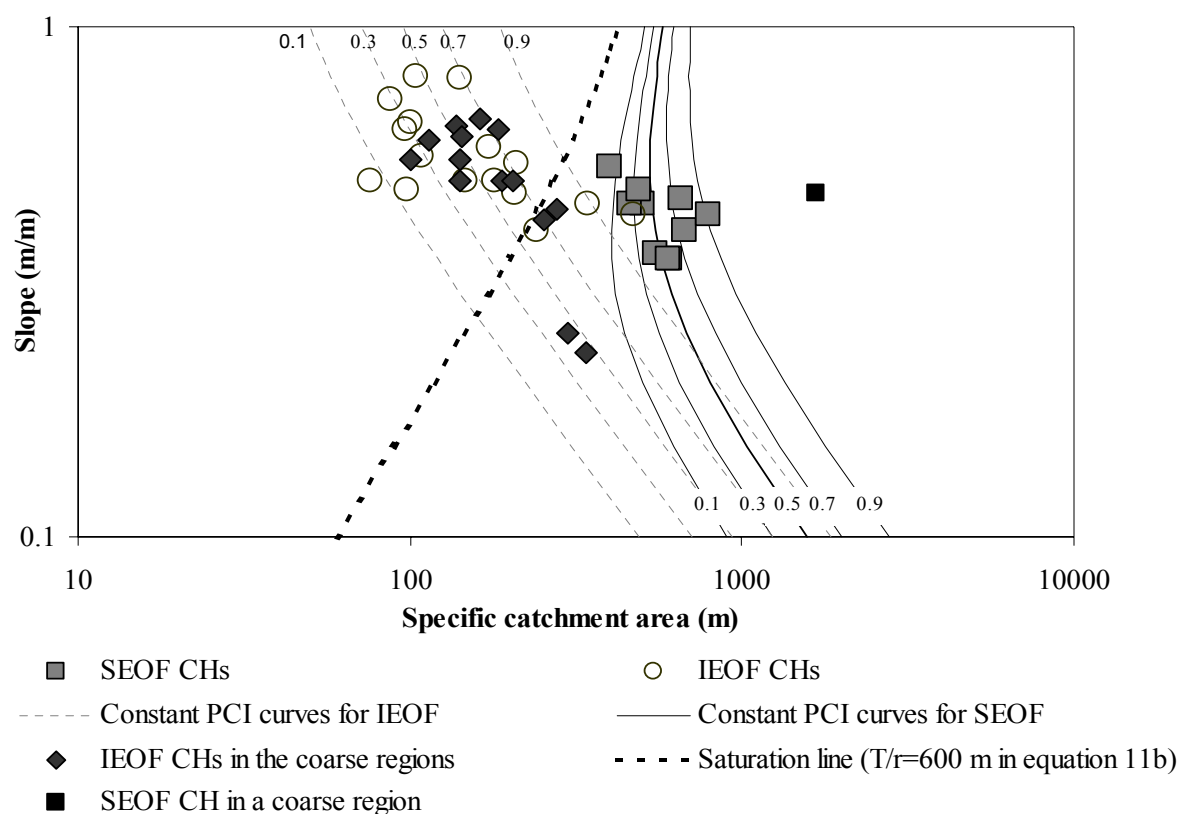
Figure 2-12. Specific catchment area versus local slope plot for channel heads in REL
Creek. Lines are the PCI curves from left to right, as labeled.

different concepts. The negative (or positive) slope-area relationships obtained from equality in equations (9) or (12) assume a fixed C at all channel heads, whereas the point of this paper has been to explore spatial and temporal variability in C, characterized using probability. Channel formation in equation (9) or (12) requires that at a point, a combination of area and slope should be greater than a certain threshold independent of the morphology of the landscape. Area-slope trends on the topography are established over the long term evolution of the landscape due to the interactions between diffusive hillslope and fluvial channel processes. Therefore depending on the C threshold at an instant in time (e.g., a thunderstorm event following a wildfire) channels may erode different hillslope positions where different processes dominate over the long term. If channelization occurs where diffusive processes dominate over the long term (convex hillslopes) then a positive relationship between area and slopes at observed channel heads is expected. The gully heads observed in Trapper Creek after significant disturbance are an example of this effect. Similarly when channel heads are observed where fluvial sediment transport is dominant (concave valleys) then the area-slope relationship would be negative. One may also observe channel heads in the field where over the long term diffusive and fluvial processes are in balance. In this case channel head data would reveal no distinct relationship between area and slope. The only case for which channel heads observed in the field may follow the functional form of the relationship between area and slope derived from the shear stress theory is the rather special case where all the model parameters of equation (10) are constant in space and time. In this case an erosional

threshold line on area-slope plots would show the transition point between hillslopes and channels (e.g., Figure 11 of *Tucker and Bras* [1998]).

Based on the observations presented in this paper we conclude that channels can incise in different topographic locations depending on the spatial and temporal variability of climate and land cover. The probabilistic channel initiation zone on the slope-area diagrams shifts back and forth along the specific catchment area axis (compare Figures 2-11 and 2-12) depending on the model input values, such as variation of runoff rates and additional roughness due to vegetation cover, that characterize climate and land cover variability.

Flow concentration due to channelization is an important mechanism in erosion and sediment transport. In this paper we have presented a probabilistic theory for modeling channel initiation and tested the theory using field data as an initial step in quantifying this process considering the inherent uncertainties in nature. In this paper we first showed that measured variability of sediment grain size is related to and accounts for a significant portion of the variability in channel initiation threshold observed in the field. We then showed that the probabilistic model developed is capable of producing a probability distribution of channel initiation threshold that matches the observed slope-area dependent channel initiation threshold (Figures 2-5 and 2-7). We recognize that probability distribution comparisons are weaker than point-wise comparisons, but have no way to quantify the specific spatial patterns of inputs necessary for more detailed point-wise tests of the model. In the probability distribution comparisons presented uniform distributions were assumed for some of the inputs. The specific form of these

may be questioned. In particular, exponential or gamma distributions are more common distributions used for rainfall. The uniform distribution was used as a convenient non-informative a-priori choice. Without specific information it is easy to understand and conceptualize equal likelihood between upper and lower bounds. Based upon our experimentation there is sufficient flexibility in the model that it is relatively insensitive to the specific form of the input distribution chosen. It is more important to quantify the variability and uncertainty using some probability distribution, rather than worry about the precise form of distribution chosen.

Estimating fluvial sediment transport from hillslopes first requires predicting the channeled portions of the terrain. A model that uses a single channel initiation threshold will predict significant erosion only in locations where channelization is predicted on a long-term basis. Our probabilistic model, provides a way to account for the less frequent contribution to erosion due to channelization even at locations that do not meet the single channelization threshold.

The effects of different land management practices on channel initiation and the erosion risk can be visualized by mapping the PCI using DEMs. In forested watersheds for example these maps may be useful for spatial planning of forest harvests and developing soil conservation techniques after wildfires. Mapping PCI can also be used in planning land use in agricultural watersheds where the effects of different crop patterns and tillage practices on PCI and the potential for gully erosion is of concern.

The hydrologic response of a basin, such as hydrograph characteristics, is strongly related to geomorphology and climate [*Rodriguez-Iturbe*, 1993]. The closer the channel

head is to the watershed divide the longer distance the flow will travel in channels rather

than on hillslopes. Expansion of ephemeral gullies to unchanneled hillslopes within a

storm event decreases flow travel times within the channel network [*Beven and Wood*,

1993]. Mapping the probability of channel initiation on the terrain (Figure 2-10) reveals

the probabilities of flow transport in both overland and channeled states and contributes

to understanding the effects of geomorphologic changes on the hydrologic response of

the watersheds.

References

Abrahams, A. D., and A. J. Parsons, Resistance to overland flow on desert pavement and its implications for sediment transport modeling, *Water Resour. Res.*, 27(8), 1827-1836, 1991.

Arcement, G. J. J., and V. R. Schneider, Guide for selecting Manning's roughness coefficients for natural channels and floodplains, *U.S. Geol. Surv. Report Number RHWA-TS-84-204*, p. 50 U.S. Geol. Surv., 1984.

ASCE, Hydrology handbook, *ASCE Manuals and Reports on Engineering Practice* No. 28, 2nd, edition, 784 p. ASCE, New York, 1996.

Barling, R. D., I. D. Moore, and R. B. Grayson, A quasi-dynamic wetness index for characterizing the spatial distribution of zones of surface saturation and soil water content, *Water Resour. Res.*, 30(4), 1029-1044, 1994.

Beven, K., and E. F. Wood, Flow routing and the hydrological response of channel networks, in *Channel network hydrology*, edited by K. Beven and M. J. Kirkby, pp. 99-128, John Wiley, New York, 1993.

Beven, K. J., and M. J. Kirkby, A physically based variable contributing area model of basin hydrology, *Hydrol. Sci. Bull.*, 24(1), 43-69. 1979.

Buffington, J. M., and D. R. Montgomery, A systematic analysis of eight decades of incipient motion studies, with special reference to gravel-bedded rivers, *Water Resour. Res.,* 33(8), 1993-2029, 1997.

Desmet, P. J. J., and G. Govers, Two-dimensional modelling of the within-field variation in rill and gully geometry and location related to topography, *Catena*, 29, 283-306, 1997.

Desmet, P. J. J., J. Poesen, G. Govers, and K. Vandale, Importance of slope gradient and contributing area for optimal prediction of the initiation and trajectory of ephemeral gullies, *Catena*, 37, 377-392. 1999.

Dietrich, W. E., and T. Dunne, The Channel Head, in *Channel Network Hydrology*, edited by K. Beven and M. J. Kirkby, pp. 175-219, John Wiley, New York, 1993.

Dietrich, W. E., C. J. Wilson, D. R. Montgomery, and J. McKean, Analysis of erosion thresholds, channel networks, and landscape morphology using a digital terrain model, *J. of Geol.*, 101, 259-278, 1993.

Dunne, T., and B. F. Aubry, Evaluation of Horton's theory of sheetwash and rill erosion on the basis of field experiments, in *Hillslope Processes*, edited by A. D. Abrahams, pp. 31-53, Allen and Unwin, Boston, 1986.

Engman, E. T., Roughness coefficients for routing surface runoff, *J. Irrig. and Drain. Engrg*, 112(1), 39-53, 1986.

Foster, G. R., L. J. Lane, M. A. Nearing, S. C. Finkner, and D. C. Flanagan, Erosion component, in *USDA - Water Erosion Prediction Project: Hillslope Profile Model Documentation*, Edited by L. J. Lane and M. A. Nearing, pp.10.1-10.12, NSERL Report No. 2, USDA-ARS National Soil Erosion Research Laboratory, West Lafayette, Indiana, 1989.

Gessler, J., Beginning and ceasing of sediment motion, in *River Mechanics*, edited by H. W. Shen, chap. 7, pp. 7.1-7.22, Colo. State Univ., Fort Collins, 1971.

Gupta, H. V., S. Sorooshian, and P. O. Yapo, Toward improved calibration of hydrologic models: Multiple and noncommensurable measures of information," *Water Resour. Res.*, 34(4), 751-763. 1998.

Horton, R. E., Erosional development of streams and their drainage basins: Hydrophysical approach to quantitative morphology, *Geol. Soc. Amer. Bull.,* 56, 275-370, 1945.

Ijjasz-Vasquez, E. J. and R. L. Bras, Scaling regimes of local slope versus contributing area in digital elevation models, *Geomorphology.*, 12(4), 299-311, 1995.

Julien, P. Y. and D. B. Simons, Sediment transport capacity of overland flow, *Trans. ASAE*, 28(3), 755-762, 1985.

Megahan, W. F., Erosion over time on severely disturbed granitic soils: A model, *USDA For. Serv. Res. Pap. INT-156*, 14 pp., Intermt. Res. Stn., For. Serv., U.S. Dep. of Agric., Ogden, Utah, 1974.

Megahan, W. F., and W. J. Kidd, Effect of logging roads on sediment production rates in the Idaho Batholith, *For Serv. Res. Pap. INT-123*, 14 pp., Intermt Res. Stn., For. Serv., U.S. Dep. of Agric., Ogden, Utah, 1972.

Megahan, Walter F., and James L. Clayton, Saturated hydraulic conductivities of granitic materials of the Idaho Batholith, *J. Hydrol.*, 84(1-2), 167-180, 1986.

Miller, M. C., I. N. McCave, and P. D. Komar, Threshold of sediment motion under unidirectional currents, *Sedimentology*, 24, 507-527, 1977.

Montgomery, D. R., Road surface drainage, channel initiation, and slope instability, *Water Resour. Res.*, 30(6), 1925-1932, 1994.

Montgomery, D. R., Erosional processes at an abrupt channel head: implications for channel entrenchment and discontinuous gully formation, in *Incised River Channels: Processes, Forms, Engineering and Management*, edited by S. E. Darby and A. Simon, pp. 247-276, John Wiley, Chichester,. 1999.

Montgomery, D. R., and W. E. Dietrich, Where do channels begin, *Nature*, 336, 232-234, 1988.

Montgomery, D. R., and W. E. Dietrich, Source areas, drainage density and channel initiation, *Water Resour. Res.*, 25(8), 1907-1918, 1989.

Montgomery, D. R., and W. E. Dietrich, Channel initiation and the problem of landscape Scale, *Science*, 255, 826-830. 1992.

Montgomery, D. R., and W. E. Dietrich, Landscape dissection and drainage area-slope thresholds, in *Process Models and Theoretical Geomorphology*, edited by M. J. Kirkby, pp. 221-246, John Wiley & Sons. 1994.

Montgomery, D. R., and E. Foufoula-Georgiou, Channel network source representation using digital elevation models, *Water Resour. Res.*, 29(12), 3925-3934, 1993.

Nearing, M. A., J. R. Simanton, L. D. Norton, S. J. Bulygin, and J. Stone, Soil erosion by surface water flow on a stony, semiarid hillslope, *Earth Surf. Process. Landforms*, 24, 677-686, 1999.

Prosser, I. P. and B. Abernety, Predicting the topographic limits to a gully network using a digital terrain model and process thresholds, *Water Resour. Res.*, 33(7), 2289-2298, 1996.

Prosser, I. P., and W. E. Dietrich, Field experiments on erosion by overland flow and their implication for a digital terrain model of channel initiation, *Water Resour. Res.*, 31(11), 2867-2876, 1995.

Prosser, I. P., and M. Soufi, Controls on gully formation following forest clearing in a humid temperature environment, *Water Resour. Res.*, 34(12), 3661-3671, 1998.

Rodriguez-Iturbe, I., The geomorphological unit hydrograph, in *Channel network hydrology*, edited by K. Beven and M. J. Kirkby, pp. 43-68 John Wiley, New York, 1993.

Rouhipour, H., C. W. Rose, B. Yu, and H. Ghadirr, Roughness coefficients and velocity estimation in well-inundated sheet and rilled overland flow without strongly eroded bed forms, *Earth Surf. Process and Landforms*, 24, 233-245, 1999.

Shields, A., Application of similarity principles and turbulence research to bed-load movement (in German), No. 26, Preuss. Vers. Anst. Wasserb. Schiffb. 1936. (English translation is available as *Hydrodyn. Lab. Publ. 67*, Hydrodyn. Lab., Calif. Inst. of Technol., Pasadena.).

Smith, T. R., and F. P. Bretherton, Stability and the conservation of mass in drainage basin evolution, *Water Resour. Res.*, 8(6), 1506-1529, 1972.

Tarboton, D. G., A new method for the determination of flow directions and contributing areas in grid digital elevation models, *Water Resour. Res.*, 33(2), 309-319, 1997.

Tarboton, D. G., R. L. Bras, and I. Rodriguez-Iturbe, A physical basis for drainage density, *Geomorphol.*, 5, 59-76, 1992.

Tiscareno-Lopez, M., V.L. Lopes, J. L. Stone, and L. J. Lane, Sensitivity analysis of the WEPP watershed model for rangeland applications II, Channel processes, *Trans. ASAE*, 37(1), 151-158, 1994.

Tucker, G. E., and R. L. Bras, Hillslope processes, drainage density and landscape morphology, *Water Resour. Res.*, 34(10), 2751-2764, 1998.

Willgoose, G. R., *A physically based channel network and catchment evolution model*, Ph.D. thesis, 464 pp., Mass. Inst. of Technol., Cambridge, 1989.

Willgoose, G., R. L. Bras, and I. Rodriguez-Iturbe, A coupled channel network growth and hillslope evolution model 1. theory, *Water Resour. Res.*, 27(7), 1671-1684, 1991.

Woolhiser, D. A., R. E. Smith and D. C. Goodrich, *KINEROS, a kinematic runoff and erosion model; documentation and user manual*, ARS-77, 130 pp., Agric. Res. Serv., U.S. Dep. of Agric., Tuscon, Ariz., 1990.

Yalin, M. S., and E. Karahan, Inception of sediment transport, *J. Hydraul. Div.*, 105, 1433-1443. 1979.

Yen, B. C., Hydraulic resistance in open channels, in *Channel Flow Resistance: Centennial of Manning's Formula*, edited by Yen, B.C., pp.1-136. Water Resour. Publ., Highlands Ranch, Colo., 1992.

CHAPTER 3

A SEDIMENT TRANSPORT MODEL FOR INCISING

GULLIES ON STEEP TOPOGRAPHY[1]

Abstract. We have conducted surveys of the gullies that developed in a small steep watershed in the Idaho Batholith after a severe wildfire followed by intense precipitation. We measured gully extent and cross sections and used these to estimate the volumes of sediment loss due to gully formation. These volume estimates are assumed to provide an estimate of sediment transport capacity at each survey cross section from the single gully forming thunderstorm. Sediment transport models commonly relate transport capacity to overland flow shear stress, which is related to runoff rate, slope and drainage area. We have estimated the runoff rate and duration associated with the gully forming event and in this paper used the sediment volume measurements to calibrate a general physically based sediment transport equation in this steep high shear stress environment. We find that a shear stress exponent of 3 which corresponds to drainage area and slope exponents of M=2.1 and N=2.25 match our data. This shear stress exponent of 3 is approximately two times higher than the exponents used for bedload transport in alluvial rivers, but is in the range of shear stress exponents observed in flume experiments on steep slopes and with total load equations. The concavity index of the gully profiles theoretically obtained from the area and slope exponents of the sediment transport equation, $\theta_c = (M-1)/N$ agrees well with the observed profile concavity of the gullies. Our results,

---

[1] Coauthored by Erkan Istanbulluoglu, David G. Tarboton, Robert T. Pack, Charles Luce.

although somewhat preliminary due to the uncertainty associated with the sediment volume estimates, suggest that for steep hillslopes such as those in our study area, a greater nonlinearity in the sediment transport function exists than that assumed in some existing hillslope erosion models which calculate sediment transport capacity using the bedload equations developed for rivers.

1. Introduction

Gullies are unstable, eroding channels formed at or close to valley heads, sides or floors [*Schumm and Harvey*, 1984]. They usually differ from stable river channels with their steep sides, low width to depth ratios and with a head cut at the upslope end [*Knighton*, 1998]. The main causes of gully erosion are natural and anthropogenic effects that increase runoff production on hillslopes and/or reduce the erosion resistance of the soil surface. Some of these causes are the clearing of natural forests [*Prosser and Slade*, 1994; *Prosser and Soufi*, 1998], forest fires [*Megahan*, 1992; *Prosser and Williams*, 1998; *Meyer et al.*, 2001], agricultural treatments and grazing [*Burkard and Kostaschuk*, 1995; *Vandekerckhove et al.*, 1998, 2000], climate change [*Coulthard et al.*, 2000] and road construction [*Montgomery*, 1994; *Wemple et al.*, 1996; *Croke and Mockler*, 2001].

There are two main stages of gully development, the incision stage and the stability or infilling stage [*Sidorchuk*, 1999]. Gully erosion usually starts at locations where the vegetation mat is broken. Under poorly vegetated conditions the critical shear stress required to scour the surface sediment decreases and overland flow can more easily cause incisions. Runoff concentration in depressions forms headcuts that may then retreat upslope due to the combination of many processes such as seepage erosion and plunge-

pool action [*Dietrich and Dunne*, 1993; *Knighton*, 1998]. The initiation stage of gully

erosion is often the most critical stage from a land management perspective, because once

the gullies have initiated and developed it is difficult to control gully erosion [*Prosser*

and Soufi, 1998; *Woodward*, 1999].

During the last four decades erosion prediction technology provided models for

soil conservation planning in small agricultural catchments [*Osterkamp and Toy*, 1997].

Most empirical models, such as the USLE approach [*Wishmeier and Smith*, 1965] and the

recent physically based distributed soil erosion prediction models such as LISEM [*Roo et*

al., 1995] and EROSION 3D [*Schmidt et al.*, 1999] have been developed for modeling

rainsplash and dispersed overland flow erosion. They often produce poor results in

relatively larger catchments where channels exist [*Takken et al.*, 1999]. The CREAMS

[*Knisel*, 1980] and EGEM [*Woodward*, 1999] models simulate field-scale gully erosion

potential. These models were developed and tested using data from relatively flat

croplands.

Recent field observations of erosion events in steep mountain drainages in the

western United States also show that large pulses of sediment could be produced due to

gully erosion [*Meyer and Wells,* 1997; *Cannon et al.,* 2001; *Meyer et al.,* 2001]. In this

paper we study the mechanistic behavior of sediment transport on steep mountains using

gully erosion observations in Idaho. We first theoretically adapt a general dimensionless

sediment transport capacity equation to incising gullies by relating the flow shear stress

and flow width to contributing area and slope assuming steady-state runoff generation

and turbulent uniform flow conditions. The dimensionless sediment transport capacity

relationship we used has two empirical parameters that need to be calibrated against data. We then present our field data comprising sediment volumes estimated from gully cross-sections in a highly erodible steep forested basin in Idaho. These gullies were developed in a single rainstorm after a severe wildfire. Following this we calibrate the empirical parameters of the sediment transport equation to this field data and compare the results with the parameter ranges published in the literature. We then used the calibrated sediment transport capacity equation with the probabilistic approach for channel initiation (PCI) *Istanbulluoglu et al*. [Chapter 2] to model the expected sediment transport capacity over the terrain and sediment delivery to streams.

We begin with a brief review of the current sediment transport functions and their geomorphic implications in order to provide motivation to the paper.

1.1. Sediment Transport Review: Functional Form and Implications

Sediment transport rate is often described as a power function of discharge and slope or shear stress [*Kirkby*, 1971; *Julien and Simons*, 1985; *Nearing et al.*, 1997]:

$$Q_s = k_1 Q^M S^N \tag{1}$$

$$Q_s = k_2 (\tau - \tau_c)^p \tag{2}$$

where Q_s is the rate of sediment transport in a channel, Q is water discharge, S is slope, τ is the average bottom shear stress, $\tau = \rho_w gRS$ where R is the hydraulic radius ρ_w is water density and g gravitational acceleration. τ_c is critical shear stress for incipient motion, k_1

is a rate constant and k_2 a transport coefficient. M, N and p are model parameters. These functional forms are interchangeable when shear stress is written as a function of discharge and slope, $\tau \propto (Q, S)$ [*Willgoose et al.*, 1991a; *Tucker and Bras*, 1998].

Many equations that describe sediment transport as a function of shear stress such as those of Meyer-Peter and Muller and Einstein-Brown and empirical total load sediment transport equations, for example, the Engelund and Hansen equation and the Bishop, Simons and Richardson's methods can be written in the form of equation (2). This equation is essentially based on the relationship between dimensionless sediment transport rate, q_{s*} and dimensionless shear stress τ_* [*Garde and Raju*, 1985]. Dimensionless sediment transport rate is commonly expressed as a nonlinear function of dimensionless shear stress in the form,

$$q_{s*} = \beta \tau_*^p \tag{3}$$

where

$$q_{s*} = \frac{q_s}{\sqrt{g(s-1)d^3}} \tag{4a}$$

$$\tau_* = \frac{\tau/(\rho_w g)}{(s-1)d} \tag{4b}$$

$$\beta = \begin{cases} \kappa(1 - \dfrac{\tau_{*c}}{\tau_*})^{p_\beta} & \tau_* > \tau_{c*} \\ 0 & otherwise \end{cases} \tag{4c}$$

In these equations, q_s is the unit sediment discharge that could be either bed or total load, β is a dimensionless transport rate, s is the ratio of sediment to water density (ρ_s/ρ_w), d is dominant grain size often taken as the median, d_{50}, the calibration parameters are κ, p and p_β and usually $p=p_\beta$. *Yalin* [1977] showed that κ is 17 at high values of τ_* for bedload transport. Many κ values were reported in the range of 4-40 in different equations [*Simons and Senturk, 1977*; *Yalin*, 1977]. The shear stress exponent p is consistently 1.5 for bedload equations developed for gentle slopes while in total load equations it varies from relatively low values of $p \cong 1.5$ up to $p=3$ depending on the mode of transport. Lower shear stress exponents correspond to predominantly bedload transport and the higher values to suspended sediment transport in the total load. Equation (3) does not fully describe the suspended load transport physics and the idea of using higher shear stress exponents for total load is to account for the additional sediment discharge due to suspended sediment in the same functional form used for bedloads [*Garde and Raju*, 1985]. Nevertheless total load equations in the form of equation (3) are easy to use and provide reasonable sediment transport capacity estimates [*Simons and Senturk*, 1977].

Equation (1) has often been used by geomorphologists and landscape evolution modelers to develop theories to explain the influence of transport limited erosion on channel network and landform evolution [*Smith and Bretherton*, 1972; *Tarboton et al.*,

1992; *Hancock and Willgoose*, 2001]. It has mathematical and computational advantages in integrating the effects of a range of discharge events to address the long-term sediment transport processes [*Willgoose et al.*, 1991a; *Tucker and Bras*, 2000]. The discharge and slope exponents M and N in (1) are often in the range of 1 to 2.5 [*Julien and Simons*, 1985; *Everaert*, 1991; *Rickenmann*, 1992; *Nearing et al.*, 1997]. The exponents M and N have significant impacts on hillslope evolution, drainage density and landscape morphology [*Band*, 1990; *Arrowsmith et al.*, 1996; *Tucker and Bras*, 1998]. They also influence landscape response timescales and the sensitivity of mountain range relief to tectonic uplift [*Whipple and Tucker*, 1999; *Niemann et al.*, 2001]. Nonlinearity in the gradient term governs the relief-uplift relationship and has a significant influence on the duration and timing of erosional response [*Tucker and Whipple, 2002*]. One of the long-term implications of a sediment transport relationship is the observed power law scaling of slope with contributing area, $S \propto A^{-\theta_c}$, where θ_c is the concavity index often in the range of 0.37 to 0.83 with a mean of 0.6 [*Tarboton et al.*, 1991]. This empirical observation was theoretically explained for the case of dynamic equilibrium when the denudation rate and erosion are everywhere in balance in a basin [*Willgoose et al.*, 1991b; *Tarboton et al.*, 1992]. The power law relationship between local slope and upslope area is

$$S = (\frac{U}{k_1})^{1/n} A^{-\theta_c}, \qquad \theta_c = \frac{M-1}{N} \qquad\qquad (5)$$

where, U is tectonic uplift or an average degradation rate and A is drainage area used as a proxy for discharge in the sediment transport equation (1). Some observations suggest that there may not be a great difference between the concavity of steady-state and non-steady-state mountain basins. The Appalachians are believed to be in a state of decline and yet Appalachian river basins reveal concavity indices consistent with the range often observed in steady-state topographies [*Willgoose*, 1994; *Tucker and Whipple,* 2002]. Discharge and slope exponents are the fundamental parameters of erosion and sediment transport and related to the scale properties of landscape and river evolution used in landscape evolution research. Thus, they are deserving of study via both field work and modeling [*Rodriguez-Iturbe and Rinaldo*, 1997; *Tucker and Whipple,* 2002]

1.2. Sediment Transport on Steep Slopes

With the recognition of the importance of erosion processes in mountain regions steep flume experiments have been conducted [*Mizuyama*, 1977; *Rickenmann*, 1992]. These experiments suggested that bed load sediment transport can be described using (1) both for gentle and steep slopes when information about grain size and density is included in the equation [*Rickenmann*, 1991]. A bed-load transport equation was developed by *Smart and Jaeggi* [1983] based on their steep flume experiments (slope range 3% to 20%) and the data of Meyer-Peter and Muller. Clear water was used as the transporting fluid in the experiments. The Smart and Jaeggi [1983] equation is

$$q_s = \frac{4}{(s-1)}(\frac{d_{90}}{d_{30}})^{0.6}(1-\frac{\tau_{*c}}{\tau_*})q_r S^{1.6} \qquad (6)$$

where, q_r is the reduced unit discharge (corrected for side wall influence), d_{90} and d_{30} are

the grain sizes at which respectively 90% and 30% by weight of the sediment is finer.

Sediment transport equations for steep slopes are often considered to be bedload

equations. On steep slopes bedload and suspended load are usually inseparable. *Smart*

[1984] suggested that for alluvial coarse sediments (mean grain size greater than 0.4 mm)

observed sediment transport can be regarded as total load or the sediment transport

capacity.

Rickenmann [1991, 1992] conducted steep flume experiments where a clay

suspension was used as transporting fluid. He analyzed his steep flume data set together

with Smart and Jaeggi's data. He developed the following equation for both clear water

and hyperconcentrated flows for slopes between 5% and 20%,

$$q_s = \frac{12.6}{(s-1)^{1.6}} (\frac{d_{90}}{d_{30}})^{0.2} (q_r - q_{cr}) S^2 \tag{7}$$

$$q_{cr} = 0.065(s-1)^{1.67} g^{0.5} d_{50}^{1.5} S^{-1.12} \tag{8}$$

where, q_{cr} is the critical discharge for the initiation of sediment motion. Equation (7) was

originally proposed by [*Bathurst et al.*, 1987] and was slightly modified by Rickenmann

to include the density factor (s-1). Ricknmann noted that as slopes increase, the

exponents for (s-1) and S should increase as well. This observation was also supported by

steep flume data of *Mizuyama and Shimohigashi* [1985] who predicted $q_s \propto S^2 /(s-1)^2$

[*Rickenmann*, 1991]. The influence of steep slopes on the exponents of the density

parameter and slope is not apparent in the Smart and Jaeggi equation. They used only

clear water data and the number of tests with S≤ 5% was significantly larger because of the Meyer-Peter and Muller data included in the analysis.

The use of equations (6) and (7), which are elaborated forms of (1) look promising for erosion modeling on steep slopes at a first glance. In addition to discharge and slope they include bed material size and fluid density as parameters. An inconsistency in these equations compared to other sediment transport studies on the same slope ranges is the discharge exponent. *Nearing et al*. [1997] recently combined experimental data for slopes between 0.5% and 30% and reported results in the form of (1) that show consistently a discharge exponent greater than 1.5. Equation (6) is linear with discharge while equation (7) is linear for discharge in excess of a threshold. We don't know if median sediment size and density ratio factors considered in (4) and (6) account for the nonlinearity of sediment transport with respect to discharge that *Nearing et al*. [1997] found. A linear dependence of sediment transport on discharge has implications for erosion and landscape evolution dynamics. In the landscape form stability theory of *Smith and Bretherton* [1972] channels and concave hillslope profiles form when M>1. In equation (5) M=1 gives θ_c=0 that implies a constant slope or a planar topography. Such conclusions can also be obtained from landscape evolution simulation experiments [*Willgoose*, 1989; *Tucker and Bras,* 1998]. Erosion will be less sensitive to hydrology when M=1 instead of M>1.5, thus erosion and landscape response to the impacts of changes in any environmental factors that influence hydrology (e.g., climate change, deforestation) and tectonics will be less severe.

Most sediment transport equations were developed for very ideal conditions, such as plane beds with no form influence and unlimited supply of bed material and are limited to the slope range for which they were developed. When these equations are applied to natural terrain to model the various fluvial processes acting on hillslopes for example to incise gullies, some other geomorphic considerations should be taken into account such as concentration of overland flow in gullies, widening and deepening of the incisions downstream, variations in the flow shape, the influence of form roughness etc. Variations of slopes in natural terrain especially in mountainous areas also imposes limitations because the sediment transport equations were developed for specific slope ranges.

An appropriate sediment transport relationship for steep mountainous settings should characterize the erosion dynamics and accurately predict the spatial and temporal erosion rates. It should also characterize the long-term implications of erosion on landscape evolution such as the concavity of the channel network, its 3D texture and terrain properties compared to the observed mountain topography [*Hancock et al.*, 2001]. Thus, for the sediment transport equations developed from flume experiments to be applicable in geomorphologic modeling they need to be calibrated and revised using field observations on scales relevant to the processes of interest. Long-term implications of selected sediment transport and erosion functions on large-scale landscape evolution need to be tested.

2. Methods

2.1. Sediment Transport Capacity of Eroding Gullies

The dimensionless sediment transport capacity equation (3) is adapted for gully erosion describing basin hydrology and flow hydraulic characteristics as a function of contributing area and slope. Steady-state discharge Q, is assumed to be proportional to contributing area A,

$$Q = rA \tag{9}$$

where, r is runoff rate which can be evaluated for infiltration and saturation excess runoff generation mechanisms. For the case of saturation excess runoff generation we expect that the runoff rate would be spatially variable due to the variations of the saturated subsurface transport rates across the landscape. In this case r would be a function of contributing area and slope [*Tucker and Bras*, 1998].

We assume that for incising gullies the hydraulic radius, R, is a function of flow cross sectional area A_f [*Foster et al.*, 1984; *Moore and Burch*, 1986],

$$R = CA_f^{0.5} \tag{10}$$

where, C is a shape constant (see Appendix A1). A_f is discharge divided by flow velocity and is estimated as a function of discharge by assuming steady turbulent uniform flow and using Manning's equation for flow velocity. Mannings roughness, n, is approximated as a function of discharge, Q [*Leopold et al.*, 1964; *Knighton*, 1998],

$$n = k_n Q^{-m_n} \qquad (11)$$

where k_n and m_n are empirical parameters. In Manings equation this then gives

$$A_f = k_n^{0.75} C^{-0.5} Q^{0.75(1-m_n)} S^{-0.375} . \qquad (12)$$

Substituting (12) into (10) gives hydraulic radius as a function of Q and S. Manning's n is assumed to be comprised of grain and additional (form) roughness components, and this leads to a partitioning of hydraulic radius into grain and additional roughness components. The grain hydraulic radius is then used to calculate the effective shear stress acting on sediment grains (Appendix A2 for details).

$$\tau_f = \rho_w g k_n^{-1.13} C^{0.75} n_{gc}^{1.5} Q^{0.375+1.13m_n} S^{0.8125} \qquad (13)$$

This is then used in equation (4b) then (3) to model sediment transport.

We also derived a relationship for flow width in terms of Q and S, by analytically describing the flow cross sectional area in the gullies as a function of flow width and depth (dependent on width through a constant width to depth ratio) and side slope ratio and then equating this analytical form to (12) and solving for flow width (Appendix A3),

$$W_f = k_s k_n^{0.375} C^{-0.25} Q^{0.375(1-m_n)} S^{-0.1875} \qquad (14)$$

where k_s is a dimensionless constant based on flow geometry. The derived relationships for flow cross-sectional area, hydraulic radius, shear stress and flow width are proportional to discharge and slope in a generic form (Table 3-1),

$$\Psi = \chi_\Psi (rA)^{m_\Psi} S^{n_\Psi} \tag{15}$$

where, ψ represents the hydraulic variable of interest and χ_ψ is a constant relating the hydraulic variable to discharge and slope, m_ψ and n_ψ are theoretically derived exponents (Table 3-1).

The general sediment transport capacity equation is derived by substituting the shear stress relationship (13) into (4b) and (4b) into (4c), and substituting (4a), (4b), and (4c) into (3) and solving for q_s and finally multiplying q_s with the flow width in (14):

$$Q_s = [\kappa \chi_c^{-1} \chi_W \chi_\tau^p d^{1.5-p} (1 - \tau_c \chi_\tau^{-1} (rA)^{-m_\tau} S^{-n_\tau})^p](rA)^M S^N \tag{16}$$

where $\chi_c = \rho^p (g(s-1))^{p-0.5}$, $M = pm_\tau + m_W$ and $N = pn_\tau + n_W$. The term in square brackets provides the theoretical basis of k_1 in (1), and is independent of discharge when $\tau_c = 0$. This could be a practical assumption for the incision stage of gullies as long as a channel initiation threshold controls gully initiation. The two calibration parameters that appear in the equation are κ and p.

Table 3-1. Physical Parameters of the Generic Hydraulic Variable Equation, $\Psi = \chi_\Psi Q^{m_\Psi} S^{n_\Psi}$

ψ	χ_ψ	m_ψ	n_ψ
Flow cross-sectional area, A_f	$k_n^{0.375} C^{-0.5}$	$0.75(1-m_n)$	0.375
Hydraulic radius, R	$k_n^{0.375} C^{0.75}$	$0.375(1-m_n)$	0.1875
Flow width, W_f	$k_s k_n^{0.375} C^{-0.25}$	$0.375(1-m_n)$	0.1875
Effective shear stress, τ_f	$\rho_w g C^{0.75} k_n^{-1.13} n_{gc}^{1.5}$	$0.375+1.13m_n$	0.8125

2.2. Calibration Methodology

Sediment transport equations in the form of (3) are often calibrated using data from flume experiments and rivers [*Yalin,* 1977]. In such experiments parameters κ and p are obtained from q_{s*} and τ_* pairs that are measured throughout the experiments. Here we developed a procedure to obtain the calibration parameters κ and p for gully sediment transport based on q_{s*} and τ_* pairs estimated from geomorphic field observations in gullies. We measured gully erosion volumes in a mountainous watershed (described later) that was recently gullied due to a thunderstorm whose magnitude and duration are approximately known. We assumed that once a gully was incised the sediment transport rate was at its transport capacity. This transport-limited erosion assumption is consistent with the flume experiments of rills and gullies for cohesionless sediments in the case of unlimited sediment supply [*Cochrane and Flanagan,* 1997; *Bennett et al.,* 2000]. Based on this assumption the average unit sediment discharge of a particular flow cross-section in the gully can be approximated by the total volume of sediment passing that point V_s (volume of total estimated erosion that originated from the upslope contributing area) divided by the total erosion duration T, and flow width W_f,

$$q_s = \frac{V_s}{TW_f} . \tag{17}$$

Writing W_f as a function of area and slope (14) and substituting (17) into (4a) we obtain the dimensionless sediment transport rate of a particular flow cross-section as a function

of sediment volume passing that cross section (field observation), upslope contributing

area and the local slope as

$$q_{s*}(V_s, A, S) = \frac{V_s}{T\chi_W (rA)^{m_W} S^{n_W} \sqrt{g(s-1)d^3}} .$$

(18)

Similarly substituting the shear stress as a function of area and slope (13) into (4b) we

have the dimensionless shear stress described in terms of area and slope

$$\tau_*(A, S) = \frac{\chi_\tau (rA)^{m_\tau} S^{n_\tau}}{\rho_w g(s-1)d} .$$

(19)

Now plotting the observed q_{s*} versus $\tau_*(1 - \tau_{*_c}/\tau_*)$ described in the equations (3), (4a),

(4b) and (4c) (we use $\tau_*' = \tau_*(1 - \tau_{*_c}/\tau_*)$ in the remainder of the paper) we obtain the

empirical parameters κ and p in equation (3) by fitting a power function to the data. The

calibration procedure described here requires field identifications of three major spatially

distributed data which are V_s, A and S at different points along the gullies and estimates

for the other sediment transport model parameters in (16) and the erosion duration and

runoff rate for the gully incising runoff event. In the following section we describe our

field area and methods used to estimate these quantities.

3. **Field Study**

The sediment transport capacity equation described above has been calibrated

using field data from the Idaho Batholith. This area consists of an extensive mass of

granitic rock approximately 16,000 mi^2 in size that covers a large portion of Idaho and

some parts of Montana. It is almost entirely mountainous and forested. Valleys are typically narrow and V shaped. Erodible coarse textured soils are found on steep gradients that often exceed 70% [*Megahan*, 1974]. Colluvium that accumulates in hollows and steep headwater channels is episodically evacuated by gullying and debris flows [*Kirchner et al.*, 2001]. Average annual precipitation is approximately 1000 mm. Localized high intensity rainstorms (25 – 50 mm/h) of short duration (<0.5 h) are common during summer. At other times of the year more widespread storms occur, often in conjunction with snowmelt. Following soil disturbance and wildfires the combination of steep topography, high-soil erodibility, and high-climate stress often results in accelerated surface erosion and landslides [*Megahan and Kidd*, 1972].

The specific study area selected is Trapper Creek within the North Fork of the Boise River in southwestern Idaho (see Figure 3-1). Trapper Creek was intensely burned by a wildfire in 1994 and extreme gullying occurred during a convective summer storm in 1995, possibly due to water repellent conditions of the surface soil. On the average the gullies were 1-2 m deep and 3-4 m wide. Relatively narrow cross-sections were observed at sites where all the colluvium was scoured to bedrock. Widening of the gully cross-sections was due to sidewall collapse at most of the sites. Cobbles and boulders up to 0.3 m in diameter which were presumably introduced by side wall collapse were deposited at the foot of the collapse or several meters downstream. Other than these coarse material deposits no significant deposition was observed in the gullies.

In the field we recorded the locations of channel heads, gully heads and heads of the continuous gullies. Here we are using the terminology channel head to refer to the

most upstream limit of erosion within definable banks, while gully heads refer to the

sequential headcuts observed downstream in the field from the channel head where

gullies were discontinuous. The continuous gully head refers to the headcut below which

the gully is continuous. In order to estimate the volume of eroded material from the

gullies we measured the gully cross sections at intervals on the average of 20 to 30 m. All

significant sediment scours observable in the discontinuous gully reaches were also

measured. Slope measurements were taken at each measurement location over a length of

10 to 20 m. This measurement protocol was applied for distances ranging between 150 m

and 500 m downslope from gully heads in 4 different gullies including one discontinuous

gully. The erosion data obtained from the discontinuous gully segment is used to discuss

the implications of a gully discontinuity on sediment transport capacity. The field data

collected is reported in Table 3-2.

4.   Field Estimates for the Model Parameters

Gully erosion volumes between two successive gully cross-sections are calculated

by multiplying the distance between the two cross-sections by the average cross-sectional

area. Total sediment passing a particular cross-section, V_s is then estimated by

accumulating all the upslope erosion measurements along the gully profile down to that

particular point. Contributing areas are derived from the 30m DEM of the study site using

the D infinity algorithm [*Tarboton*, 1997]. There was a forest road located uphill of the
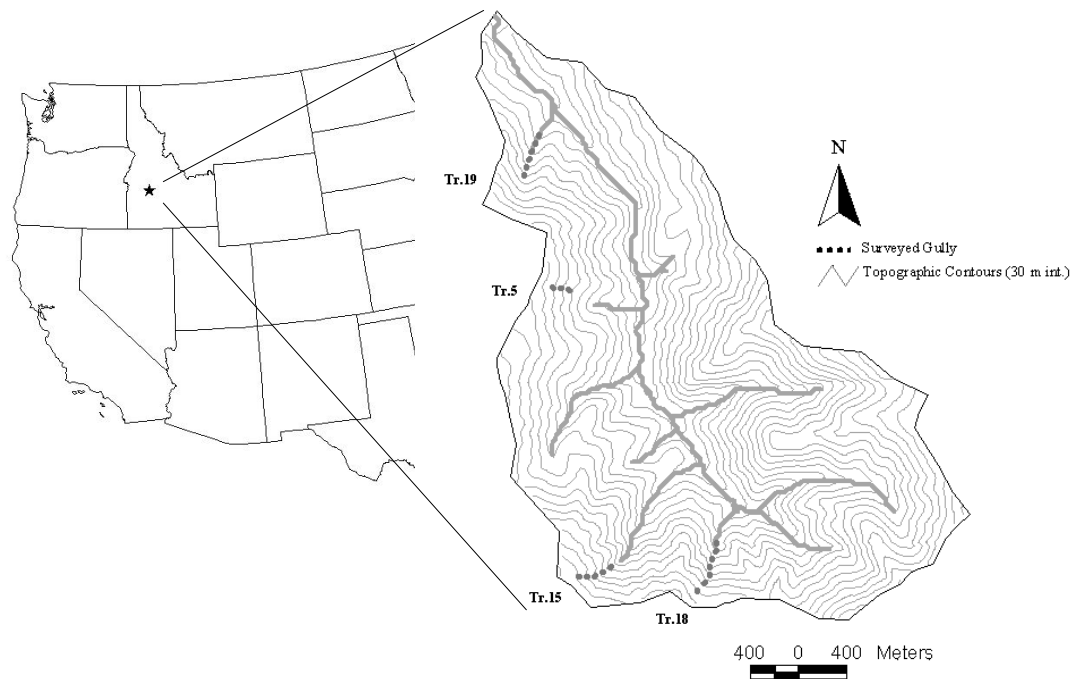
Figure 3-1. Location map of the study area and the four gullies studied in the field. In the figure Tr. is an abreviation used for Trapper Creek and the following number is the gully numbered in the field.

gullies that may have an influence on the drainage pattern of the hollows. We used the mapped road flow directions and road structures to detect any road induced abnormalities. Except for one of the gullies we did not see any significant road induced drainage pattern changes. For that particular gully (Tr.15 in Figure 3-1) 25000 m^2 of additional contributing area was added due to the road drainage from the surrounding hillslopes.

The plotting position of q_{s*} versus τ_*' described above requires the estimates of median sediment size of the eroding material d, runoff rate r, erosion duration T, Manning's roughness for grains n_{gc}, parameters k_n and m_n for the total channel roughness

Table 3-2. Gully Erosion Data Collected in the Trapper Creek Study Site

Gully No	Distance from GH[1] (m)	Local slope (m/m)	Cross-sectional area (m^2)	Gully No	Distance from GH[1] (m)	Local slope (m/m)	Cross-sectional area (m^2)
Tr.05	0	0.36	0.210	Cont. Tr18	180	0.4	2.250
	6	0.36	0.600		200	0.4	6.000
	24	0.35	1.492		240	0.44	3.000
	33	0.55	3.840		260	0.43	9.000
	40	0.55	7.000		280	0.35	8.400
	50	0.55	2.560		300	0.29	20.000
	57	0.55	1.750		310	0.29	18.000
	87	0.28	1.000		340	0.3	20.000
	114	0.55	3.600		360	0.37	18.000
	121	0.55	2.000		380	0.3	42.000
	133	0.53	0.300		400	0.28	32.500
	148	0.5	2.610		420	0.2	70.000
	155	0.35	5.880		440	0.13	45.000
	166	0.33	5.200		460	0.24	63.000
Tr15	30	0.34	16.000		480	0.24	24.000
	60	0.39	10.500	Tr.19	0	0.45	3.000
	70	0.45	7.200		10	0.48	0.300
	100	0.55	8.000		30	0.46	1.400
	140	0.50	3.500		50	0.45	1.950
	160	0.49	3.150		70	0.4	3.000
	180	0.41	9.750		80	0.4	2.500
	200	0.40	20.000		100	0.35	0.250
	220	0.49	24.000		110	0.35	0.960
	260	0.32	45.000		130	0.45	2.000
	280	0.4	60.000		150	0.32	2.100
Tr.18	0	0.44	0.021		170	0.31	0.400
	20	0.51	0.015		190	0.18	2.250
	30	0.47	0.000		240	0.19	2.500
	40	0.61	0.090		280	0.2	5.200
	60	0.60	0.100		290	0.18	1.150
	80	0.64	0.850		320	0.17	0.200
	100	0.65	0.291		340	0.16	0.750
	130	0.50	0.400		380	0.2	1.820
	140	0.50	0.560		400	0.18	1.000
	160	0.6	1.440		440	0.23	4.950

[1]GH: Gully head

estimates from discharge, and channel shape and cross-sectional constants. All of these parameters could vary in space and time as gullies erode, however we made estimates for each of the parameters based on field observations to characterize the average conditions as described below.

We do not have specific information about the eroded sediment size in the gullies. We were unable identify the deposits of individual gullies in the main creek, because the deposition process we observed was mostly size selective. Some coarse material coming out of the gullies was deposited in main channel in several locations and fine sediment presumably kept moving downslope. We measured an average median sediment size of 2 mm for the surface sediment in Trapper Creek on hillslopes surrounding the gully heads. Sediment sizes visually observed on the gully walls were coarser than a median sediment size of 2 mm due to the increased fraction of gravel sizes. In the overall Idaho batholith soils are mostly poorly graded sands with very little silts and clays [*Megahan*, 1992]. *Gray and Megahan* [1981] reported size distributions of sediment samples taken from various soil depths in an experimental watershed in the area with median sediment size in the range of coarse sand and fine gravel. Several unpublished sediment sieve analysis also show similar results. Here we used a median sediment size of 3 mm for gully sediment transport and took τ_{*c}=0.045 which is a commonly accepted value [*Suszka*, 1991]. The selected τ_{*c} = 0.045 is consistent with the τ_{*c} values reported by *Buffington and Montgomery* [1997] for coarse sand and fine gravel observed in our field areas, yet under high shear stresses τ_{*c} does not have very much influence on sediment transport.

We do not know the exact rainfall rate of the storm that incised the channels in Trapper Creek. However some forest service personnel were exposed to that storm and they approximated that more than an inch of rain fell in less than half an hour. It is conceivable that this kind of a convective storm event could result in local intensities of between 50 mm/h and 100 mm/h. We selected a steady-state runoff rate of 35 mm/h

generated by the thunderstorm from presumably water–repellent soils. This is the average rate of the uniform probability distribution for runoff rate used by *Istanbulluoglu et al*. [(Chapter 2)] for the same event in Trapper Creek. In the area convective summer storms often last less than or approximately half an hour. Since we do not know the exact duration of both the rainfall and erosion we assumed that all the gully incisions occurred in half an hour and took T=0.5h.

Grain roughness (n_{gc}) for fine gravel is selected as 0.025 [*Chow*, 1959; *Arcement and Schneider*, 1984]. The at-a-station Manning's roughness relationship (equation 11) gives total roughness n as a function of parameters k_n, m_n and discharge which in our case is obtained from runoff rate and contributing area [*Leopold et al.*, 1964; *Knighton*, 1998]. In Tr.19 we observed small boulders up to 300 mm in diameter, exposed rocks on the sides of the channel, and logs at several locations along the gully channel. Based on these observations we rated the degree of irregularity of the channel and the effects of obstructions as "severe" for the gully-incising event. Additional Manning's roughness values, n_{ac} for such conditions can be in the range of 0.05 to 0.1 [*Chow*, 1959; *Arcement and Schneider*, 1984] which with n_{gc}=0.025 implies total roughness, n=n_{gc}+n_{ac}, in the range 0.075 to 0.125. In the surveyed sections of Tr.19 the discharge is calculated in the range 0.15 to 1.9 m^3/s. We therefore estimated k_n=0.08 in equation (11) to match this total roughness range. The roughness conditions in the rest of the gullies (Tr.5, Tr.15, Tr.18) were not as severe as Tr.19. The channels were relatively clear of obstructions. For these three gullies we took k_n=0.045. This results in additional roughness values in the range of 0.015 to 0.055 for the calculated discharge range of 0.05 to 2.2 m^3/s. This range

corresponds to moderate to severe effect of obstructions for the gully incising event [*Chow*, 1959; *Arcement and Schneider*, 1984]. A parabolic flow cross-section with a width to depth ratio of 2 was used to obtain the shape parameters C and k_s that are used in the flow hydraulic calculations.

The presence of sediment at high concentrations in the flow may change the fluid properties, decrease the flow velocity and increase its depth [*Aziz and Scott*, 1989]. As the sediment concentration increases in the flow, flow hydraulics becomes much more complicated compared to clear water flow due to the interactions among solid particles [*Hashimoto*, 1997; *Jan and Shen*, 1997]. There is however theoretical and experimental evidence that even debris flows can be regarded as a special type of flow that can be described by similar hydraulic formulations such as Manning and Chezy equations for flow velocity [*Jeppson and Rodriguez*, 1983; *Jan and Shen*, 1997; *Julien*, 1997]. In this paper flow velocities and shear stresses are calculated assuming hydraulic properties of clear water flow.

5. Results and Discussions

5.1. Calibration Results

The relationship between q_{s*} and $\tau_*^{'}$ obtained using the field data is presented in Figure 3-2. The area and slope exponents for shear stress (m_τ=0.6, n_τ=0.8125) and the flow width (m_w=0.3, n_w=-0.1825) are calculated using the expressions in Table 3-1 with a selected m_n=0.2 [*Knighton*, 1998]. The figure also plots the fitted power function relationship in the form of (3) with κ=20 and p=3. The Meyer-Peter Muller and Govers

sediment transport relationships were also plotted on Figure 3-2 for comparison with the

fitted relationship. Details of these equations are given below All the data points except

for the first 13 points of Tr. 18 show good correspondence with the theoretical

derivations.

The major sources of sediment discharge in gullies are sediment detachment from

the bed, widening by undercutting and side slope failures [*Selby*, 1993]. In Figure 3-2

thirteen data points (circled by dashed line) from gully Tr.18 fall significantly below the

trend of the fitted dimensionless sediment transport capacity curve. The first four data
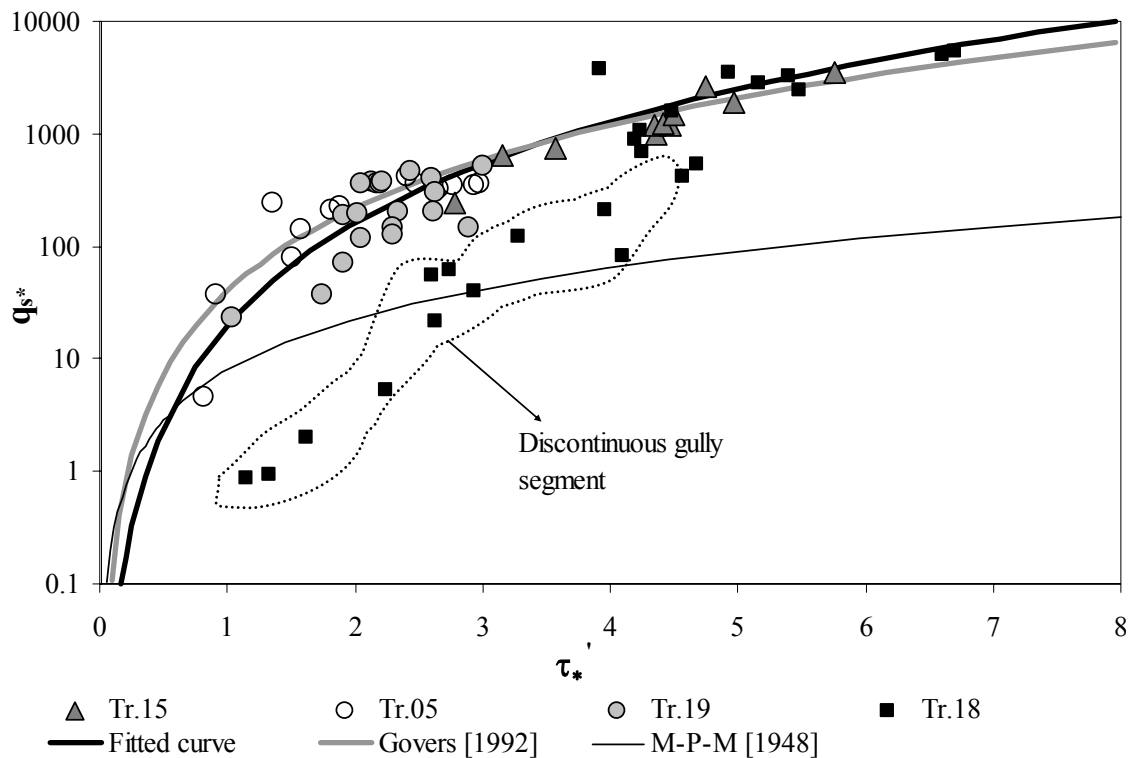
Figure 3-2. Relationship between q_{s*} and $\tau_*^{'}$ obtained using the field observations. The solid lines are fitted power relationships in the form of equation (3).

points represent the sediment transport in the first 60 m of the gully reach starting from the channel head that has two discontinuous channel segments each about 30 m long and 5 to 20 cm deep. No side slope failures were observed and the incisions were presumably due to sediment detachment from the bed and partly from the walls of the channels. Downslope of the 60m long discontinuous channel segment the gully is continuous and incision depths start increasing abruptly and reach to about 1.20 m at about 120 m down the channel head. Beyond this point side slope failures were observed at short intervals. Presumably these subsequent side failures supply considerable sediment to the flow and flow reaches to its transport capacity (Figure 3-2). The growth of Tr.18 was evidently slower than the other gullies where significant scours were observed in relatively very short distances. Since the q_{s*}-τ_*' pairs plotted in figure 3-2 were calculated assuming channeled sediment transport it is consistent that detachment (around the flow cross-section) and supply limited channel segments would plot below the transport capacity relationship.

The dimensionless shear stress exponent p we found is consistent with the total load equations in the form of (3). This exponent is not an artifact of the model inputs. The theory uses spatially distributed observations of gully erosion volumes, drainage areas and slopes, and assumes the rest of the model inputs spatially constant. Therefore q_{s*} and τ_* used in figure 3-2 (equations 18 and 19) are scaled quantities of the field observations as

$$q_{s*} \propto \frac{V_s}{A^{m_w} S^{n_w}} \tag{20}$$

$$\tau_* \propto A^{m_\tau} S^{n_\tau}. \tag{21}$$

Figure 3-3 plots field observations of $V_s / A^{0.3} S^{-0.1875}$ used as a surrogate for sediment discharge, versus $A^{0.6} S^{0.8125}$ used as a proxy for shear stress. A power relationship with an exponent p=3 has been fit to this data,

$$\frac{V_s}{A^{0.3} S^{-0.1875}} \propto (A^{0.6} S^{0.8125})^3. \tag{22}$$
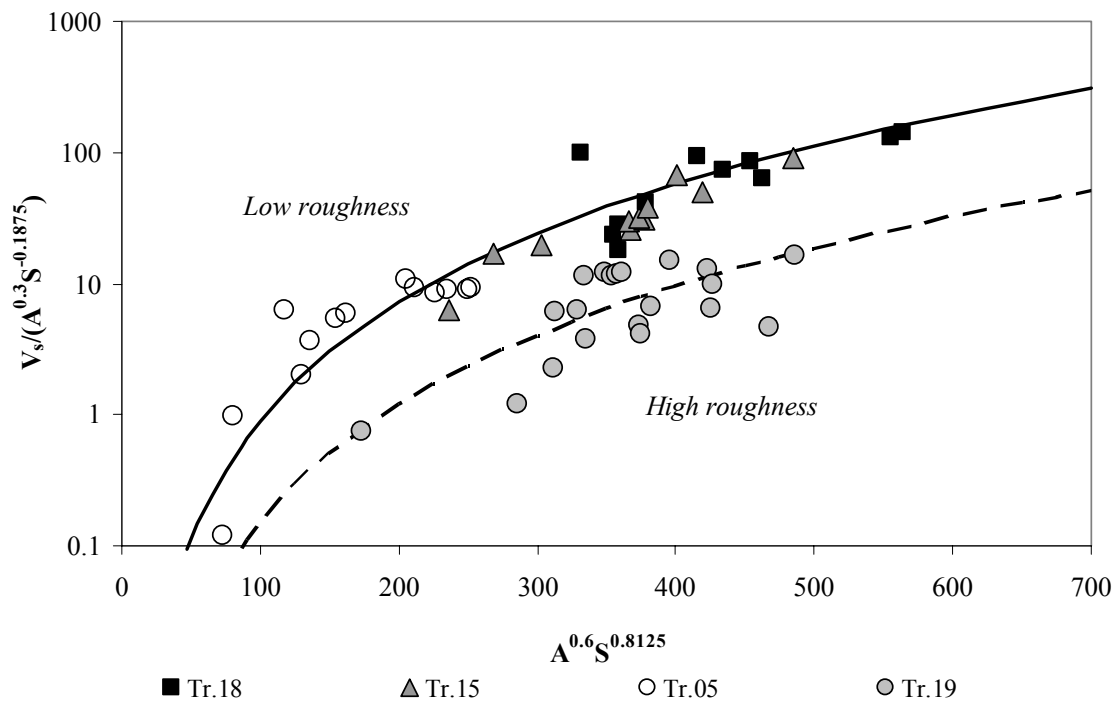
Figure 3-3. Field observations of $V_s / A^{0.3} S^{-0.1875}$ used as a surrogate for sediment discharge versus $A^{0.6} S^{0.8125}$ used as a proxy for shear stress.

The outliers in figure 3-2 were excluded from the plot since the tested theory is for sediment transport capacity conditions. Except for Tr. 19, where rougher channel conditions were observed, the data plots close to the same curve (solid line on Figure 3-3). Tr. 19 data plots below the rest of the data but shows the same functional form (22) (dashed line). When the roughness of Tr.19 is characterized with a higher constant all the data collapses on to one functional relationship equation (3) (Figure 3-2). Figure 3-3 shows the field evidence that sediment transport capacity on steep gullies is a nonlinear function of shear stress with p=3. This figure also indicates that sediment transport capacity is reduced with the rougher conditions observed in Tr.19. This is theoretically described in equations A7 to A11 which show that as the total roughness coefficient increases due to additional roughness elements such as non-transportable grains and obstructions, the fraction of the shear stress acting on transported grains decreases and reduces the sediment transport rate.

In many hillslope erosion models [*Foster et al.*, 1989; *Woolhiser et al.*, 1990; *Coulthard et al.*, 2000] the transport capacity of overland and rill flows are represented by adopting existing bed load equations developed from observations of alluvial rivers and channels [*Julien and Simons*, 1985]. The hydraulic conditions of shallow flows on steep slopes can be different from much deeper channel flows [*Abrahams and Parsons*, 1991; *Ferro*, 1998]. *Govers* [1992] tested the performance of a number of bed load equations using his data set obtained simulating rill flow on slopes ranging from 1.7% to 21% in a laboratory flume and other data sets giving the sediment transport capacity of overland flow. He found that bed load equations are inappropriate for overland flow on

slope ranges steeper than they were originally developed. He suggested that overland

flow does not necessarily show a bedload type transport behavior and that the shear stress

exponent p in (2) should be ~2.5 for the transport capacity of shallow flows on steep

slopes. In Govers' equation the exponent p=2.5 therefore accounts for both suspended

and bedload transport. In order to test Govers' conclusions we compared the Meyer-Peter

& Muller and Govers sediment transport equations with our data by plotting their

dimensionless forms on figure 3-2. In the Meyer-Peter & Muller bedload equation κ=8

and p=1.5. *Govers* [1992] equation has the form of (2) and is not consistent for

nondimensionalization in the form of equation (3), unless κ is written as a function of

sediment size and sediment specific gravity as; $\kappa_G = 34.70(s-1)^2 d^{0.15}$ for clear water as

transporting fluid (see Appendix A4).

When the (τ_*'-q$_*$) curve for the M-P-M equation is compared to the data one can

see that classical bedload equations with p=1.5 would significantly underpredict sediment

transport on very steep slopes at high shear stresses. Bedload equations for alluvial rivers

such as the Meyer-Peter & Muller equation were tested for slopes in the range of 0.1% up

to 2% and in the τ_* range of 0.1 to 1. They often give good results in the slope range of

0.1% and 0.3% [*Yalin*, 1977]. Therefore high flow shear stresses on steep slopes are

significantly above their test range. In addition to that even bedload equations are

sometimes regarded as transport capacity equations under high shear stresses on steep

slopes, Meyer Peter & Muller equation can not be considered among that type because of

the limited slope ranges used in the model experiments [*Smart*, 1984]. This comparison

allows us to visualize how a hillslope erosion model using a generic bedload equation

may underpredict sediment transport in rills and gullies [*Foster et al.*, 1989]. In

distributed models such mispredictions may not be detected since models are often

calibrated optimizing several parameters using basin outlet data. However, biased

spatially distributed erosion estimates may severely affect spatial model results. The

dimensionless form of the Govers equation for shallow overland/rill flow for steep slopes

corresponds well with the field data.

Figure 3-4 plots the total sediment transport volumes calculated from equation

(16) with the derived exponents M=2.1 and N=2.25 (based on p=3, m_τ=0.6, n_τ=0.8125,

m_w=0.3, n_w=-0.1825 and m_n=0.2) against the estimated volumes in the field. The outliers

in figure 3-2 were excluded from the plot. Regression coefficients (R^2) and Nash-

Sutcliffe error measures (NS) [e.g., *Gupta et al.*, 1998]

$$NS = 1 - \frac{\sum (Q_s T - V_s)^2}{\sum (V_s - \overline{V}_s)^2} \tag{23}$$

are calculated for group of gullies where the model inputs were selected constant.

According to equation (16) spatially constant model parameters implies that

$Q_s = const. A^{2.1} S^{2.25}$. The combined data from Tr.05, Tr.15 and Tr.18 revealed both R^2

and NS equal to 0.83 indicating that 83% of the spatial variability of the sediment

transport rates can be represented by the model. For Tr 19 we obtained R^2=0.5 and

NS=0.44. This means that only 44% of the variability of the sediment transport rates over

the terrain can be represented by the model. The reason for a significantly lower model
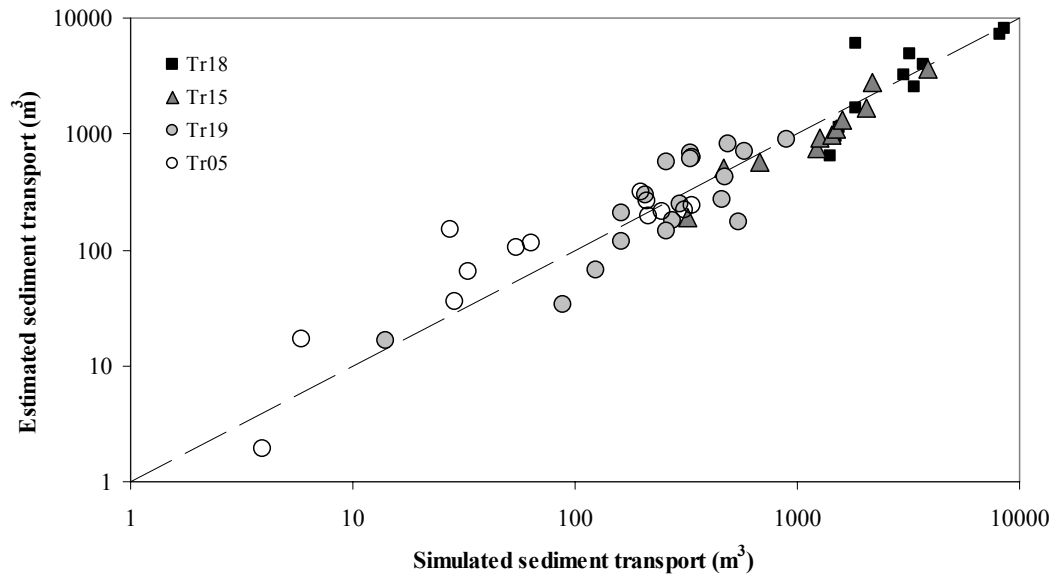
Figure 3-4. Comparison of the calculated sediment transport using the calibrated model parameters of κ=20 and p=3 to the estimated sediment transport in the field. For the combined data for gullies Tr.05, Tr.15 and Tr.18, R^2=0.84 and NS=0.83. For the Tr.19 data set alone R^2=0.5, NS=0.44.
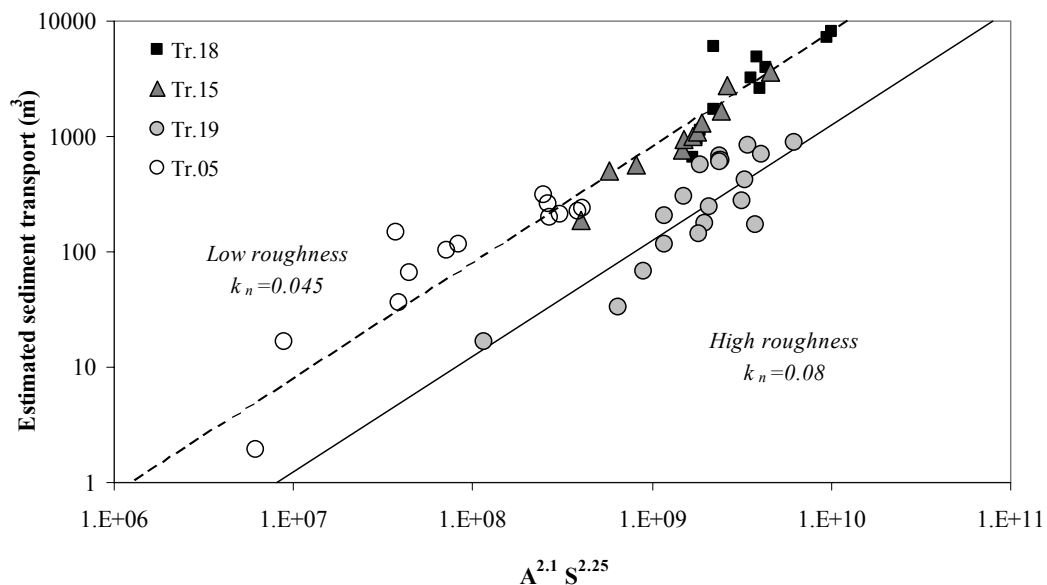
Figure 3-5. Estimated sediment transport as a function of contributing area and slope using their derived exponents at surveyed gully segments. The lines plot equation (16). The solid line is for k_n=0.08 which is for higher roughness conditions observed in Tr.19 and the dashed line for k_n=0.045 for the rest of the gullies.

performance in Tr.19 is we believe due to the observed logs, boulders and exposed rocks inside the gully that may limit the applicability of the model.

To show the relationship between topography and sediment transport we plotted the estimated sediment transport volumes in the field as a function of $A^{2.1}S^{2.25}$ (Figure 3-5). In the figure the solid line plots equation (16) for relatively high and the dashed line for low total channel roughness conditions based on the field estimates of the model inputs. Figure 3-5 shows the importance of contributing area and slope in channelized erosion.
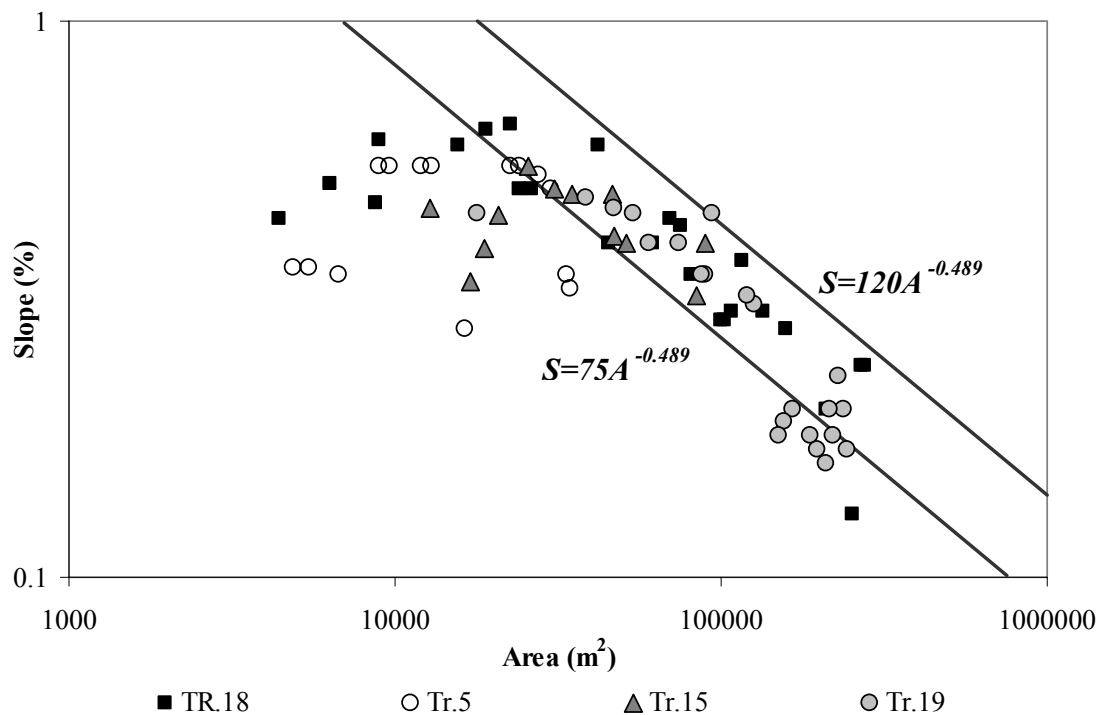
Figure 3-6. Slope-area plot of the gully profiles observed in the field. Lines are the power-law relationships of the profile concavity between area and slope (equation 3) plotted as the upper and lower bounds of the data that shows an inverse relationship between slope and area. M=2.1 and N=2.25.

Topographic concavity expresses the long term effects of sediment transport and provides another check on sediment transport functions. Figure 5-6 presents the slope-area plot of the gully profiles observed in the field. Lines are the power-law relationships between area and slope that characterizes the hillslope profile concavity (equation 5). The lines are plotted as the upper and lower bounds of the data points which show an inverse relationship between slope and area. The concavity index is calculated using the area and slope exponents M=2.1 and N=2.25 of the sediment transport relationship. This figure implies that the form of the sediment transport equation derived using field data from a single gully-forming event may be consistent with the fluvial transport processes acting over the long term.

5.2. Modeling Sediment Transport over the Watershed Scale

Modeling the sediment input to mountain streams is crucial for assessing the impacts of landuse on erosion, predicting the influence of sediment on changing the hydraulic conditions in the river and on the habitat for fish and invertebrates [*Wilcock*, 1998; *Kirchner et al.*, 2001]. In this section we coupled the sediment transport model with the probabilistic model for channel initiation [*Istanbulluoglu et al.*, (Chapter 2)] and mapped the expected sediment transport capacity on the DEM of the study site and calculated the sediment inputs to the main channel of Trapper Creek.

Channel initiation due to the concentration of dispersed overland flow into gullies is identified based on a probabilistic threshold criterion. The probability of channel initiation (PCI) at a point on the landscape is [*Istanbulluoglu et al*., (Chapter 2)],

$$PCI = \text{Probability}(C \le aS^{\alpha}) = \int\limits_{0}^{aS^{\alpha}} f_c(C)dC \qquad (24)$$

where, $f_C(C)$ is a probability density function describing random spatial variability in C,

and $\alpha=1.167$ for channel initiation due to overland flow [*Willgoose et al.*, 1991a; *Istan-*

bulluoglu et al., (Chapter 2)] derived C based on the assumption that channels are formed

where overland flow shear stress exceeds a critical shear stress threshold for incipient

motion,

$$C = \left(\frac{\tau_{*c}g(\rho_s - \rho_w)d_{50}}{\rho_w gn_{go}^{1.5}(n_{go} + n_{ao})^{-0.9}r^{m_1}} \right)^{1.667}. \qquad (25)$$

In this equation, n_{go} is Manning's roughness coefficient for overland flow on bare soil

calculated as a function of d_{50} from Strickler's equation [*Julien and Simons*, 1985], n_{ao} is

the additional roughness of overland flow. In the PCI theory d_{50}, n_{ao}, $n_{go}=f(d_{50})$ and r are

random variables.

The PCI model parameters are obtained from *Istanbulluoglu et al.* (Chapter 2)

where median sediment size, d_{50} of the surface sediment is lognormally distributed with

an average and a standard deviation of 2 mm and 0.48 mm (from field observations of the

surface sediment on hillslopes), and r and n_{ao} are uniformly distributed, r between 15 and

55 mm/h and n_{ao} between 0.015-0.1. Figure 3-7 plots the cumulative distributions of the

observed aS^{α} at channel heads and the derived C thresholds using the Monte Carlo

simulation approach where 1500 random numbers are used for r, d_{50} and n_{ao}. Field data

used in figure 7 is presented in *Istanbulluoglu et al.* (Chapter 2). The PCI map for the
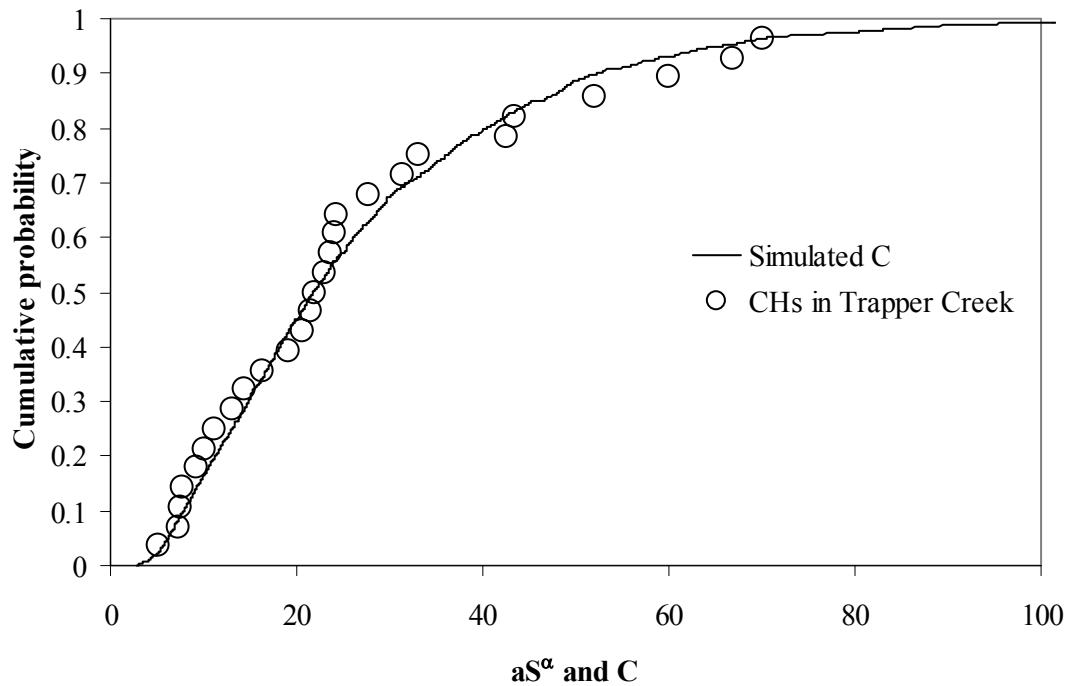
Figure 3-7. Comparison of the cumulative distribution from the simulations of C to the cumulative distribution of observed aS^α at channel heads in Trapper.

study area and the channel and continuous gully heads observed in the field are presented

in figure 3-8. Channel head locations towards the end of the high PCI zones are

consistent with the theory.

Expected total sediment transport in gullies within the erosion event is calculated

as the product of sediment transport capacity (16) and PCI at each grid cell of the DEM.

Figure 3-9 shows the expected total sediment transport over the terrain. No sediment

transport is shown for the main channel of Trapper Creek as this may require more

complex sediment transport formulations and longer term simulations [*Benda and Dunne*,

1997] that are beyond the scope of this paper. Instead we calculated the total sediment

input volumes to along the main channel from tributaries and hillslopes where PCI>0.

Figure 3-10 plots the sediment inputs versus the drainage area of the main channel. Each

point on the plot shows the sediment input to a main channel grid cell and the bold black line shows sediment accumulation along the channel. The total amount of sediment that laterally enters the main channel is 114,000 m^3. Sediment introduced from individual gullies ranges from 0.01 m^3 to 39,000 m^3. Almost 43% of the total sediment comes from gullies draining larger hollows in the headwaters of the basin. Relatively smaller sediment contributions can be observed close to the mouth of the basin (drainage area > 7 km^2) where the basin width narrows and the drainage areas of individual hollows get smaller. Similar intense erosion events are typical especially after forest fires in the Idaho batholith where approximately 80% of the long-term erosion rates are due to infrequent episodic gullying [*Kirchner et al.*, 2001].

6. Conclusions

Sediment transport capacity is often parameterized as a nonlinear function of shear stress or interchangeably discharge or contributing area and slope in theoretical geomorphology. Although extensive data sets exist that decipher the nonlinearity in relationships between sediment transport and shear stress, discharge and slope (equations 1 and 2) in experimental flume scales we know of no study that examines the theoretical foundations of these equations for naturally eroded gullies surveyed in the field.

In this paper we adapted a generic dimensionless sediment transport function (3) to incising gullies on steep slopes by describing the hillslope hydrology and flow hydraulics based on contributing area and local slope. We calibrated the parameters of the dimensionless sediment transport function, an empirical constant κ and a shear stress
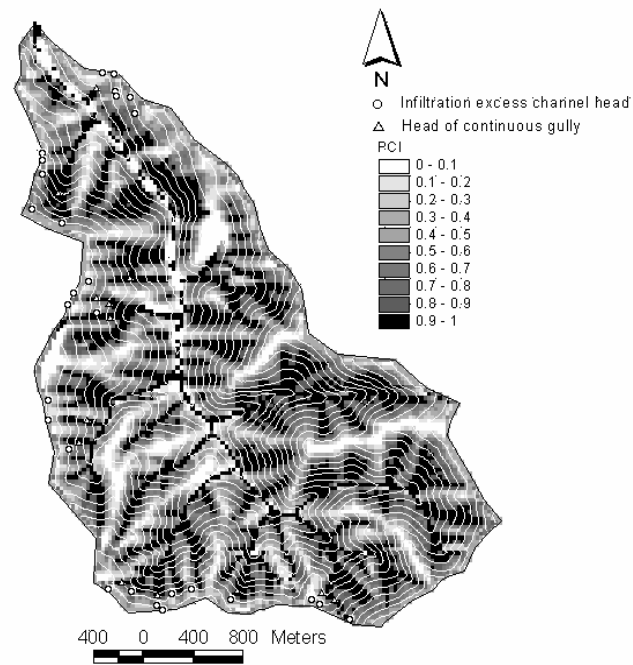
Figure 3-8. Probability of channel initiation (PCI) map of the study area.
Contour interval is 30 m.
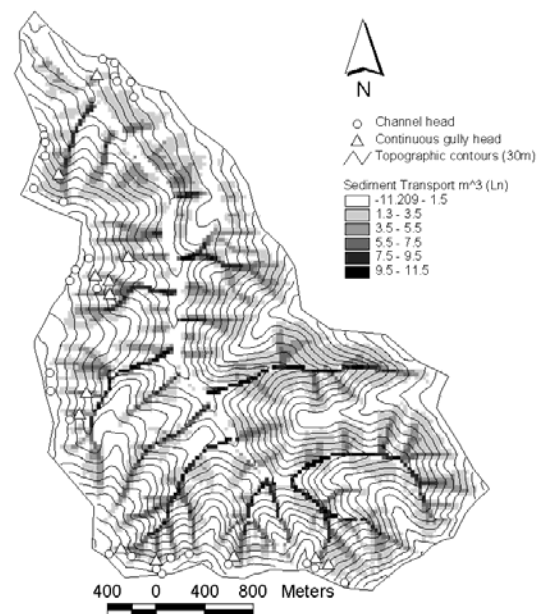
Figure 3-9. Expected total sediment transport from gullies for the thunderstorm that
incised the gullies in Trapper Creek. Contour interval is 30 m.
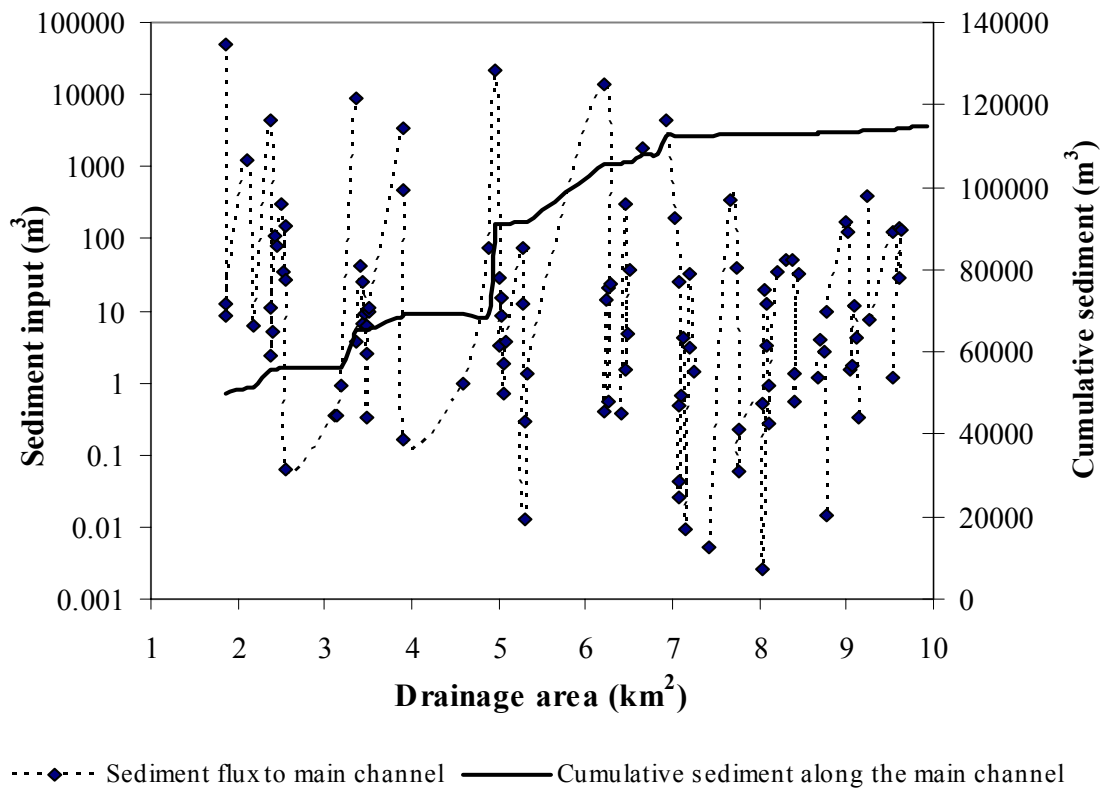
Figure 3-10. Modeled sediment fluxes to the main channel from the hillslopes where PCI>0 and the accumulated fluxes to the main channel of Trapper Creek.

exponent p for the case of recent gully erosion using field data from a steep mountainous

basin in southwestern Idaho.

Our field data suggested that under high shear stresses, p=3. This exponent is

twice the shear stress exponents used in classical bed load equations but consistent with

the total load equations [*Garde and Raju*, 1985]. Engelund and Hansen noted that starting

from the incipient motion of bed load the τ_* exponent increases from 1.5 to 2.5 and even

up to 3 under high shear stresses in equation (3) as the flow intensity and the suspended

load movement increases [*Chien and Wan*, 1999]. Bed and total load equations were

mostly developed for alluvial rivers with gentle slopes and bedforms, and under relatively lower τ_* ranges than we calculated for our gullies. Thus, their applicability on steep hillslopes can be questionable. However Govers' flume experiments on steep slopes with well-sorted mixtures also reveal a shear stress exponent p=2.5 and shows good correspondence with the field data (Figure 3-2). We suggest that sediment transport capacity of incising gullies can be modeled using equation (16) either with the model calibration parameters obtained in this study or the parameters derived from the Govers equation.

The model driven by spatially constant inputs represents 83% of the spatial variability of the sediment transport rates in gullies Tr.05, Tr.15 and Tr.18 located in three different hollows. The reason for this good performance is attributed to the rather spatially homogenous model inputs such as the sediment sizes and the roughness conditions observed in these gullies. For the case of Tr.19 the model explains only 44% of the spatial variability of the sediment transport rates. The reason for a significantly lower model performance in Tr.19 is we believe due to the heterogeneities in the roughness conditions in the field that are not spatially characterized in the model.

The shear stress exponent p=3 theoretically corresponds to exponents M=2.1 and N=2.25 in the sediment transport equation (1). Figure 3-5 plots field estimates of the erosion volumes as a function of $A^{2.1}S^{2.25}$. The lines shown in the figure plot equation (16) for constant model parameters. This plot shows the importance of topography in concentrated erosion. In the literature several M and N exponents were presented for different sediment transport processes such as creep, soil wash and rivers [*Kirkby*, 1971;

Arrowsmith et al., 1996]. For soilwash and gullying reported values of area and slope exponents are in the range of M=1-2 and N=1.3-2. The exponents we find are higher than the upper limit of these published values. In the literature however contributing area is represented as the specific catchment area (contributing area per unit contour width) instead of concentrated area and the exponents were empirically developed based on longer observation periods.

One of the implications of the sediment transport function on landscape morphology is the concavity of the channel network. The concavity index $\theta_c = (M-1)/N$, obtained from the area and slope exponents of the sediment transport equation agrees well with the observed profile concavity of the gullies. This shows that the sediment transport equation developed using a single erosion event is consistent with the functional form of sediment transport over the long term.

The probability of channel initiation and the expected total sediment transport maps presented in Figures 3-8 and 3-9 show the importance of topographic variables on channelized erosion and also reflect the climate, landuse and lithologic conditions. Since the theory showed is calibrated using field observations we believe that these maps communicate reliable information for our field site and the model developed could be used for evaluating the influence of climate and land-use conditions on sediment yields. In order to extend and test the equations presented here more field data from different climate and lithological settings are required.

References

Abrahams, A. D., and A. J. Parsons, Resistance to overland flow on desert pavement and its implications for sediment transport modeling, *Water Resour. Res.*, 27(8), 1827-1836. 1991.

Arcement, G. J. J., and V. R. Schneider, Guide for selecting Manning's roughness coefficients for natural channels and floodplains, *U.S. Geol. Surv. Report Number RHWA-TS-84-204*, 50 p. U.S. Geol. Surv., 1984.

Arrowsmith, J. R., D. D. Pollard, and D. D. Rhodes, Hillslope development in areas of active tectonics, *J. Geophys. Res.*, 101(B3), 6255-6275. 1996.

Aziz, N. M., and D. E. Scott, Experiments on sediment transport in shallow flows in high gradient channels, *Hydrol. Sci. J.*, 34, 465-479. 1989.

Band, L. E., Grain size catenas and hillslope evolution, *Catena Supl.*, 17, 167-176. 1990.

Bathurst, J. C., W. H. Graf, and H. H. Cao, Bedload discharge equations for steep mountain rivers, in *Sediment Transport in Gravel Bed Rivers*, edited by Thorne et al., pp. 453-477, John Willey, New York, 1987.

Benda, L., and T. Dunne, Stochastic forcing of sediment supply to channel networks from landsliding and debris flow, *Water Resour. Res.*, 33(12), 2849-2863. 1997.

Bennett, S. J., J. Casali, K. M. Robinson, and K. C. Kadavy, Characteristics of actively eroding ephemeral gullies in an experimental channel, *Trans. ASAE*, 43(3), 641-649, 2000.

Buffington, J. M., and D. R. Montgomery, A systematic analysis of eight decades of incipient motion studies, with special reference to gravel-bedded rivers, *Water Resour. Res.*, 33(8), 1993-2029, 1997.

Burkard, M. B., and R. A. Kostaschuk, Initiation and evolution of gullies along the shoreline of Lake Huron, *Geomorphol.*, 14, 211-219, 1995.

Cannon, S. H., E. R. Bigio and E. Mine, A process for fire-related debris flow initiation, Cerro Grande fire, New Mexico, *Hydrol. Processes*, 15, 3011-3023, 2001.

Chien, N. and Z. Wan, *Mechanics of sediment transport*, ASCE Press, 913 p., 1999.

Chow, V. T., *Open channel hydraulics*, McGraw-Hill., XXX p., New York, 1959.

Cochrane, T. A., and D. C. Flanagan, Detachment in a simulated rill, *Trans. ASEA*, 40(1), 111-119, 1997.

Coulthard, T. J., M. J. Kirkby, and M. G. Macklin, Modelling geomorphologic response to environmental change in an upland catchment, *Hydrol. Processes*, 14, 2031-2045, 2000.

Croke, J., and S. Mockler, Gully initiation and road-to-stream linkage in a forested catchment, Southeastern Australia, *Earth Surface Process. Landforms*, 26, 205-217, 2001.

Dietrich, W. E., and T. Dunne, The Channel Head, in *Channel Network Hydrology*, edited by K. Beven and M. J. Kirkby, pp. 175-219, John Wiley, New York, 1993.

Everaert, W., Emprical relations for sediment transport capacity of interrill flow, *Earth Surface Process. Landforms*, 16, 513-532, 1991.

Ferro, V., Evaluating overland flow sediment transport capacity, *Hydrol. Processes*, 12, 1895-1910, 1998.

Foster, G. R., L. F. Huggins, and L. D. Meyer, A laboratory study of rill hydraulics: I. Velocity relationships, *Trans. ASCE*, 27(3), 790-796, 1984.

Foster, G. R., L. J. Lane, M. A. Nearing, S. C. Finkner, and D. C. Flanagan, Erosion component, in *USDA - Water Erosion Prediction Project: Hillslope Profile Model Documentation*, Edited by L. J. Lane and M. A. Nearing, pp.10.1-10.12, NSERL Report No. 2, USDA-ARS National Soil Erosion Research Laboratory, West Lafayette, Indiana, 1989.

Garde, R. J., and K. G. R. Raju, *Mechanics of sediment transportation and alluvial stream problems*, 2 nd. Edition, 618 pp., John Wiley, New York, 1985.

Govers, G., Evaluation of transporting capacity formulae for overland flow, in *Overland flow hydraulics and erosion mechanics*, edited by A. J. Parsons, and A. D. Abrahams, pp. 243-273, Chapman & Hall, New York, 1992.

Gray, D. H., and W. F. Megahan, Forest vegetation removal and slope stability in the Idaho Batholith., *For Serv. Res. Pap. INT-271*, 23 pp., Intermt Res. Stn., For. Serv., U.S. Dep. of Agric., Ogden, Utah, 1981.

Gupta, H. V., S. Sorooshian, and P. O. Yapo, Toward improved calibration of hydrologic models: multiple and noncommensurable measures of information, *Water Resour. Res.*, 34(4), 751-763, 1998.

Hancock, G., and G. Willgoose, Use of a landscape simulator in the validation of the SIBERIA catchment evolution model: declining equilibrium landforms, *Water Resour. Res.*, 37(7), 1981-1992, 2001.

Hancock, G. R., G. R. Willgoose, and K. G. Evans, Testing the Siberia landscape evolution model using the Tin Camp creek, northern territory, Australia, field catchment, *Earth Surface Process. Landforms*, 27(2), 125-143. 2001.

Hashimoto, H., A comparison between gravity flows of dry sand and sand-water mixtures, in *Recent Developments in Debris Flows*, edited by A. Armanini and M. Michiue, pp. 70-92, Springer-Verlag, New York, 1997.

Jan, C. D., and H. W. Shen, Review dynamic modeling of debris flows, in *Recent Developments in Debris Flows*, edited by A. Armanini and M. Michiue, pp. 93-116, Springer-Verlag, New York, 1997.

Jeppson, R. W., and S. A. Rodriguez, Hydraulics of solving unsteady debris flows, *Hydraulics and Hydrology Series*, 88 pp., Utah State Univ., Logan, 1983.

Julien, P., Dynamics of debris flows, in *Recent Developments on Debris Flows*, edited by A. Armanini and M. Michiue, pp. 65-69, Springer-Verlag, New York, 1997.

Julien, P. Y. and D. B. Simons, Sediment transport capacity of overland flow, *Transac. ASAE*, 28(3), 755-762, 1985.

Kirchner, J. W., R. C. Finkel, C. S. Riebe, D. E. Granger, J. L. Clayton, J. G. King, and W. F. Megahan, Mountain erosion over 10 yr, 10 k.y., and 10 m.y. time scales, *Geology*, 29(7), 591-594, 2001.

Kirkby, M. J., Hillslope process-response models based on the continuity equation, in *Slopes Form and Processes*, Institute of British Geographers, Special Publication No. 3., pp.15-30, 1971.

Knighton, D., *Fluvial Forms and Processes*, 383 pp., Arnold, London, 1998.

Knisel, W. G., CREAMS: A field scale model for chemical, runoff and erosion from agricultural management systems, USDA ARS, *Report no: 26, 474-485*, U.S. Dep. of Agric., 1980.

Leopold, L. B., M. G. Wolman, and J. P. Miller, *Fluvial processes in geomorphology*, 522 pp., Freeman, San Francisco, 1964.

Megahan, W. F., Erosion over time on severely disturbed granitic soils: A model, *USDA For. Serv. Res. Pap. INT-156*, 14 pp., Intermt. Res. Stn., For. Serv., U.S. Dep. of Agric., Ogden, Utah, 1974.

Megahan, W. F., An overview of erosion and sedimentation processes on granitic soils, in *Proc. Decomposed Granite Soils Conf.*, edited by S. Sari, pp. 11-30, Redding, CA; Davis, CA, 1992.

Megahan, W. F., and W. J. Kidd, Effect of logging roads on sediment production rates in the Idaho Batholith, *For Serv. Res. Pap. INT-123*, 14 pp., Intermt Res. Stn., For. Serv., U.S. Dep. of Agric., Ogden, Utah, 1972.

Meyer, G. A., J. L. Pierce, S. H. Wood, and A. J. T. Jull, Fire, storms and erosional events in the Idaho batholith, *Hydrol. Processes*, 15, 3025-3038. 2001.

Meyer, G. A., and S. G. Wells, Fire-related sedimentation events on alluvial fans, Yellowstone National Park, U.S.A., *J. Sedimentary Res.*, (A67), 776-791, 1997.

Mizuyama, T., *Bedload transport in steep channels,* PhD., Thesis, 300 pp. Kyoto University, Kyoto, 1977.

Mizuyama, T., and H. Shimohigashi, Influence of fine sediment concentration on sediment transport rates, *Japan. Civil Eng. J.*, 27(1), 46-49, 1985.

Montgomery, D. R., Road surface drainage, channel initiation, and slope instability, *Water Resour. Res.*, 30(6), 1925-1932, 1994.

Moore, I. D., and G. J. Burch, Sediment transport capacity of sheet and rill flow: Application of unit stream power theory, *Water Resour. Res.*, 22(8), 1350-1360. 1986.

Nearing, M. A., L. D. Norton, D. A. Bulgakov, G. A. Larinov, L. T. West, and K. M. Dontsova, Hydraulics and erosion in eroding rills, *Water Resour. Res.*, 33(4), 865-876, 1997.

Niemann, J. D., N. M. Gasparini, G. E. Tucker, and R. R. Bras, A quantitative evaluation of Playfair's law and its use in testing long-term stream erosion models, *Earth Surface Process. Landforms*, 26, 1317-1332, 2001.

Osterkamp, W. R., and T. J. Toy, Geomorphic consideration for erosion prediction, *Environ. Geol.*, 29(3/4), 152-157, 1997.

Prosser, I. P., and C. J. Slade, Gully formation and the role of valley floor vegetation, southeastern Australia, *Geology*, 22, 1127-1130, 1994.

Prosser, I. P., and M. Soufi, Controls on gully formation following forest clearing in a humid temperature environment, *Water Resour. Res.*, 34(12), 3661-3671, 1998.

Prosser, I. P., and L. Williams, The effect of wildfire on runoff and erosion in native Eucalyptus forest, *Hydrol. Processes*, 12, 251-265, 1998.

Rickenmann, D., Bedload transport and hyperconcentrated flow at steep slopes, in *Fluvial Hydraulics of Mountain Regions*, edited by A. Armanini and G. D. Silvio, pp. 429-441, Springer-Verlag, New York, 1991.

Rickenmann, D., Hyperconcentrated flow and sediment transport at steep slopes, *J. Hydr. Engrg.*, 117(11), 1419-1439, 1992.

Rodriguez-Iturbe, I. and A. Rinaldo, *Fractal River Basins*, 547 pp., Cambridge University Press, New York, 1997.

Roo, A. P. J. D., C. G. Wesseling, V. G. Jetten, and C. J. Ritsema, *Limburg Soil Erosion Model*, A User Manual. Version 3.1., 48 pp., Dep. Phys. Geogr. Utrecht Univ., Laon, France, 1995.

Schmidt, J., M. v. Werner, and A. Michael, Application of the EROSION 3D model to the CATSOP watershed, The Netherlands, *Catena*, 37, 449-456. 1999.

Schumm, S. A., Harvey, M.D., and Watson, C.C., 1984, *Incised channels*: *Morphology Dynamics and Control,* 200 pp., Water Resourcess Publications, Littleton, 1984.

Selby, M. J., *Hillslope Materials and Processes*, 451 pp., Oxford University Press, New York, 1993.

Sidorchuk, A., Dynamic and static models of gully erosion, *Catena*, 37, 401-414, 1999.

Simons, D. B., and F. Senturk, *Sediment Transport Technology*, 807 pp., Water Resour. Pub., Fort Collins, 1977.

Smart, G., Sediment transport formula for steep channels, *J. Hydr. Engrg.*, 100(3), 267-276, 1984.

Smart, G. M., and M. Jaeggi, Sediment transport on steep slopes. Mitteilung der Versuchsanstalt fur Wasserbau, Hydrologie und Glaziologie, No. 64, ETH Zurich, 1983.

Smith, T. R., and F. P. Bretherton, Stability and the conservation of mass in drainage basin evolution, *Water Resour. Res.*, 8(6), 1506-1529, 1972.

Suszka, L., Modification of transport rate formula for steep channels, in *Fluvial Hydraulics of Mountain Regions*, edited by A. Armani and G. G. Silvio, pp. 59-70. Springer-Verlag, New York, 1991.

Takken, I., L. Beuselinck, J. Nachtergaele, G. Govers, J. Poesen, and G. Degraer, Spatial evaluation of a physically-based distributed erosion model (LISEM), *Catena*, 37, 43-447, 1999.

Tarboton, D. G., A new method for the determination of flow directions and contributing areas in grid digital elevation models, *Water Resour. Res.*, 33(2), 309-319, 1997.

Tarboton, D. G., R. L. Bras, and I. Rodriguez-Iturbe, On the extraction of channel networks from digital elevation data, *Hydrol. Processes*, 5(1), 81-100, 1991.

Tarboton, D. G., R. L. Bras, and I. Rodriguez-Iturbe, A physical basis for drainage density, *Geomorphol.*, 5(1/2), 59-76. 1992.

Tucker, G. E., and R. L. Bras, Hillslope processes, drainage density and landscape morphology, *Water Resour. Res.*, 34(10), 2751-2764, 1998.

Tucker, G. E., and R. L. Bras, A stochastic approach to modeling drainage basin evolution, *Water Resour. Res.*, 36(7), 1953-1964, 2000.

Tucker, G. E., and K. X. Whipple, Topographic outcomes predicted by stream erosion models: Sensitivity analysis and intermodel comparison, *J. Geophys. Res.*, 107, (B9), 2179, doi:10.1029/2001JB000162, 2002.

Vandekerckhove, L., J. Poesen, D. O. Wijdenes, and T. d. Figueiredo, Topographic thresholds for ephemeral gully initiation in intensely cultivated areas of the Mediterranean, *Catena*, 33, 271-292, 1998.

Vandekerckhove, L., J. Poesen, D. O. Wijdenes, J. Nachtergaele, C. Kosmas, M. J. Roxo and T. d. Figueired, Thresholds for gully initiation and sedimentation in Mediterranean Europe, *Earth Surface Process. Landforms*, 25, 1201-1220, 2000.

Wemple, B. C., J. A. Jones and G. E. Grant, Channel network extension by logging roads in two basins, western cascades, Oregon, *Water Resour. Bulletin.*, 32(6), 1195-1207, 1996.

Whipple, K. X., and G. E. Tucker, Dynamics of the stream-power river incision model: implications for height limits of mountain ranges, landscape response timescales, and research needs, *J. Geophys. Res.,* 104(B8), 17,661-17,674, 1999.

Wilcock, P. R., Two-fraction model of initial sediment motion in gravel-bed rivers, *Science*, 280, 410-412. 1998.

Willgoose, G. R., A physical explanation of an observed area-slope relationship for catchments with declining relief, *Water Resour. Res.*, 30, 151-159. 1994.

Willgoose, G. R., *A physically based channel network and catchment evolution model*, Ph.D. thesis, 464 pp., Mass. Inst. of Technol., Cambridge, 1989.

Willgoose, G., R. L. Bras, and I. Rodriguez-Iturbe, A coupled channel network growth and hillslope evolution model 1. theory, *Water Resour. Res.*, 27(7), 1671-1684, 1991a.

Willgoose, G., R. L. Bras, and I. Rodriguez-Iturbe, A physical explanation of an observed link area-slope relationship, *Water Resour. Res.*, 27(7), 1697-1702, 1991b.

Wishmeier, W. H., and D. D. Smith, Predicting rainfall-erosion losses from cropland east of the Rocky Mountains, *Agr. Handbook 282.*, U.S Dept. Agr., Washington, D.C., 1965.

Woodward, D. E., Method to predict cropland ephemeral gully erosion, *Catena*, 37, 393-399, 1999.

Woolhiser, D. A., R. E. Smith and D. C. Goodrich, *KINEROS, a kinematic runoff and erosion model; documentation and user manual*, ARS-77, 130 pp., Agric. Res. Serv., U.S. Dep. of Agric., Tuscon, Ariz., 1990.

Yalin, M. S., *Mechanics of Sediment Transport*, 2nd. edition, 219 pp., Pergamon, Oxford, 1977.

CHAPTER 4

MODELING OF THE INTERACTIONS BETWEEN FOREST VEGETATION, DISTURBANCES AND SEDIMENT YIELDS[1]

Abstract. The controls of forest vegetation, natural (wildfires) and anthropogenic (harvest) vegetation disturbances on the frequency and magnitude of sediment delivery from a small watershed (~ 3.9 km^2) in the Idaho batholith are investigated through numerical modeling. Simulation results compare well with field observations of event sediment yields and long term averages over ~10,000 years. The model simulates soil development based on continuous bedrock weathering and the divergence of diffusive sediment transport on hillslopes. Soil removal is due to episodic gully erosion, shallow landsliding and debris flow generation. In the model, forest vegetation provides root cohesion and surface resistance to channel initiation. Forest fires and harvests reduce the vegetation. Vegetation loss leaves the land susceptible to erosion and landsliding until the vegetation cover reestablishes in time. When vegetation is not disturbed by wildfires over thousands of years, sediment delivery is modeled to be less frequent but with larger event magnitudes. Increased values of root cohesion (representing denser forests) lead to lower event magnitudes. Wildfires appear to control the timing of sediment delivery. Compared to undisturbed forests, erosion is concentrated during the periods with low erosion thresholds often called "Accelerated Erosion Periods" (AEP) following wildfires. We find that the drainage density that results is inversely proportional to root cohesion and under the same forest cover conditions wildfires increase the drainage density. We

---

[1] Coauthored by Erkan Istanbulluoglu, David Tarboton, Robert T. Pack and Charles H. Luce.

compare the sediment yields under anthropogenic (harvest) and natural (wildfire) disturbances. Harvest disturbances appear to increase the frequency of sediment delivery however sediment delivery following wildfires seems to be more severe. Different sediment delivery regimes explored in this paper have different implications for the engineering design of water structures and stream habitats. We suggest that when the concern is the amount of sediment episodically delivered to streams (e.g., for engineering design purposes of reservoirs) then the possibility of sediment delivery after wildfires needs to be taken into account. However, if the concern is the disturbances on the aquatic ecosystem and stream habitats then forest management practices should be planned to mimic natural disturbance regimes.

1. Introduction

Episodic debris flows and gully erosion are the major geomorphic processes involved in the development of steep mountainous regions in tectonically active humid environments [*Selby*, 1993]. Episodic erosion delivers a punctuated sediment supply to channels that may cause property damage and life loss [*Sidle et al.*, 1985; *Crozier*, 1986], kill fish, disturb aquatic habitats [*Pollock*, 1998; *Reeves et al.*, 1998] and cause silting in reservoirs that significantly reduces their operational lifespan. Understanding the factors that control the natural rates of erosion, their variability and timing in mountainous basins is important for assessing the environmental risks associated with erosion events and predicting the impacts of landuse on erosion [*Dietrich et al.*, 2000; *Kirchner et al.*, 2001].

It has been argued that in rivers most of the sediment is carried by floods which recur at least once in five years [*Wolman and Miller*, 1960]. The importance of extreme

events in geomorphology on the scale of hillslopes however has been a neglected topic because of the lack of data and techniques to date past low frequency and large magnitude events [*Selby*, 1993]. *Kirchner et al.* [2001] compared long term erosion rates over 10 thousand year time scales with short term measurements (10-84 years) in steep forested Idaho watersheds and found that long term average sediment yields are on the average 17 times higher than the short term stream sediment fluxes. This significant difference suggests that sediment delivery from mountainous watersheds is extremely episodic and long-term sediment delivery is dominated by catastrophic rare events [*Kirchner et al.*, 2001]. In steep forested basins of the Western U.S. catastrophic erosion events are often linked to extreme storms and wildfires [*Montgomery*, 1994; *Cannon et al.*, 2001; *Meyer et al.*, 2001]. Wildfires reduce the stabilizing effects of vegetation and leave the soil susceptible to fluvial erosion and landsliding. Vegetation disturbances together with climate forcing trigger geomorphologic responses that supply catastrophic amounts of sediment and large woody debris to streams. Human disturbances such as clearcutting and road construction in forested basins have also been shown to dramatically accelerate erosion rates over rates in undisturbed forests [*Megahan et al.*, 1978; *Gray and Megahan*, 1981; *Sidle et al.*, 1985; *Johnson et al.*, 2000; *Montgomery et al.*, 2000]. Although the short-term effects of forest disturbances are well documented in many locations there is still a lack of information on their longer term consequences [*Sidle et al.*, 1985]. *Kirchner et al.* [2001] suggested that human influence on erosion should be considered from two different perspectives. First if human influences increase incremental erosion rates they may result in significant harm to aquatic ecosystems that

are naturally adjusted to episodic disruptions and second human activities may alter the size of the catastrophic events that deliver sediment to streams.

Various internal (e.g., weathering rates, soil cohesion) and external (climate forcing, fires etc.) factors influence the occurrence of episodic erosion events. Their significance and the risks associated with them can be recognized and managed when their frequency and magnitude and the physical factors contributing to their episodic behavior is known [*Selby*, 1993]. *Benda and Dunne* [1997a, 1997b] modeled the interactions between the stochastic sediment supply due to mass wasting driven by random rainstorms and fires, and the topology of the channel network to generate spatial and temporal sediment fluxes and storages over large areas (~200 km^2) in the Oregon Cost Range. In a recent paper *Lancaster et al.* [2001] developed a numerical model similar to Benda and Dunne's to explore the dynamics of the interaction between sediment and wood supply and transport.

In this paper our specific emphasis is the influence of forest vegetation and natural and anthropogenic vegetation disturbances on the frequency and magnitude of erosion events in a typical steep forested headwater basin in the Idaho batholith. We developed a physically based numerical model to explore the following questions: (1) How do forest cover conditions (i.e., poor, good, dense) influence the magnitude and frequency of sediment yields? (2) How do the natural (e.g., wildfires) and anthropogenic (e.g., forest management) disturbances alter the frequency and magnitude of sediment yields? (3) What is the influence of vegetation growth rates on erosion?

The model was developed to characterize the dominant erosion processes of the granitic mountains of central Idaho where both fluvial erosion and saturation slope failures are observed [*Megahan et al.*, 1978; *Gray and Megahan*, 1981]. Figure 4-1 shows a flow chart of the model. The model uses digital elevation model (DEM) grid cells as model elements, and operates on yearly time steps. Soil depths are evolved in time due to the mass balance between soil production from underlying bedrock and the divergence of diffusive sediment transport. Soil removal is modeled by fluvial sediment transport, landsliding and debris flow scour. In the model vegetation is grouped into overstory (e.g., trees) and understory (e.g., grass) vegetation cover types. Overstory vegetation is assumed to provide deep root cohesion while the understory vegetation provides the surface resistance to erosion. Forest disturbances kill the vegetation and reduce the root cohesion and surface resistance. Following disturbance, vegetation properties recover in time to their pre-disturbed levels. The vegetation module simulates a yearly time series of the spatially uniform response of vegetation related variables (e.g., root cohesion, overland flow vegetation roughness coefficient) to temporal occurrences of forest fires and forest harvests. The hydrology module characterizes the hydrologic forcing driving erosion and landslides using probability distributions of the largest summer thunderstorms and winter/spring water input events (that include snowmelt) and calculates spatially uniform runoff rates and the wetness of the soil profile based on topography.

In what follows we first describe the geomorphology, hydrology and different erosion patterns observed in our field area in the Idaho batholith. Second we presented

our theoretical framework for modeling episodic sediment yields. We then describe our

simulation experiments and our conclusions.
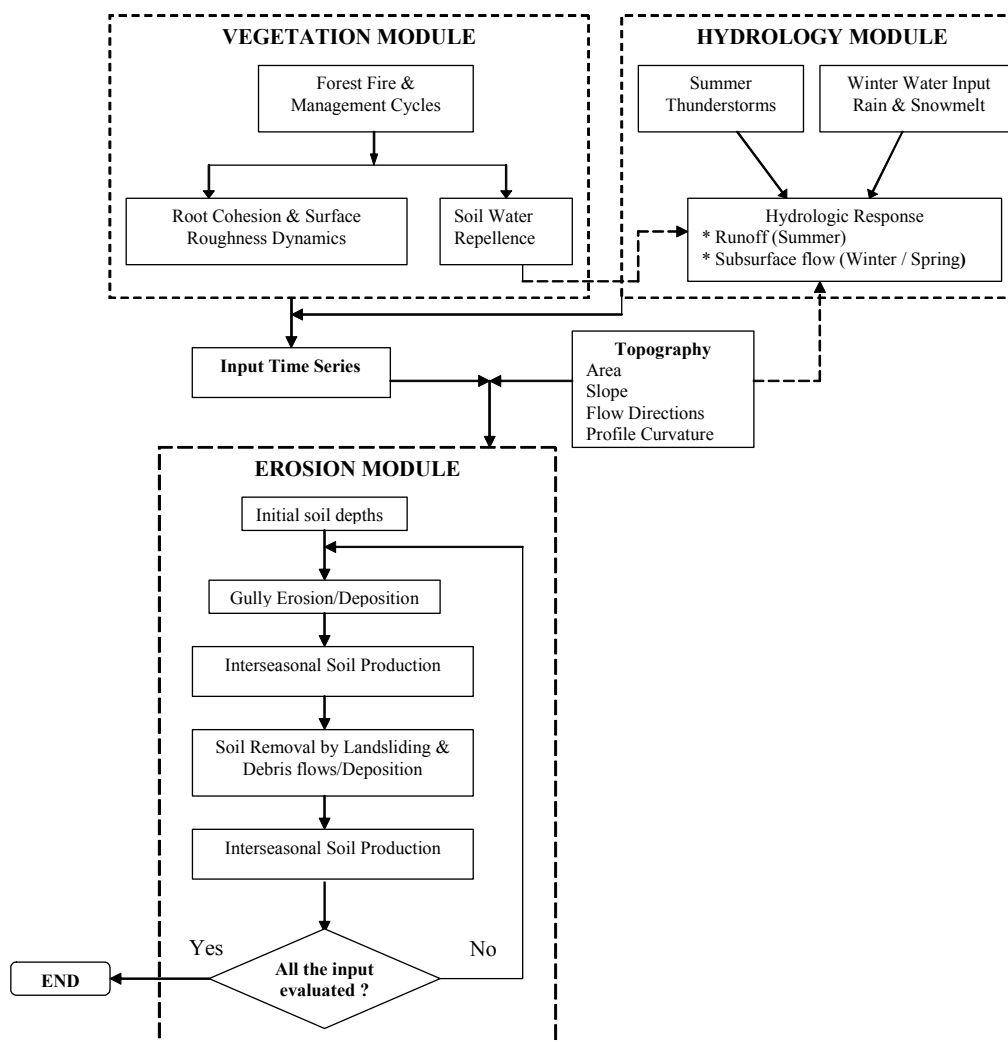
Figure 4-1. Model flow chart.

2. Study Site

The study area is a 3.8 km^2 watershed in the headwater drainages of Trapper

Creek within the North Fork of the Boise River (NFBR) in the southwestern Idaho

batholith (see Figure 4-1). Here we selected this site to take advantage of the available

data on event sediment yields [*Istanbulluoglu et al.*, (Chapter 3)]. We focused on the

headwaters of Trapper because the area is small enough to assume spatially uniform

climate, soil and vegetation characteristics [*Benda and Dunne*, 1997a; *Lancaster et al.*,

2001].
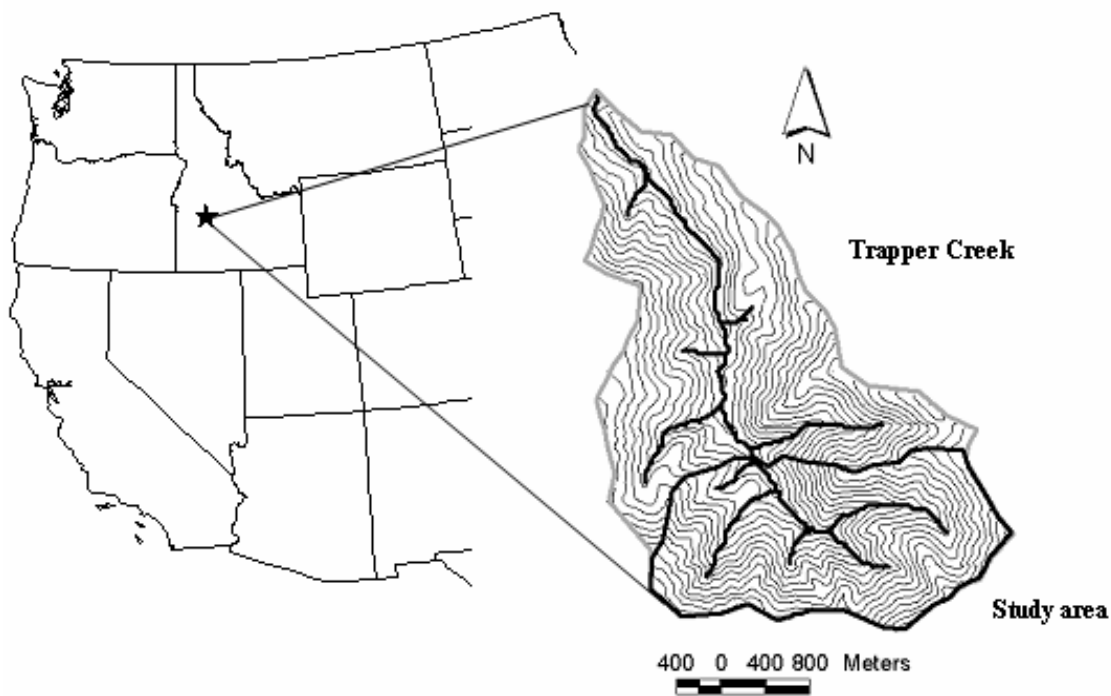
Figure 4-2. Trapper Creek watershed location map with the study basin outlined by a
black solid line.

The Idaho batholith consists of an extensive mass of granitic rock that covers a large portion of Idaho and some parts of Montana. In the study watershed valleys are typically narrow and V shaped with an average valley floor width of approximately 50 m. The elevation of the study watershed ranges from 1637 m to 2231 m above see level. The average slope is 47 % with a maximum of 98 % in the study area. The colluvium is grussy, clay-poor and was produced due to the disintegration of Idaho batholith rocks [*Meyer et al.*, 2001]. It shows little or no cohesion and is subject to runoff erosion and mass wasting especially following vegetation disturbances [*Gray and Megahan*, 1981].

Stand-replacing wildfires are often considered to be one of the major causes of the episodic erosion rates in Idaho [*Clayton and Megahan*, 1997]. They are mostly weather related and often ignited by lightning during summer drought conditions [*Barret et al.*, 1997]. The dominant overstory vegetation in the area is Douglas-fir and Ponderosa pine with an understory vegetation cover of mostly sage-grass. *Karsian* [1995] reports that in the current fire regime spanning roughly the last 2000 years, natural stand-replacing fires have a probability of $P_F = 0.005$ in a given summer in this region.

In the Idaho batholith about 60-70% of the precipitation falls as snow during the winter. Snow accumulation usually starts in the second half of October and continues till March when snowmelt starts. Snowmelt usually ends in April. Most of the remainder of the precipitation occurs as widespread low intensity long duration cyclonic storms in conjunction with snowmelt from March through May [*Megahan*, 1978; *Megahan et al.*, 1983; *Meyer et al.*, 2001]. In the summer-fall period similar cyclonic storms may occur, however high intensity short duration convective storms are more common in the summer

and fall. This type of storm usually produces localized heavy rainfalls in less than half an hour [*Meyer et al.*, 2001]. A storm intensity of 76 mm/h has a return period of 4 years in the central Idaho batholith [*Kidd*, 1964; *Clayton et al.*, 1979].

The Idaho batholith summer and winter climate regimes cause two distinct erosion patterns. Erosive overland flow is uncommon on undisturbed forested basins [*Megahan*, 1983; *Clayton and Megahan*, 1997]. Hydrophobic soil formation following wildfires [*Shakesby et al.*, 2000; *Benavides-Solorio and MacDonald*, 2001] significantly reduces the infiltration rates and promotes infiltration excess runoff generation especially in dry summer months. Extreme gully erosion initiated by high intensity thunderstorms is often observed during dry summer periods following forest fires [*Megahan*, 1992; *Meyer et al.*, 2001; *Istanbulluoglu et al.*, (Chapter 2)]. Soil water-repellence decreases or completely vanishes following prolonged rainy periods and spring snowmelts. During these wet periods saturation overland flow may develop [*Burcar et al.*, 1994; *Doerr and Thomas*, 2000; *Jaramillo et al.*, 2000; *Shakesby et al.*, 2000] and initiate slope failures [*Clayton and Megahan*, 1997].

3. Model Formulation and Initial Conditions

In every year of model simulation a winter/spring surface water input and a summer thunderstorm are modeled using probability distributions of the largest annual climate events observed in the region. Winter/spring water input increases pore-pressures and triggers shallow landsliding and debris flows that scour the soil to the watershed outlet. Summer thunderstorms trigger gully erosion. Soil production by bedrock weathering and accumulation due to creep occur continuously between erosion events.

Fires are simulated using a Poisson process. Vegetation death and regrowth is modeled to represent the response of surface roughness and root cohesion to disturbances. These responses are related to the mechanics of erosion and landslide initiation respectively. Initiation of fire induced hydropohobicity with wildfires and recovery of watershed infiltration capacity is modeled. The equations used to model these processes are described in the following sections.

3.1. Hydrology

3.1.1. Water input

In order to estimate the winter-spring water input rates we analyzed 20 years of available daily meteorological data for winter-spring months from three sites at elevations 1688, 1703 and 1830 meters approximately 20 miles SE of Trapper Creek (Atlanta stations). Daily water input rate, *wi* (mm/day) is calculated according to the difference between the snow depths, SD in subsequent days multiplied by the ratio of snow density to the density of water, RSW and adding the amount of precipitation, P observed in the same day,

$$wi_i = (SD_{i-1} - SD_i)RSW + P_i \qquad SD_i < SD_{i-1} \qquad \text{(1a)}$$

$$wi_i = 0 \qquad SD_i \geq SD_{i-1}. \qquad \text{(1b)}$$

When there is an increase in the snow depth between two daily observations the water input rate is taken 0, assuming that all the precipitation is in the form of snow. The equations above assume snowmelt and precipitation rates are steady throughout the day

and constant over the watershed. The largest water input rate of each year is selected. The cumulative distribution of these largest events corresponded well with the Extreme value type-I (Gumbel) distribution (Figure 4-3). The Gumbel distribution is often used for the extreme values of distributions that have an upper tail falling off in an exponential manner (eg., normal and gamma distributions) [*Benjamin and Cornell*, 1970]. In each yearly iteration of the model a random water input rate is generated from Gumbel distribution and used to calculate the maximum possible wetness parameter of the soil profile across the watershed. A random water input event is generated numerically as,

$$wi = F_{WI}^{-1}(\varepsilon) \tag{2a}$$

where

$$F_{WI}(wi) = \exp[-e^{-\alpha(wi-u)}]. \tag{2b}$$

In the equations, α and u are the parameters of the Gumbel distribution for *wi* and ε is a uniformly distributed random number between 0 and 1. Because we are using yearly time steps in the model, all the pore-pressure induced landsliding and debris flow activities in a year are associated with the maximum water input event. A similar assumption was also made by *Benda and Dunne* [1997a].
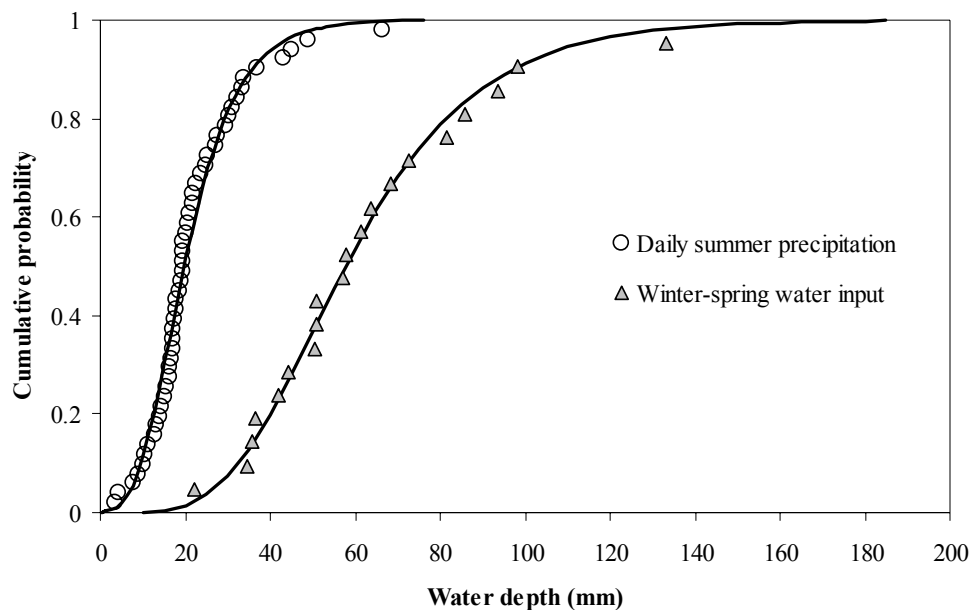
Figure 4-3. Cumulative Gumbel probability distributions fitted to the maximum annual daily water input rates calculated for the winter-spring period and daily summer thunderstorms observed in the area.

.
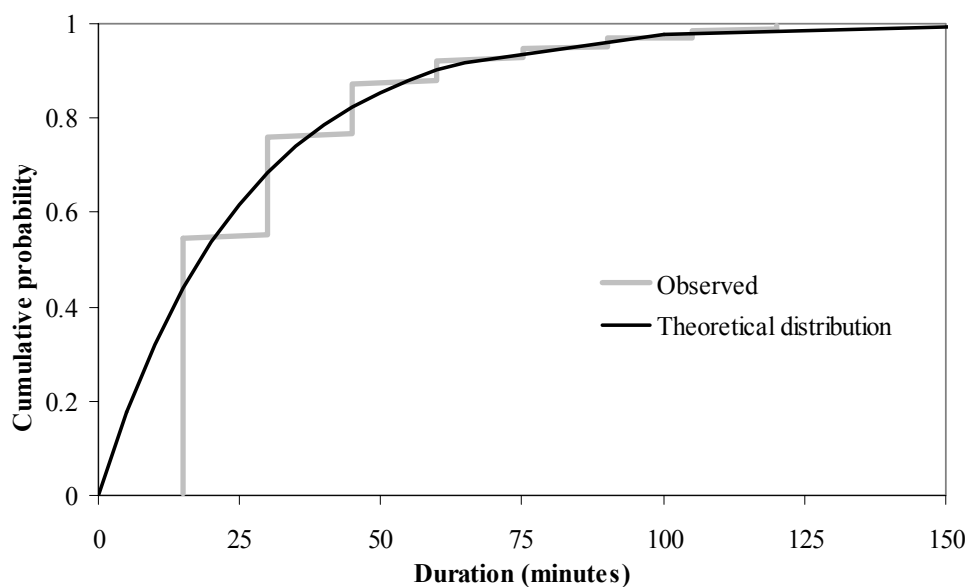
Figure 4-4. Cumulative exponential distribution fitted to observed thunderstorm durations. (The stepped nature of the observations is due to the 15 minute discretization of precipitation data)

We selected the maximum of daily summer precipitation events from 50 years of observations available in the area to characterize the extreme summer thunderstorms. These maximum daily values are used to obtain the parameters of the Gumbel distribution (2a and 2b) for summer thunderstorms (Figure 4-3). Table 4-1 includes the parameters from the Gumbel distribution fit to this data.

The analysis of daily water input alone does not provide information on storm duration. In order to approximate the durations associated with the thunderstorms we used the nearest rainfall gage that records 15 minute precipitation. This is further away approximately 60 miles South of Trapper Creek and at a lower elevation (862 m). Figure 4-4 shows that an exponential probability density function with a mean of 26 minutes fits the durations of all storms recorded at this location that occurred in the summer months (June - August) for the years 1972-2001.

Similar to the water input rates one random thunderstorm is used to model gully incisions in the area. This neglects the contribution to erosion from thunderstorms smaller than the maximum event. Average rainfall rate, $\bar{p}$ is calculated by dividing the total random precipitation depth, P by storm duration, D,

$$\bar{p} = P / D .\tag{3}$$

In the model D can be either held constant or selected at random from the exponential distribution. In sampling from the exponential distribution for D we censored the distribution to D>25 minutes. Because unreasonable $\bar{p}$ occurs if P is large and D is small.

The climate forcing (annual maximum winter and summer water inputs and durations) is assumed to be a stationary random process. This assumption neglects any changes in the climate regime. It has been reported that in the Western U.S. mountain erosion rates are not sensitive to moderate climate changes except glaciation [*Riebe et al.*, 2001; *Kirchner et al.*, 2001]. In the Idaho batholith long term sediment yield estimates from watersheds that show evidence of Pleistocene glaciation are in the same range as sediment yields observed in watersheds that were not glaciated [*Riebe et al.*, 2001; *Kirchner et al.*, 2001]. This field evidence made it possible to compare the model results driven by a stationary climate regime with the reported long term average erosion rates in the region.

3.1.2. Runoff generation

Considering the effects of soil disturbances on runoff generation, erosive runoff events are modeled by the infiltration excess runoff generation mechanism. Field observations of fire related hydrophobicity on small field plots show that hydrophobicity may significantly increase runoff rates [*Walsh et al.*, 1998; *Shakesby et al*., 2000; *Jaramillo et al.*, 2000]. However there is not yet much field information available on the spatial contiguity of hydrophobicity and its influence on watershed runoff generation [*Shakesby et al.*, 2000]. In the absence of detailed observations we assume that hydrophobic soils result in a fraction Δ of the watershed being impervious and that the average instantaneous runoff rate over an area is the sum of runoff generated on both pervious and impervious watershed fractions according to

$$r = \begin{cases} (p - I_c)(1 - \Delta) + p\Delta & p > I_c \\ p\Delta & p \leq I_c \end{cases}$$ (4)

where, p is the instantaneous precipitation rate, and I_c a uniform infiltration capacity across the watershed.

Rainfall rate is highly variable in time (e.g., in monthly and daily time periods, individual storms and during storms) and space [*Hutchinson*, 1995; *Schaake et al.*, 1996]. In a model of landscape evolution *Tucker and Bras* [2000] showed that variability in the average storm rates result in higher erosion rates because of the non-linearity of sediment transport to discharge. This led to higher drainage density and reduced relief in transport-limited catchments over geomorphic time scales. Similar to the variability in the average storm rates over the long term, temporal rainfall variability during storms which may trigger rapid fluctuations on the watershed hydrograph especially in small basins seems to be important for erosion modeling [*Smith et al.*, 1995]. Here we represented temporal rainfall variability during storms probabilistically. Gamma, exponential, Weibull, lognormal, skewed normal distributions are among the probability distributions used to characterize rainfall variability at different time scales [*Eagleson*, 1978; *Yu*, 1998]. We used the exponential distribution to characterize rainfall intensity variability during storms using the average rainfall rate given in (3),

$$F_P(p) = 1 - \exp(-\frac{p}{\overline{p}}) .$$ (5)

$F_P(p)$ is the cumulative distribution function for rainfall rate p, and gives the fraction of the storm duration when the rainfall rate is less than or equal to p [*Yu*, 1998]. The probability density function of runoff rate is obtained by solving equation (4) for p, $p = r + I_c (1 - \Delta)$ when $p > I_c$, and $p = r / \Delta$ for $p \leq I_c$, and substituting p into (5) and differentiating with respect to r,

$$f_R(r) = \begin{cases} f_{R1}(r) = (1/\Delta\overline{p})e^{(-\frac{r}{\Delta\overline{p}})} & r \leq I_c\Delta \\ f_{R2}(r) = (1/\overline{p})e^{(-\frac{r + I_c(1-\Delta)}{\overline{p}})} & r > I_c\Delta \end{cases} . \tag{6}$$

The expected value of the distribution in (6) is the mean runoff rate:

$$\overline{r} = \int_0^{I_c\Delta} r f_{R1}(r)dr + \int_{I_c\Delta}^{\infty} r f_{R2}(r)dr = \overline{p}\left[\Delta + e^{-I_c/\overline{p}}(1 - \Delta)\right]. \tag{7}$$
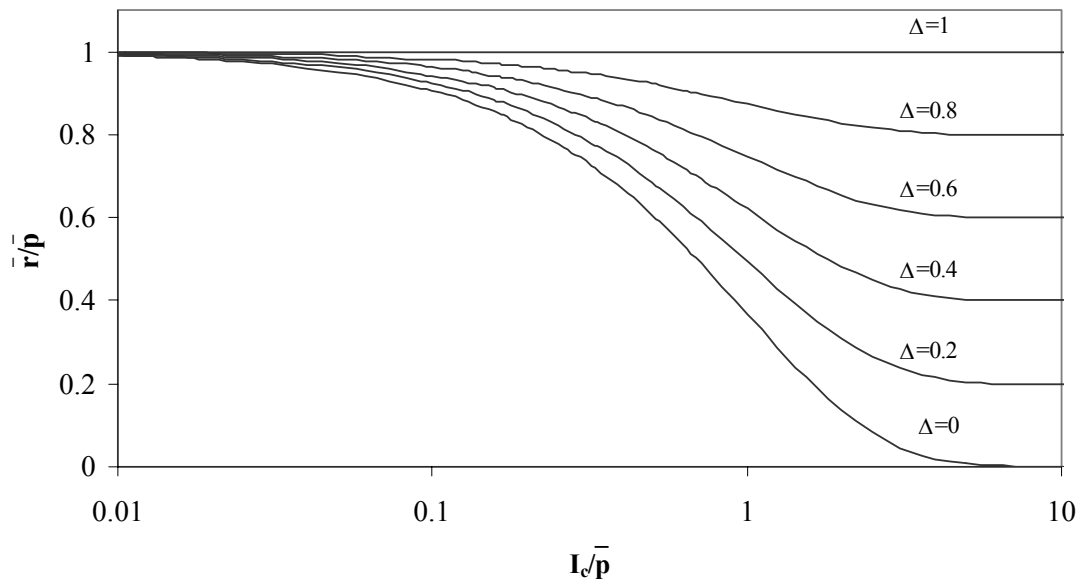
Figure 4-5. Relationship between the mean runoff rate and infiltration capacity both normalized by the mean storm rate for different impervious watershed fractions.

Figure 4-5 illustrates the behavior of equation (7) by plotting the mean runoff rate

nondimensionalized by the average storm rate as a function of the ratio of infiltration

capacity to the average storm rate for different impervious watershed fractions. The

figure shows that assuming rainfall variability during storms results in the generation of

runoff when the average storm rainfall rate is less than the watershed infiltration capacity

($I_c / \overline{p} > 1$).

3.2. Hillslope Mass Transport

In steep soil-mantled landscapes soil thickness plays an important role on slope

stability, the magnitude of landslide and debris flows and fluvial erosion rates [*Benda and*

Dunne, 1997a; *Tucker and Slingerland*, 1997]. Soil thickness shows significant spatial

variations [*Dietrich et al.*, 1995]. Soils are often thin or absent on steep ridges with

divergent morphology and in channels depending on the frequency of flow in the latter,

and usually thick in unchanneled valleys located in convergent topography [*Dietrich et*

al., 1995; *Tucker and Slingerland*, 1997; *Heimsath et al.*, 1997]. Modeling the temporal

and spatial variability of soil depths is crucial for long-term predictions of the frequency

and magnitude of hillslope erosion especially in mountainous settings [*Iida*, 1999]. In this

model soil development by "continuous" hillslope processes (chp) such as soil creep is

modeled based on the production rate of soil from the underlying bedrock and the

downslope change in the rate of slope dependent sediment transport, $q_s = -K\nabla z$. The

conservation of mass equation for soil thickness is written as [*Tucker and Slingerland*,

1997; *Heimsath et al.*, 2001]

$$\left.\frac{\partial h_s}{\partial t}\right|_{chp} = -\frac{\rho_r}{\rho_s}\frac{\partial z_{b-s}}{\partial t} + -\nabla(-K\nabla z) \,, \tag{8}$$

where h_s is the soil thickness, ρ_r and ρ_s are rock and soil bulk densities respectively, z is the elevation of the soil surface and z_{b-s} is the elevation of bedrock-soil interface, and $\partial z_{b-s}/\partial t$ is the lowering rate of the weathering front. In theory bedrock soil production rate is usually assumed as a function of soil depth [*Cox*, 1980; *Dietrich et al.*, 1995; *Heimsath et al.*, 1997]. In various theoretical relationships, the mechanical weathering rate is usually assumed to decrease exponentially with soil thickness, while chemical weathering is first assumed to increase with thickening soil, then attain a maximum value at some finite soil depth and then to decrease with further soil thickening. In seven different environments [*Heimsath et al.*, 1997, 1999, 2000, 2001] used cosmogenic radionuclide measurements and topographic controls on soil depth to quantify the soil production function. They consistently found that soil production rate declines exponentially with increasing soil depth. The distinctions between mechanical and chemical weathering in the Idaho batholith are obscure and they complement each other synergistically [*Clayton et al.*, 1979]. There are not enough field observations in the area to calibrate theoretical relationships between bedrock weathering rate and soil thickness. Therefore for the sake of simplicity we will use a constant rate of bedrock weathering in this paper. However this assumption should be taken with caution. For example without any gullying and landsliding soil depths will progressively thicken when the weathering rate is constant. Whereas steady-state soil depths may develop especially on planar and divergent slopes when bedrock weathering rate decreases exponentially with increasing

soil thickness. However soil creep from hillslopes to hollows is on the average two times

greater than soil production from bedrock weathering in the study watershed with the

selected parameter values presented in Table 4.1. Therefore we feel that limitations from

assuming a constant bedrock weathering do not significantly impact the results.

3.3. Gully Erosion

Channel initiation due to the concentration of dispersed overland flow into gullies

is identified based on a probabilistic threshold criterion. The probability of channel

initiation (PCI) at a point on the landscape is [*Istanbulluoglu et al.*, (Chapter 2)],

$$PCI = \text{Probability}(C \leq aS^{\alpha}) = \int_0^{aS^{\alpha}} f_c(C)dC \tag{9}$$

where $f_C(C)$ is a probability density function describing random spatial variability in C,

and α=1.167 for channel initiation due to overland flow [*Willgoose et al.*, 1991], a is

specific catchment area and S is topographic slope obtained from the DEM [e.g.,

Tarboton, 1997]. *Istanbulluoglu et al.* [(Chapter 2)] derived C based on the assumption

that channels are formed where overland flow shear stress exceeds a critical shear stress

threshold for incipient motion,

$$C = \left(\frac{\tau_{*c}(\rho_s - \rho_w)d_{50}}{\rho_w g n_{go}^{1.5}(n_{go} + n_{ao})^{-0.9}} \right)^{1.667} (1/r). \tag{10}$$

In this equation, τ_{*c} is the nondimensional critical shear stress, ρ_w, ρ_s are water and

sediment density, g is gravity of acceleration, n_{go} is Manning's roughness coefficient for

overland flow on bare soil calculated as a function of median sediment size d_{50} from Strickler's equation [*Julien and Simons*, 1985], n_{ao} is the additional roughness of overland flow. In the PCI theory [*Istanbulluoglu et al.*, (Chapter 2)] d_{50}, n_{ao}, n_{go}=f(d_{50}) and r are random variables.

Here we employed a Monte Carlo simulation approach to calculate the mean and variance of the C thresholds (10) to characterize the probability distribution of the spatial variability of C thresholds for each annual storm event using 1500 random numbers for d_{50} and n_{ao}. The mean and variance of C are then used to parameterize a Gamma distribution used to represent PCI at each grid cell. The gamma distribution was shown [*Istanbulluoglu et al.*, (in press)] to provide a reasonable match to the distributions of area-slope thresholds measured and modeled at channel heads in the field. Although *Istanbulluoglu et al.*, (in press) modeled the spatial variability in r using a uniform distribution for a thunderstorm event in Trapper Creek here we ignored the spatial variability in r and took the mean runoff rate (7) as a constant input in the Monte Carlo procedure for each annual storm event. Uncertainty in n_{go} is characterized using field observations of median sediment sizes that showed a log-normal distribution [*Istanbulluoglu et al.*, (Chapter 2)]. In this paper we assume that n_{ao} is solely due to vegetation roughness, n_V. Vegetation is subject to wildfire and harvest disturbances, therefore n_V exhibits temporal variations due to the interaction between the rate and magnitude of disturbances and the vegetation regrowth rate. We model the temporal variability in n_V for each summer period (see section 3.5.2) assuming spatially uniform vegetation disturbance and growth. We assume that the modeled n_V for each summer

represents a spatially average value for vegetation roughness. Spatial variability in vegetation roughness is characterized using a uniform distribution between upper and lower bounds that average to the n_V modeled for each summer. *Istanbulluoglu et al.* [(Chapter 3)] used uniformly distributed additional roughness values between 0.015 and 0.1 which describe ± 73.4 % deviation from the mean value of 0.0575. Assuming that ± 73.4 % deviation is constant for every summer, maximum value for additional roughness is calculated by $n_v + 0.734.n_V$ and the minimum value by $n_v - 0.734.n_V$ and they are used as the upper and lower bounds of the uniform distribution selected for additional roughness.

An undisturbed channel network is defined by referring to Robert E Lee Creek, a neighboring drainage to Trapper Creek that was not significantly influenced by the wildfire in 1994 [*Istanbulluoglu et al.*, (Chapter 2)]. Based on field observations of seepage and saturation excess overland flow we found that a channel initiation threshold, $C_F = 500$ m, used with $aS^\alpha > C_F$ mapped the channels in Robert E Lee Creek from the DEM. Episodic erosion is assumed to only occur in years when the average of the 1500 simulated C values (equation 10) is less than C_F. In these years a PCI grid is defined for each simulated thunderstorm and erosion is calculated using the method given below.

For channels where easily detachable non-cohesive material is available, flow is often assumed to be at its sediment transport capacity. This assumption limits the sediment transport, and the erosion amount from a location would be equal to the excess (downstream change) of sediment transport capacity [*Willgoose et al.*, 1991; *Tucker and Bras*, 1998],

$$-\frac{\partial h_s}{\partial t}\bigg|_{fluvial} = \frac{\rho_s}{\rho_b}\nabla q_s,$$ (11)

where, q_s is unit sediment discharge (L^2/T), ρ_b is soil bulk density.

The instantaneous sediment discharge in a channel can be modeled as a non-linear function of shear stress in excess of a threshold,

$$Q_s = \gamma W_f(\tau_f - \tau_c)^{p_f},$$ (12a)

where

$$\gamma = \frac{\kappa\sqrt{g(s-1)d^3}}{(\rho_w g(s-1)d)^{p_f}}$$ (12b)

in the equations, Q_s is the volumetric sediment discharge (L^3/T), τ_f is the shear stress acting on grains, τ_c is critical shear stress, γ is a transport coefficient, κ is a constant, d is sediment size and p_f is an exponent that is typically 1.5 for bedload and higher for total load equations [*Garde and Raju*, 1985]. Assuming steady, uniform flow and using Manning's equation for flow velocity, flow width and effective shear stress can be written as a power function of discharge and slope,

$$W_f = \chi_w Q^{m_w} S^{n_w}$$ (13a)

$$\tau_f = \chi_\tau Q^{m_\tau} S^{n_\tau}$$ (13b)

where the parameters χ_w and χ_τ are functions of channel cross-section shape and the latter both channel shape and roughness. The exponents are m_w=0.3, n_w=-0.1875, m_τ=0.6 and n_τ=0.8125 (for derivations see e.g., *Willgoose* [1989] and *Istanbulluoglu et al.*, [(Chapter 3)]). Substituting (13a) and (13b) into (12), and assuming τ_c=0, sediment transport capacity as a function of discharge and slope is written as,

$$Q_s = \left\langle \gamma \chi_w \chi_\tau^{P_f} \right\rangle Q^M S^N .$$ (14)

Discharge and slope exponents are $M = p_f m_\tau + m_W$ and $N = p_f n_\tau + n_W$ respectively. Here we assume τ_c=0 for sediment transport in gullies. Under high shear stresses τ_c does not have much influence on sediment transport [*Istanbulluoglu et al.*, (Chapter 3)].

In order to write Q in terms of runoff we assumed that the instantaneous discharge is proportional to the instantaneous runoff rate that is uniform across the basin and drainage area,

$$Q = rA .$$ (15)

Substituting (15) into (14) gives sediment transport as a function of drainage area and slope. We now obtain the average sediment transport rate of a storm by integrating the instantaneous sediment transport capacity equation over the probability distribution of runoff during a storm (6) and multiplying with PCI,

$$\overline{Q}_s = PCI \int_0^\infty Q_s f(r)dr = \left\langle \gamma \chi_W \chi_\tau^{P_f} \int_0^\infty r^M f_R(r)dr \right\rangle A^M S^N PCI .$$ (16)

This integral is solved analytically. Here we reported the equation as a function of a parameter that absorbs all the hydrologic and hydraulic variables χ_{Q_s}, and topographic variables A, S and PCI as

$$\overline{Q}_s = \chi_{Q_s} A^M S^N PCI \tag{17a}$$

where χ_{Q_s}:

$$\chi_{Q_s} = \gamma \chi_W \chi_\tau^{p_f} \overline{p}^M [\Delta^M \Gamma(M+1, \frac{I_c}{\overline{p}}) + e^{-I_c(1-\Delta)/\overline{p}} (\Gamma(M+1) - \Gamma(M+1, \frac{I_c \Delta}{\overline{p}}))] \tag{17b}$$

where $\Gamma(\ )$ is the gamma function and $\Gamma(\ ,\ )$ the incomplete gamma function [*Benjamin and Cornell*, 1970]. In equations (9) and (10) PCI is a function of r. However we feel that the PCI concept is applicable to time intervals longer than storm events, not within storm variability in r, therefore we used PCI as a function of $\overline{r}$ from equation (6) in equation (16) rather than including it in the integral.

3.4. Landsliding and Debris Flows

Recent technology for the mapping of landslide susceptibility uses the infinite slope stability equation to map the areas prone to shallow landsliding based on DEMs [*Montgomery and Dietrich*, 1994; *Wu and Sidle*, 1995; *Pack et al.*, 1998]. The infinite slope stability model we used is in the form given by [*Pack et al.*, 1998];

$$FS = \frac{C_r + C_s}{h_s \rho_b g \sin \theta} + \frac{\cos \theta \tan \phi [1 - Rw\rho_w / \rho_b]}{\sin \theta} \tag{18}$$

where C_r and C_s are root and soil cohesion, respectively; h_s is the soil thickness perpendicular to slope, θ and ϕ are slope angle of the ground and soil internal friction angle, respectively; Rw is the relative wetness which is defined as the ratio of subsurface flow depth flowing parallel to the soil surface to soil thickness. Assuming that lateral discharge at each point is in equilibrium with a steady state water input rate wi (L/T) and that the capacity for lateral water flux at each point is $K_s h_s Sin\theta$, where K_s is the lateral saturated hydraulic conductivity (L/T) of the soil, Rw is written as the ratio of lateral discharge to the lateral flux capacity,

$$Rw = \min\left(\frac{wia}{K_s h_s \sin\theta}, 1\right). \tag{19}$$

The relative wetness has an upper bound of 1 with any excess assumed to be saturation excess overland flow.

In the V-shaped hollows of the Idaho batholith landslides are mostly triggered by spring snowmelt and rain on snow events when the hollow axis is saturated. This saturated slide material often triggers a debris flow that erodes the hollow axis to bedrock or flows in pre-existing gullies [*Megahan et al.*, 1978]. Although the physics of debris flow scour is as yet poorly understood [*Jan and Shen*, 1997] (for example the influence of standing tress and topographic shape to local scour) erosion in debris flow channels may be modeled using a generic excess shear stress erosion law similar to (12) [*Lancaster et al.*, 2001]. According to excess shear stress erosion theories we may expect erosion to be a function of the product of drainage area and slope [*Whipple and Tucker*, 1999; *Niemann*

et al., 2001]. However we could not infer much dependence between topography and local scour in the field data we obtained from a debris flow in the South Fork of the Payette River (SFPR) basin in the Idaho batholith. Instead we observed completely scoured debris flow runout channels. In the model we assumed that all the unstable elements where FS<1 produce landslides that trigger debris flows and completely scour the colluvium to bedrock. This assumption is consistent with the field observations both in the Idaho batholith [*Megahan et al.*, 1978] and in the Pacific Northwest where channels with slopes greater than 10° are usually scored to bedrock by debris flows [*Benda and Cundy*, 1990]. Debris flows are routed downhill in the steepest direction toward one of the eight surrounding grid cells. *Benda and Cundy* [1990] and *Benda and Dunne* [1997a] used a critical channel slope criteria of 3.5^o to predict locations of debris flow deposition. The average main channel slope obtained from the DEM for the study watershed used in this paper is 6°. Therefore no debris flow deposition is assumed in the basin. This is also consistent with or observations in the field that no significant deposition was observed in the study area after an intense debris flow erosion event.

3.5. Vegetation Component

Vegetation roots tend to stabilize the slopes by providing root cohesion. In the infinite slope stability model factor of safety, FS (equation (18)) is linearly proportional to root cohesion. Similarly field observations show that presence of surface vegetation cover protects the land from erosion by increasing the erosion thresholds [*Prosser and Dietrich*, 1995]. In the PCI theory channel initiation threshold increases as a function of additional roughness (see equation 10). Here we modeled the death and regrowth of tree

roots that provide deep root cohesion and vegetation cover. We also modeled the temporal behavior of the hydrophobic impermeable watershed fraction, Δ by relating the recovery of hydrophobicity to vegetation cover spread. We divided the vegetation into two groups, overstory and understory vegetation. Root cohesion provided by the understory vegetation is ignored due to its relatively lesser contribution and the understory vegetation cover is assumed to provide additional roughness on the surface that enhances the surface resistance to erosion.

3.5.1. Root cohesion

The net root strength of a forested hillslope parcel subject to vegetation removal is the sum of decaying root cohesion due to the removed trees and regeneration of the root cohesion by new growing plants [*Sidle*, 1992]. The rate of root strength decay following vegetation disturbances has been shown to follow a negative exponential function [*Sidle*, 1992],

$$D_r = \exp(-k_C t^{n_C}) \tag{20}$$

where, D_r is dimensionless root strength decay ($0 < D \leq 1$), t is time since the vegetation removal and k_C and n_C are vegetation dependent empirical constants. *Sidle* [1991, 1992] described the rate of root regrowth of planted or invading vegetation by a sigmoid curve,

$$R_r = c_C + 1/(a_C + b_C \exp(-\xi_C t)) \tag{21}$$

where, R_r is the dimensionless root strength recovery ($0 < R_r \leq 1$) and a_C, b_C, c_C and ξ_C are empirical constants. The total root cohesion following vegetation death is,

$$C_r(t) = C_{pre}D_r(t) + C_m R_r(t).$$ (22)

In the equations; t is the time after disturbance, C_{pre} is the root cohesion at the time of vegetation disturbance and C_m is mature root cohesion. This equation says that as the root cohesion of the disturbed trees decay from a pre-disturbed cohesion value, vegetation invading the site starts producing cohesion and can grow up to maturity.

3.5.2. Vegetation roughness

Vegetation increases the total flow roughness and reduces the fraction of shear stress acting solely on soil grains. A very simple approach to calculate vegetation roughness is used in this paper. For a more sophisticated physical approach the reader is directed to [*Freeman et al.*, 2000].

In order to model the influences of the understory vegetation on erosion rates over time, we first related vegetation cover conditions to overland flow vegetation roughness, n_V and second developed a theory to model the temporal variations in the understory vegetation cover to obtain temporal dynamics of vegetation roughness.

The flow roughness coefficients for stream channels and water conveyance structures under different channel cover material, shape, irregularity etc., have been documented [*Chow*, 1959; *Arcement and Schneider*, 1984]. However very few data sets exist for shallow overland flow roughness on natural surfaces. Overland flow roughness values obtained from experimental studies are often classified for different surface cover and treatment conditions such as sparse, poor, good vegetation cover, etc. [*Ree et al.*, 1977; *Foster et al.*, 1980; *Engman*, 1986]. These observations suggest a connection

between cover density and roughness. Based on this field evidence we start with

assuming that surface roughness provided by a certain type of vegetation can be

considered proportional to its fractional ground cover, F_{gc}, $n_v \propto F_{gc}$, which could range

from 0 to a maximum value under optimum growth conditions $F_{gc} \leq \max F_{gc} \leq 1$. We

further assume that the proportionality of fractional ground cover of a vegetation type to

the fractional ground cover of a reference vegetation, F_{gc}^R that has a known roughness

coefficient, n_v^R is equal to the fraction of their roughness values,

$$\frac{F_{gc}}{F_{gc}^R} = \frac{n_v}{n_v^R}. \tag{23}$$

This assumption allows us to estimate the roughness of any type of vegetation from its

ground cover by comparing it to the fractional cover of the reference vegetation,

$$n_v = n_v^R \frac{F_{gc}}{F_{gc}^R}. \tag{24}$$

Here dense forest cover is selected as the reference vegetation and its fractional ground

cover is assumed 1.

Fires and forest harvests may disturb all of the understory vegetation or some

fraction of it. In this model we assumed that both disturbances kill all the understory

vegetation. After vegetation is disturbed it will regrow in time and the surface resistance

to erosion will gradually recover to pre-fire levels. This regrowth time frame may range

from several months to years depending on the vegetation and site conditions [*Megahan*

and Molitor, 1975; *Prosser and Soufi*, 1998; *Prosser and Williams*, 1998]. The rate of biomass regrowth is often related to soil productivity, seasonal and site specific conditions such as temperature and soil moisture, solar radiation, available plant biomass and ground cover density [*Alberts et al.*, 1989; *Arnold et al.*, 1995; *Tucker and Bras*, 1999]. Here we took a very simple approach to modeling surface vegetation growth. We ignored the influences of seasonal and site conditions to the biomass growth rate and assumed that the rate of biomass growth, dB_m / dt is proportional to a potential rate of biomass growth rate on a bare soil, k_B and the existing vegetation ground cover fraction according to

$$\frac{dB_m}{dt} = k_B k_V (1 - F_{gc}) \tag{25}$$

where, k_V is an hypothesed parameter to relate the available bare soil surface to the growth rate. This equation says that biomass growth rate will be relatively fast immediately after a vegetation disturbance (i.e., because of the availability of soil supplies necessary for plant growth) and it will approach to zero as the ground is fully covered with vegetation (i.e., due to the competition for supplies).

In the WEPP model [*Alberts et al.*, 1989; *Arnold et al.*, 1995; *Tucker and Bras*, 1999] an exponential relationship is used to relate vegetation canopy cover, plant height and plant ground cover to vegetation biomass. Fractional ground cover as a function of biomass is written as

$$F_{gc} = 1 - e^{-B_m B_c} . \tag{26}$$

where B_c is a plant related constant. Substituting (26) into (25) gives the rate of biomass growth as a function of available biomass,

$$\frac{dB_m}{dt} = k_B k_V e^{-B_m B_c}.$$
(27)

With the assumption that disturbance completely removes the understory vegetation, we solve this equation starting from $B_m=0$ at $t=0$. This initial value problem can be solved by separating variables and integrating to give

$$B_m = \frac{1}{B_c} Ln(k_B k_V B_c t + 1).$$
(28)

Now substituting (28) into (26) gives the fractional ground cover as a function of time following vegetation death,

$$F_{gc}(t) = 1 - 1/(k_B k_V B_c t + 1).$$
(29)

and substituting (29) into (24) and limiting the fractional ground cover to a maximum value that the plants can cover, Manning's roughness of understory vegetation as a function of time can be written as

$$n_v(t) = n_v^R \frac{\min[1 - 1/(k_B k_V B_c t + 1), F_{gc}^{max}]}{F_{gc}^R}.$$
(30)

3.5.3. Hydrophobic soil formation
and recovery

Here a very simple approach is described to model the effects of water repellency on runoff generation and soil erosion. We assume that water repellence due to wildfires is only experienced by some fraction of a devegetated surface, R_f. We write the post-fire pervious fraction, P_f^{post} of a burnt area as a reduced fraction of its pre-fire pervious fraction, P_f^{pre} as

$$P_f^{post} = P_f^{pre}(1 - R_f)$$ (31)

We assume that as vegetation grows on a devegetated impervious surface, vegetation roots will break the water repellent layers, form preferential micro channels and enhance the infiltration rates [*DeBano*, 1981; *Shakesby et al.*, 2000]. Therefore the impervious fraction of an area after a wildfire, $(1 - P_f^{post})$ will gradually recover in time as the ground cover increases, and it is completely removed when the ground cover fraction attains its maximum possible value. Changes in the pervious fraction following wildfires is therefore modeled based upon the vegetation recovery equation (29) as

$$P_f(t) = P_f^{post} + \frac{\min[1 - 1/(k_B k_V B_c t + 1), F_{gc}^{max}]}{F_{gc}^{max}}(1 - P_f^{post}),$$ (32)

and the impervious fraction of the watershed, Δ is

$$\Delta(t) = 1 - P_f(t).$$ (33)

Δ is used in equations (6, 7 and 17b) to relate fire induced hydrophobicity to runoff generation and erosion processes.

The vegetation model is calibrated based on the field observations of vegetation response to disturbances in the Idaho batholith. Figure 4-6 shows an example of the vegetation response to wildfire disturbances by plotting the dimensionless root cohesion (21), vegetation roughness (as the ratio of fractional ground cover recovery in time (29) to the fractional ground cover prior to wildfires) and hydrophobicity (as a fraction of water-repellent watershed area (33)) based on the model parameters given in Table 4-1 selected to be representative of the region (see section 3.6). In the example fire consumes all the vegetation at time 0. The destruction of the surface vegetation biomass abruptly brings down the vegetation roughness to a selected residual value and causes hydrophobicity. Understory vegetation typically recovers within several years following wildfires and breaks the hydrophobic soil layers (Figure 4-6), as was suggested by field observation [*Benavides-Solorio and MacDonald*, 2001; *Megahan*, 1992; *Inbar et al.*, 1998]. During the understory vegetation recovery period significant soil erosion may be observed due to low surface roughness values that increases the fraction of shear stress acting on soil grains and enhanced runoff generation due to hydrophobicity [*Wells*, 1987; *Cannon et al.*, 1998; *Benavides-Solorio and MacDonald*, 2001]. Root cohesion produced by trees attain the lowest levels in 10 years following the wildfire and leave the land susceptible to landsliding and debris flow generation [*Megahan et al.*, 1978; *Gray and Megahan*, 1981]. Finally about 80 % of the mature root cohesion recovers by the end of 60 years after tree death.

3.6. Initial Conditions and Parameter Values

The model parameter values that we think best represent the climate, erosion and vegetation conditions in our study watershed in the Idaho batholith are given in Table 4-1. These are used in the model runs presented later, except where we mention specific parameters changes implemented to explore specific hypotheses or sensitivities.

Climate parameters are obtained from the climate data available in the area (described in Section 3.1.). Nondimensional watershed infiltration capacity for an average storm rate ($I_c / \bar{p}$ where, $\bar{p} = (\overline{PD}^{-1})$) is taken as 10. This gives $I_c \tilde{=} 400$ mm/h. According to the rainfall-runoff model developed in this paper a nondimensional infiltration capacity of 10 does not generate runoff from average storm rates when the impervious fraction of the watershed, Δ is 0 (Figure 4-5). This is consistent with the field observations in the area [*Megahan*, 1983].

Lateral flow transport in the soil is controlled by the saturated lateral hydraulic conductivity, K_s. Saturated lateral hydraulic conductivity may vary orders of magnitude in the field [*Moore et al.*, 1986; *Lancaster*, 2001]. In our model the smaller (or higher)
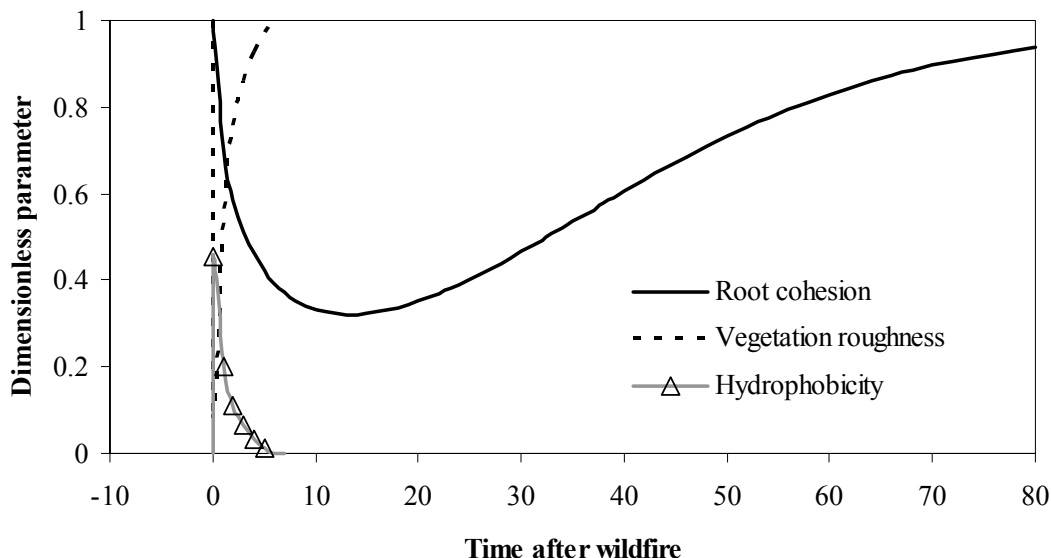
Figure 4-6. Vegetation response to wildfire disturbances based on the vegetation model parameters reported in Table 4-1 selected for Idaho batholith conditions.

the K_s, the higher (or lower) the frequency of failures. Landslides and debris flows remove soil from hillslopes. Therefore an increase in K_s in the model allows thicker soil depths to develop or vice versa. Here we calibrated K_s by running simulations with different K_s values and selected K_s= 60 m/day. This selected value produces soil depths ~1 m on the hollow axis under the current climate and fire regime and is consistent with our field observations. For comparison *Montgomery* et al. [2002] reported saturated lateral hydraulic conductivity values from 8 m/day up to 86.4 m/day in the Oregon cost range.

To apply the soil development model for continuous hillslope processes (8) we need an estimate of the diffusion constant, K, the bedrock weathering rate, $\partial z_{b-s} / \partial t$ and the ratio of bedrock to soil density. All these parameters are assumed to be spatially and temporally constant in the model. Typical values are used for the bedrock and soil bulk

Table 4-1. Constant Model Parameter Values Used in Simulations

Parameter	Value	Applicability	Source
Mean summer precipitation depth & duration; $\overline{P}$, $\overline{D}$	21.6 mm, 0.5 h	Trapper Creek	Weather station data
Mean winter water input rate; $\overline{wi}$	42 mm/day	Trapper Creek	Weather station data

Parameters of Gumbel probability distribution;
  Winter/spring water input; u, α
  Summer thunderstorms; u, α
	
	50 mm/day 0.048 day/mm
	16.64 mm/day 0.1 day/mm
		Trapper Creek area	Distribution parameters fit to climate data.

Dimensionless infiltration capacity; $I_c/(\overline{P}\,\overline{D}^{-1})$	10		Selected so that surface runoff does not occur under undisturbed conditions. Corresponding I_c = 400 mm/h
Saturated lateral hydraulic conductivity; K_s	60 m/day	Trapper Creek	Calibrated
Weathering rate constant; $\partial z_{b-s}/\partial t$	1.1 x 10^{-4} m/y	Idaho batholith	*Kirchner et al.* [2001]
Diffusion constant; K	4 x 10^{-4} m^2/y	Trapper Creek	Measured in the field by L. Benda and D. Miller based on the method described in *Benda and Dunne* [1998a]
Rock, sediment and soil bulk density; ρ_r, ρ_s	2650 and 1500 kg/m^3	Universal	
Sediment transport rate constant and exponent; κ, p_f	20, 3	Steep slopes with non-cohesive sediment	Calibrated using data from Trapper Consistent with *Govers* [1992]
Transport coefficient; γ	1.15 x 10^{-7} m^{5}s^{5}kg^{-3}	Theoretical	Chapter 3
Shear stress constant; χ_τ	303 kg m$^{-2.8}$ s$^{-1.4}$	Theoretical	Chapter 3

Table 4-1. Constant Model Parameter Values Used in Simulations, Continued.

Parameter	Value	Applicability	Source
Flow width constant; χ_W	$0.9 \text{ m}^{0.1} \text{ s}^{0.3}$	Theoretical	Chapter 3
Median size of sediment in transport; d	3 mm	Trapper Creek	Field data
Internal friction angle; ϕ	38°	Idaho batholith	*Hampton et al.* [1974]
Mature root cohesion; C_m	9 kPa	Douglas fir	*Burroughs and Thomas*
Root strength parameters for decay; k_C, n_C	0.376, 0.595	parameters for the	[1977] and *Sidle* [1991]
Root strength parameters for regrowth; a_C, b_C, c_C, ξ_C	$0.85, 4.7, -0.18, 0.057 \text{ yr}^{-1}$	Rockies.	
Overland flow roughness for mature forest; n_V^m	0.8	Universal	*Huggins and Burney* [1982]
Maximum fractional ground cover; $max (F_{gc})$	0.8	Idaho batholith	*Clayton and Megahan* [1997]
Biomass growth on a bare surface; k_B	$1.4 \text{ kg m}^{-2} \text{ yr}^{-1}$	Idaho batholith	Calibrated based on the observed surface
Plant related constant; B_c	1 kg^{-1}		vegetation recovery rates *Megahan* [1992]
Probability of wildfire; P_F	0.005	Trapper Creek	Kathleen G-Hayes' unpublished data.

densities (Table 4-1) [*Clayton and Megahan*, 1997]. No field observation exists for the long term bedrock weathering rates in our field area. Long term average weathering rates may be inferred from the sediment mass balance of watersheds assuming that under dynamic equilibrium the sediment carried away from the basin is equal to the amount produced from bedrock [*Clayton and Megahan*, 1986; *Kirchner et al.*, 2001]. Here we used a denudation rate of 1.1×10^{-4} m/y for bedrock weathering. This value is the average of the rates reported for some watersheds in the Idaho batholith that are close to the size of our study area [*Kirchner et al.*, 2001]. The diffusion constant was estimated by L. Benda and D. Miller from field observations by solving the slope dependent linear sediment transport equation, $q_s = K|\nabla z|$ for the diffusion constant, K using estimated sediment fluxes, q_s from dated colluvium samples [*Benda and Dunne*, 1998a]. When surveying the sample sites slope gradients were measured over distances commensurable to those estimated from the DEMs with the intent that the numbers obtained could be used directly with a DEM to model soil flux volumes. Diffusion constants were found in the range of 1 to 9×10^{-4} m^2/y with an average rate of 3×10^{-4} m^2/y. In the soil evolution theory (8) spatial variation of curvature dictates spatial variation in local soil thicknesses. On divergent hillslopes where $\nabla^2 z < 0$, bedrock appears at the surface when

$$-(\frac{\rho_r}{\rho_b}\frac{\partial z_{b-s}}{\partial t})/K \geq \nabla^2 z. \tag{34}$$

In the field we have observed bed rock on sharply curved ridge tops and topographic noses. Experimenting with different diffusion constant estimates from field observations

using (34), we found that K= 4 x 10^{-4} m^2/y gives reasonable bedrock exposure patterns over the study watershed and therefore used this value in all simulation runs.

Parameters of the fluvial sediment transport model are obtained from [*Istanbulluoglu et al.* (Chapter 3)]. A parabolic flow cross-section with a constant width to depth ratio of 2 is used. Soil internal friction angle is taken as 38^0 based on *Hampton et al.* [1974] who reports observations from various watersheds in the Idaho batholith. Clayton's data has 50 observation points with a mean and a standard deviation of 38° and 5.5^o, respectively, and ranges between 27° and 48.5^o.

A Manning's roughness value of 0.8 for timberland with deep forest litter and dense grass was reported [*Huggins and Burney*, 1982]. *Engman* [1986] reported overland flow Manning's roughness up to 0.66 for grass. We took 0.8 for the reference Manning's roughness coefficient for overland flow (23). *Clayton and Megahan* [1997] reported ground cover fractions of an undisturbed forest floor in south central Idaho batholith for a period of 4 years in the range of 0.2 to 1 with an average of 0.8. In the model we set the maximum fractional ground cover of the understory vegetation (30) to 0.8. This predicts that when the understory vegetation grows to maturity it will provide a vegetation roughness of 0.64. For comparison this value is a little less than the upper value for the Manning's roughness coefficient for grass [*Engman*, 1986].

Root strength parameters for decay ($k_C = 0.376$, $n_C = 0.595$) and regrowth ($a_C = 0.85$, $b_C = 4.71$, $c_C = -0.18$, $\xi_C = 0.057$ yr^{-1}) and mature cohesion ($C_m = 9$ kPa) of the root cohesion model are selected for Rocky Mountain Douglas fir [*Burroughs and Thomas*, 1977; *Sidle*, 1991]. We used the potential rate of understory vegetation biomass growth

on a bare surface, $k_B = 1.4$ kg/m^2/yr in (25). This biomass growth rate, with $B_c = 1$ kg^{-1} in (26) provides 80% of the post-fire fractional ground cover recover in the third year following wildfires (29) as was suggested in field observations [*Meyer et al.*, 2001; *Benavides-Solorio and MacDonald*, 2001].

We obtained an initial condition for soil depths by allowing soil evolution by diffusion and bedrock weathering over 3000 years (as in e.g., *Dietrich et al.*, [1995]). This procedure fills the hollows with colluvium and develops thinner soils on the ridges. In each of the simulations described below the model is run for 10,000 years. The first 3000 years in each simulation is taken as a spin up period to limit the sensitivity to the initial conditions. This period was chosen by plotting the average soil thickness in the eroding portions of the watershed (Figure 4-7).

4.   Results and Discussions

4.1. Varying Root Cohesion

First we consider the case where forests are not disturbed by either fires or human activities and geomorphic response is not influenced by such disturbances. Under this assumption the triggering mechanism for erosion and mass movements is the combination of climate forcing and the thickening of colluvium. Different forest vegetation types or the same vegetation type under various soil productivity conditions may provide different values of root cohesion [*Gray and Megahan*, 1981]. Here we performed 4 simulation experiments with progressively increasing root cohesion. We first used 1 kPa to characterize a generic poor forest growth condition [*Sidle*, 1991].
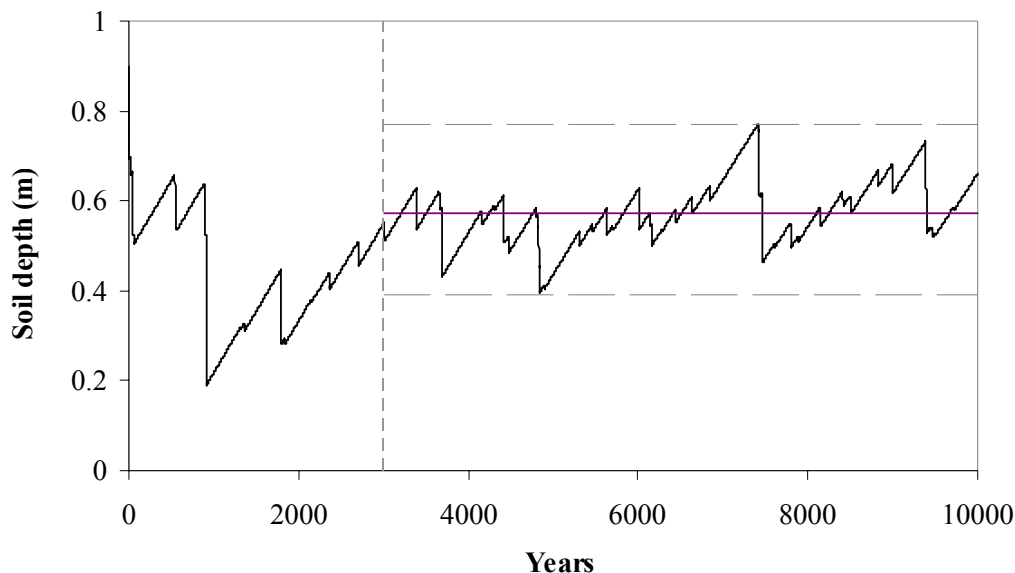
Figure 4-7. Variation of the soil thicknesses in the eroding portions of the watershed during 10,000 years. The model is driven by a stochastic climate and forest fires with a return interval of 200 years. Vegetation is Rocky Mountain Douglas fir with C_m= 9 kPa. The vertical dashed line separates the spin up period of the model (0-3,000 years) from the experimental period (3,000 to 10,000). Horizontal lines show the minimum, average and maximum average soil depths.

Mature root cohesion for Rocky Mountain Douglas fir (dominant vegetation in our

watershed) was reported in the range of 4 to 14 kPa [*Burroughs and Thomas*, 1977;

Hammond et al., 1992]. We used minimum, average and maximum mature root cohesion

values 4, 9 and 14 kPa respectively to characterize progressively increasing site

productivity conditions for Rocky Mountain Douglas fir. A 10 thousand year long

climate data set is generated and used for all four simulations and in the rest of the

simulations described in this section.

We plotted the probability distributions of time between erosion events that give

the time available for the stream hydraulic conditions and fish communities to recover

between subsequent disturbances (Figure 4-8a). We also plotted the probability

distributions of sediment yields for episodic events to show the natural range of sediment

inputs under different root cohesions (Figure 4-8b). Table 4-2 presents the mean, 0.05

and 0.95 quantiles of time between events and sediment yields.

In Table 4-2 when the cumulative probability of the time between events starts

from a higher probability than the 0.05 quantile, the value corresponding to the minimum

cumulative probability is reported. In the simulations an increase in root cohesion leads

to an increase in the time between erosion events and event sediment yields (Table 4-2).

In figures (4-7a) and (4-7b) probability distributions shift to the right as root cohesion

increases.

Cohesion provided by vegetation roots increases the stability of a potential failure

surface in the infinite slope stability model (18). The stabilizing effect of vegetation

allows thickening of colluvium on hillslopes due to the continuous hillslope processes.

Table 4-2. Simulation Statistics for the Runs with Varying Root Cohesion without Forest
Fire Disturbances

Simulation	Time between events (years)			Sediment yield (T. km^{-2}/ event)		
	Mean	$q^{¶}$=0.05	q=0.95	Mean	q=0.05	q=0.95
C_r=1 kPa	3.86	1(0.17)§	9	728	101	2,400
C_r=4 kPa	30.6	1.8	102	3,313	483	10,000
C_r=9 kPa	100	6	371	8,162	1,258	27,100
C_r=14 kPa	191	10	524	8,841	2,050	40,300

[¶] q represents quantile

[§] Number in parantheses is the minimum cumulative probability

(a)

(b)
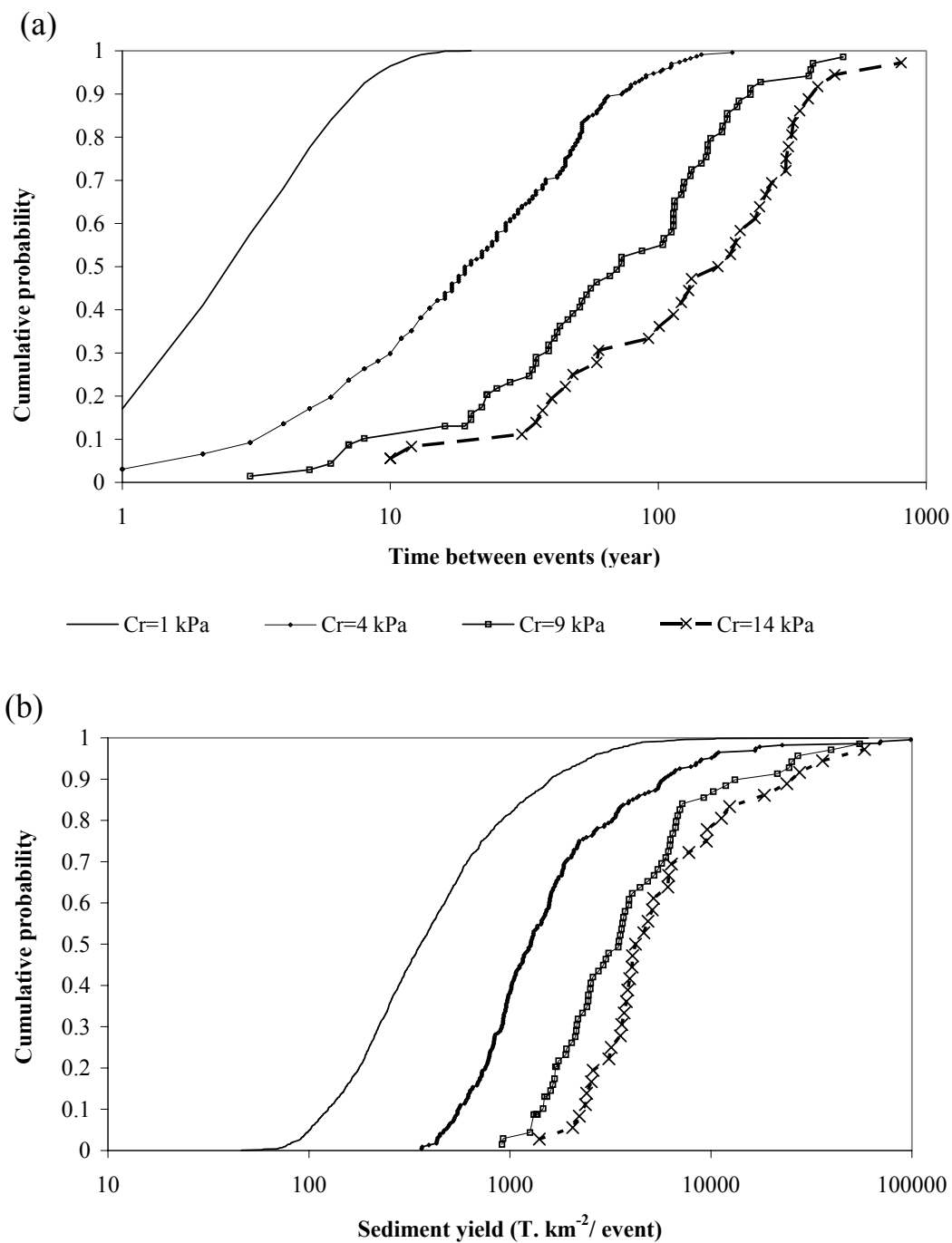
Figure 4-8. Simulation results for undisturbed forests with progressively increasing root cohesion. (a) Probability distribution of sediment yields, (b) probability distributions of the time between events.

Thickening of the colluvium enhances the lateral subsurface flow transport rate in the soil column that decreases the relative wetness of the soil in (18) for a given storm event. However at the same time soil depth thickening gradually increases the shear forces provided by the soil weight that in time overcomes the shear strength produced by the roots and causes landsliding. Figure 4-9 plots the variation of soil depth during the simulations at a selected point along the convergent valley network that has a slope and area of 40 % and 6.21 ha with a curvature of 1.98. In the figure gradual increases in soil depth show soil production by continuous hillslope processes and sudden drops represent either landslides originated at that point or debris flows that scour the colluvium stored along the debris flow tracks. Longer time intervals between two subsequent debris flows allow soil thickening at the point. For example in the case of C_r= 4 kPa, the point is scoured to bedrock 13 times in 7000 years which gives a mean return period of about 586 years. Between debris flow events soil depth on the average thickens up to 0.4 m depth. However for the case of C_r= 14 kPa, debris flows happen in every 2000-3000 years.

Longer time intervals between events allow soil accumulations up to 3 m deep. The model suggests that individual debris flows triggered due to the thickening of colluvium over thousands of years in undisturbed forests can be more destructive than debris flow triggered more frequently under the same climate and topographic conditions (Figure 4-8b). This model behavior is consistent with some field observations [*Johnson et al.*, 2000].

The functional form assumed for bedrock weathering rate would have some influence on sediment yields presented in Table 4-2 for different cohesion values. For

example in the case of a bed rock weathering function where production rate decreases

with increasing soil depth more frequent soil removal (i.e., due to low root cohesion)

would lead to higher rates of bed rock weathering, quicker soil accumulation and down

wasting by climate forcing or vice versa. Such implications of bedrock weathering

functions on sediment yields primarily due to debris flows are not discussed in the paper

because in the convergent hollows morphology modeled soil creep was generally a higher

contributer to soil accumulation than local bedrock weathering.

The upslope extent of erosion in the valley network has important implications for

the spatial pattern of the vegetation disturbances [*Naiman et al.*, 1998], biodiversity

[*Pollock*, 1998], stream temperatures [*Welch et al.*, 1998], and the hydrologic response

[*Ziemer and Lisle*, 1998] in forested catchments. Figure 4-10 maps the areas where
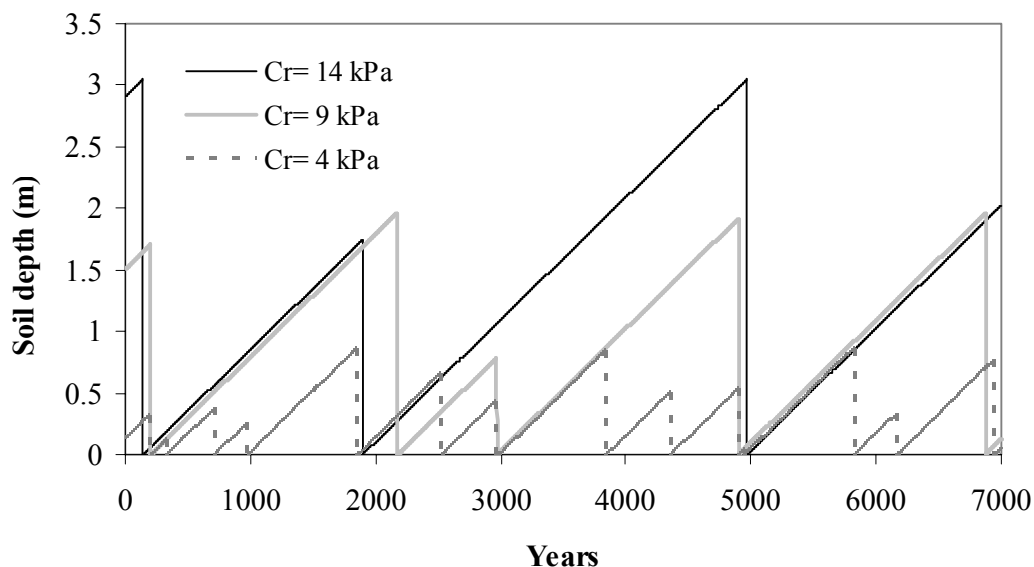
Figure 4-9. Soil depth variation in time at a selected point along the valley network (see Figure 4-10 for the location of the point) in response to changes in constant root cohesion.

episodic sediment scour by debris flows is greater than infilling by diffusion processes, a

criteria that is usually suggested to identify the hillslope-valley transition. This gives the

areas subject to net erosion compared to the initial soil depths imposed at the beginning

of the model run. The maps do not necessarily show the locations currently channeled but

rather they show the locations which are channeled most of the time over the simulation

period. No fluvial erosion is observed in the simulations so that the maintenance of the

channel network here is solely due to landsliding and debris flow scour [*Dietrich and

Dunne*, 1993; *Montgomery and Dietrich*, 1994]. Figure 4-10 clearly shows the stabilizing

effects of vegetation. As the value of root cohesion increases the spatial extend of erosion

retreats. In the lowest case of root cohesion (C_r= 1 kPa, Figure 4-10a) channels extend up

to the ridge tops in most cases and shallow landsliding is observed even in some

divergent hillslope positions. The simulation example driven by C_r= 14 kPa shows the

other end member of the simulations (Figure 4-10d). In this example erosion is confined

to the valley bottoms and shows discontinuities. Here the discontinuities would occur

when scour is rare enough to allow the diffusion processes to evolve soil depths greater

or equal to the initial soil depths. Debris flows are only triggered in the axis of major

hollows. Simulation with C_r= 9 kPa also shows a similar pattern (Figure 4-10c) with

several more tributaries initiated along the main branches. This is consistent with field

observations that drainage density tends to decrease with increasing vegetation cover or

under more humid climates that promotes vegetation [*Strahler*, 1964; *Gregory*, 1976;

Moglen et al., 1998].

When the spatial extent of the simulated erosion patterns in Figure 4-10 are

Compared to the contours of the current topography, the erosion pattern in Figure 4-10b

(C_r=4 kPa) most reasonably captures the convergent valleys.

4.2. Forest Fires

Second we considered the effects of forest fires on the episodic nature of sediment

yields. A stochastic approach to modeling forest fires is developed based on the

probability of wildfires in Trapper Creek (P_F = 0.005). We assumed that fires kill all the
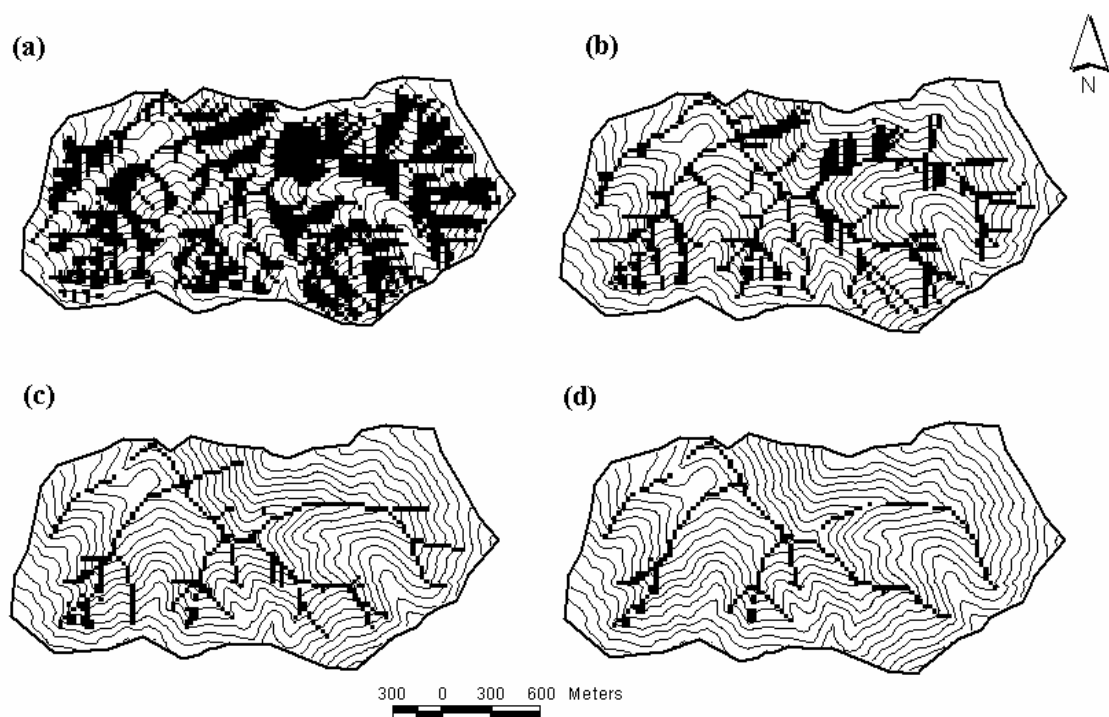
Figure 4-10 Simulated impact of a constant undisturbed root cohesion (a) C_r=1 kPa, (b) C_r=4 kPa, (c) C_r=9 kPa, and (d) C_r=14 kPa, on the spatial extent of the channel network in undisturbed forests. The channel network is here predicted where sediment scour by debris flows is higher than the amount of sediment infilling by diffusive processes (Net Erosion) over the long term.

vegetation completely and cause a random fraction of each pixel to be water repellent. In the model the occurrence of a wildfire in a given year is determined based on a uniformly distributed random number between 0 and 1 generated for each year, being greater than or equal to the probability of no wildfire fire event (1- P_F). The fraction of the grid cells that show hydrophobicity, R_f is also determined by a uniformly distributed random number. Some water drop tests conducted by the USDA Forest Service Rocky Mountain Research Station in Boise Idaho on hydrophobic soils shortly after the Trail Creek fire in Atlanta (approximately 20 miles SE of Trapper Creek) in the summer of 2001 showed hydrophobicity at up to 90 % of the sample points. Based on this information we set the upper bound of the hydrophobic fraction of the grid cells to 0.9 and we used 0.4 for the lower bound.

The model simulated 35 random forest fires during 7000 years of the numerical experiment ranging with intervals between fires from 6 to 577 years used in all three simulations. In the simulations we used the minimum, average and maximum mature root cohesion values, 4, 9 and 14 kPa, respectively, for Rocky Mountain Douglas fir analogous to different site productivity conditions.

The same time series of the climate events used in the simulations for undisturbed forest conditions is utilized in all of the runs simulating wildfires. Figure 4-11 plots the probability distributions of sediment yields and time between erosion events both for undisturbed (the previous simulation with no fires) and disturbed (due to wildfires) forest conditions. Table 4-3 reports the simulation statistics for the wildfire simulations.
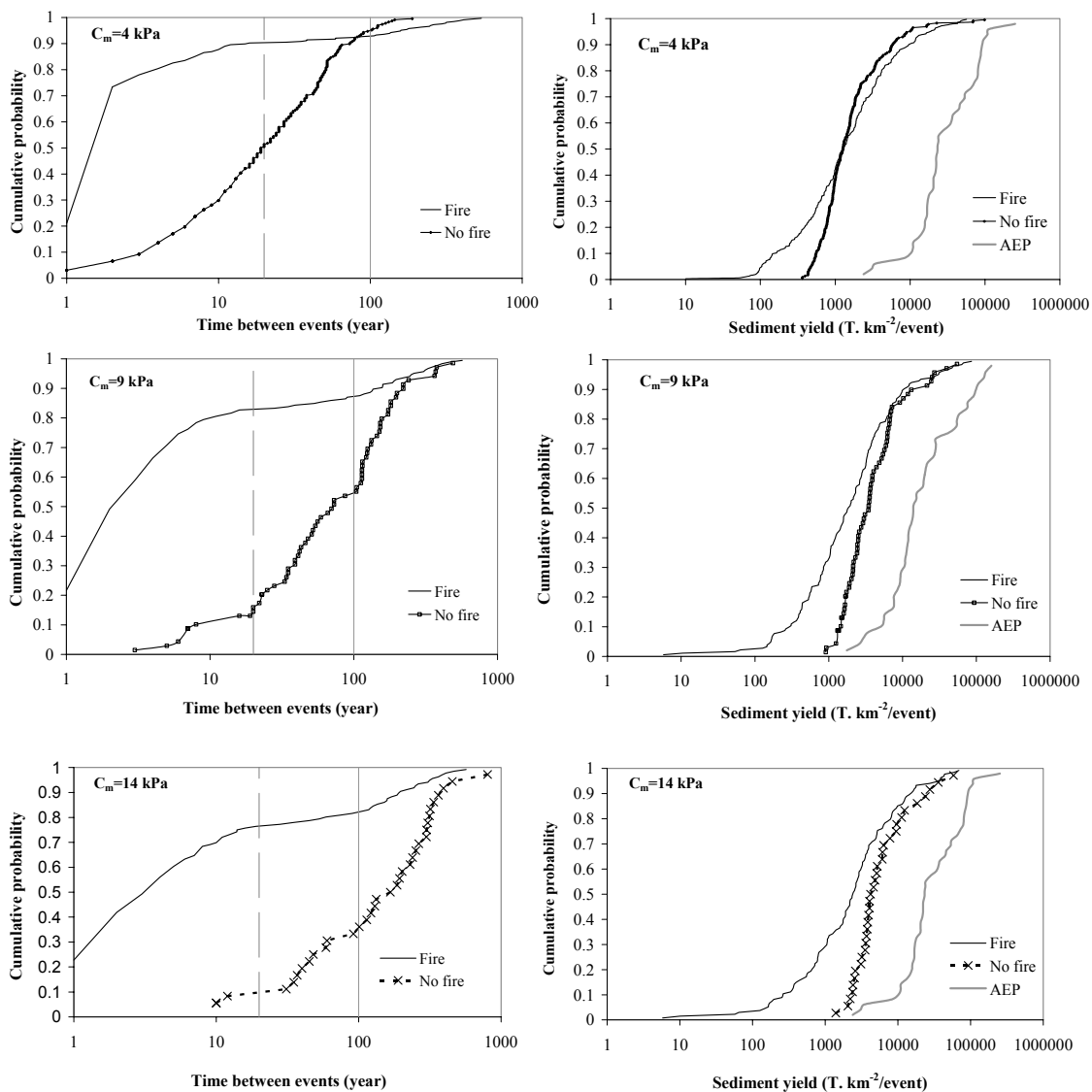
Figure 4-11. Probability distribution of sediment yields and time between erosion events under forest fire disturbances for Rocky Mountain Douglas fir with mature root cohesion values of 4, 9, and 14 kPa .

Similar to the case with no forest disturbances, our simulation results with

wildfires suggest an increase in the mean time between erosion events as the mature root

cohesion increases. Although in the simulations the wildfires kill all the trees, the

Table 4-3. Simulation Statistics for the Runs with Varying Root Cohesion with Wildfires

Simulation	Time between events (years)			Sediment yield (T. km^{-2}/ event)		
	Mean	q=0.05	q=0.95	Mean	q=0.05	q=0.95
C_m=4 kPa	21	1(0.21)	159	3,870	104	18,796
C_m=9 kPa	36.7	1(0.22)	262	5,363	164	30,960
C_m=14 kPa	50	1(0.23)	322	5,947	160	36,000

minimum values of root cohesion would be about 30 % of the mature cohesion (Figure 4-6) [*Gray and Megahan*, 1981]. The increase in the mean time between erosion with increasing root cohesion allows soil thickening on hillslopes that promotes an increase in the mean episodic sediment yields (Table 4-3). In the simulations with fire disturbances, wildfires caused a 32% decrease in the mean time between erosion events for the case with minimum mature root cohesion (4 kPa) and approximately a 3-fold decrease for the other simulations (Tables 4-3) compared to the undisturbed forest conditions (Table 4-2) under the same climate forcing. This reduction let to more frequent erosion events with lesser average magnitudes. The probability distributions of the time between erosion events for undisturbed and naturally disturbed forests show two distinct patterns (Figure 4-11). In the wildfire simulations most of the erosion is concentrated in the first 20-30 years following wildfires during the vegetation recovery period (Figure 4-6). This period is often known as the "Accelerated Erosion Period" (AEP) and its length depends on the rate of root cohesion decay and recovery and the arrival of high magnitude climate events when root cohesion value is relatively low [*Gray and Megahan*, 1981; *Megahan*, 1992]. On the average 6 discrete erosion events were triggered in each AEP depending on the

root cohesion, with; 9 events for $C_r = 4$ kPa, 5 events for $C_r = 9$ kPa and 4 events for $C_r = 14$ kPa. For example if there is gullying in the year of wildfire and then debris flows are triggered sometimes between 10 to 30 years after the fire when the root cohesion is low we may expect the time between events up to 20-30 years belong to the AEPs. In the simulations on the average about 82% of the events has time between events less than or equal to 20 years (90 % for $C_r = 4$ kPa, 82 % for $C_r = 9$ kPa and 76 % for $C_r = 14$ kPa). During the AEP in the simulations there is usually a large event followed by relatively smaller events. This behavior causes a longer tail on the probability distribution of sediment yields under wildfire disturbances (Figure 4-11). In environmental management not only the individual events but also the total amount of sediment produced by multiple events in the AEP may be important. In Figure 4-11 we have also plotted the probability distributions for the total amount of erosion triggered in the AEP of each simulated fire event. It is clearer in the plots that total sediment that may enter the streams in the AEPs following fires may be far more than the sediment produced in undisturbed forests in 20-30 years.

Since all the hollows susceptible to landsliding (i.e. due to thickening of colluvium) are evacuated during the AEPs, the AEP is usually followed by infilling periods that extend till the next fire event. Erosion triggered due to climate forcing is rare between two wildfires. This model behavior can be observed in the probability plots of time between events (Figure 4-11). The probability curves for all three runs flatten off starting approximately from 20 to 100 years. This shows that the probability of time between erosion events being between 20 and 100 years is very small. Then the

probability curves steepen slightly after 100 years. In our experiments with the model we found that this second raise in the probability curve coincides to the time between the last and the first erosion events of two subsequent AEPs following wildfires.

To show the implications of forest fires on the development of erosion dominated valleys, we mapped the locations where sediment scour dominates sediment infilling, or where net erosion is observed during the simulations (Figure 4-12). Stabilizing effects of higher root cohesion can be still seen even under wildfire disturbances. The extent of the valley network for the case of C_m= 9 kPa agrees reasonably well with the converging topographic contour lines in Figure 4-12b.

How sensitive is the episodic behavior of sediment yields to the understory vegetation cover? To discover the implications of the surface roughness produced by the understory vegetation on sediment yields, we altered the maximum fractional ground cover and potential biomass growth rates within their possible ranges. According to observations by *Clayton and Megahan* [1997] the ground cover fraction can be in the range of 0.2 to 1 with an average of 0.8 in undisturbed forests in the Idaho batholith. We used $F_{gc}^{max} = 0.8$ in the previous simulations. Here first we experimented with $F_{gc}^{max} = 1$ and $F_{gc}^{max} = 0.2$. These cover fractions imply Manning's roughness values of 0.8 and 0.16 respectively for undistrurbed forest conditions. Second we altered the growth time period for the understory vegetation by using k_B= 0.65 kg/m^2/yr and k_B= 4 kg/m^2/yr. Using B_c = 1 kg^{-1} along with these growth rates results in 80 % vegetation recovery in the first 6 and 1 years following wildfires respectively. These are possible ranges that may be observed
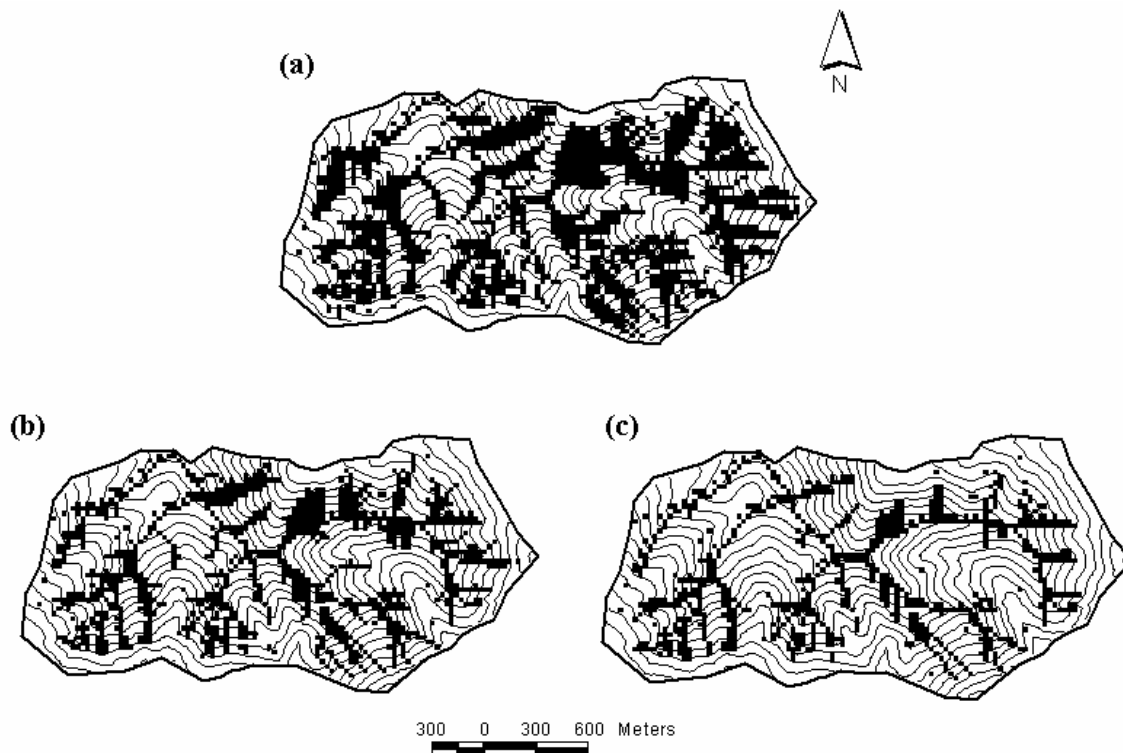
Figure 4-12. Simulated impact of mature root cohesion (a) C_m=4 kPa, (b) C_m=9 kPa, (c) C_m=14 kPa and on the spatial extent of the channel network under wildfire disturbances. The channel network is here predicted where sediment scour is higher than sediment infilling by diffusive processes (Net Erosion) over the long term.

due to variable site conditions. We ran the model utilizing the same climate and wildfire events as used in the previous simulations. Figure 4-13 plots the probability distributions of time between events and sediment yields and Table 4-4 reports the simulation statistics of the runs.

The simulation with $F_{gc}^{max} = 1$ produced the same exact results with $F_{gc}^{max} = 0.8$ that was reported earlier in Figure 4-11 and Table 4-3. Because wildfires disrupt the understory vegetation totally and gully erosion is usually triggered in the same year of

fires. However when $F_{gc}^{max} = 0.2$, we observed more than 3-fold decrease in the mean

time between erosion events that accounted for approximately a 3-fold decrease in the

mean episodic sediment yields. In this simulation the runoff generated during some

intense thunderstorms was able to initiate erosion due to a relatively low surface

resistance value. While 20% of the total soil loss was due to gullying when $F_{gc}^{max} = 1$, it

increased to 40% without any significant change in the total amount of erosions when

$F_{gc}^{max} = 0.2$. For both cases mean average sediment yield is approximately 160

tons/km^2/yr. The signs of the AEPs caused by wildfires can be no longer distinguishable

in the probability plot of time between events (Figure 4-13a). In the case of a slower

growth rate of understory vegetation, the mean time between erosion events slightly

decreased and so did the mean episodic sediment yields. The soil surface is more prone to

gullying when the surface vegetation recovery rate is slow. This promoted a slight

increase in the gullying activity (only about 5%) in the AEPs.

Table 4-4. Simulation Statistics for the Runs with Varying Maximum Ground Cover
Fraction and Potential Understory Vegetation Growth Rate.

Simulation	Time between events (years)			Sediment yield (T. km^{-2}/ event)		
	Mean	q=0.05	q=0.95	Mean	q=0.05	q=0.95
max.(F_{gc})=0.2	10	1(0.13)	60	1,612	6	5,146
max.(F_{gc})=1	36.7	1(0.22)	262	5,363	164	30,960
k_B=0.65 kg/m^2/yr	29	1(0.24)	230	4,400	18	20,500
k_B=4.0 kg/m^2/yr	39	1(0.16)	300	5,790	232	32,000
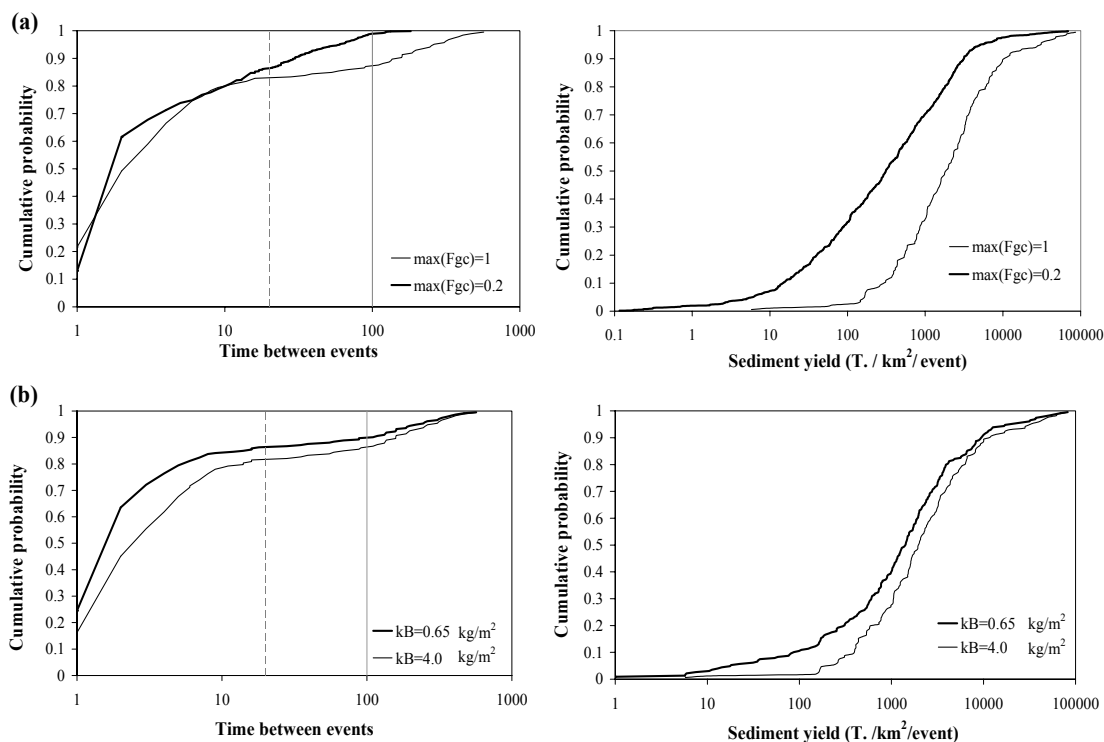
Figure 4-13. Probability distribution of sediment yields and time between erosion events under forest fire disturbances with overstory tree cover of Rocky Mountain Douglas fir C_m= 9 kPa, (a) with maximum fractional ground cover of 1 and 0.2 and (b) with potential biomass growth rate of 0.65 and 4 kg/m^2.

The simulations conducted with different maximum fractional ground cover and understory vegetation growth rates show that the model is not sensitive to 1) maximum fractional ground cover as long as it is dense enough to prevent gully initiation in undisturbed forest conditions and 2) several years of differences in understory vegetation growth periods.

4.3. Comparisons with Field Observations

We compared the mean episodic event sediment yields (Mean ESY), and the long term annual averages (LASY) of the simulation (Table 4-3 and Figure 4-11 for $C_m = 9$ kPa) we ran using the model parameter values given in Table 4-1, with field observations of event sediment yields and short- and long- term annual average sediment yields (SASY and LASY) measured for several catchments in the Idaho batholith using ^{10}Be [*Kirchner et al.*, 2001] (Figure 4-14).

We used event sediment yields reported by *Istanbulluoglu et al.* [(Chapter 3)] for the gullies initiated in Trapper Creek due to a thunderstorm event following a wildfire in 1995. We used two debris flow sediment yields reported by *Meyer et al.* [2001] one in a burned and the other in an unburned unforested site both triggered in 1997 due to a prolonged rain on snow event in the South Fork of the Boise River (SFBR) in the Idaho batholith. We also included our observations of a debris flow event that was triggered 8 years after a stand-replacing fire during the same 1997 rain on snow event in the South Fork of the Payette River (SFPR). Sediment yield data for the gullies in Trapper Creek and in the SFPR are reported for cross-sections surveyed along gullies in Figure 4-14. *Meyer et al.* [2001], however, only reports the sediment yield at the basin outlet. SASY and LASY are reproduced from *Kirchner et al.* [2001] for the basins approximately in the size of the study watershed. SASY observations on the plot represent annual averages of sediment yield over 10 to 28 years of observations whereas the LASY represent the averages over ~10,000 years.

Gully erosion data for Trapper Creek shows an order of magnitude variation for a

given drainage area, which was discussed in *Istanbulluoglu et al.* [(Chapter 3)]. The

upper bound of the Trapper Creek gully erosion sediment yield data and data reported by

[*Meyer et al.*, 2001] are approximately the same (~50,000 tons/km^2). The debris flow

event data observed in the SFPR lies between the upper and lower range of the Trapper

Creek data for a given basin area. Although the SFPR debris flow event
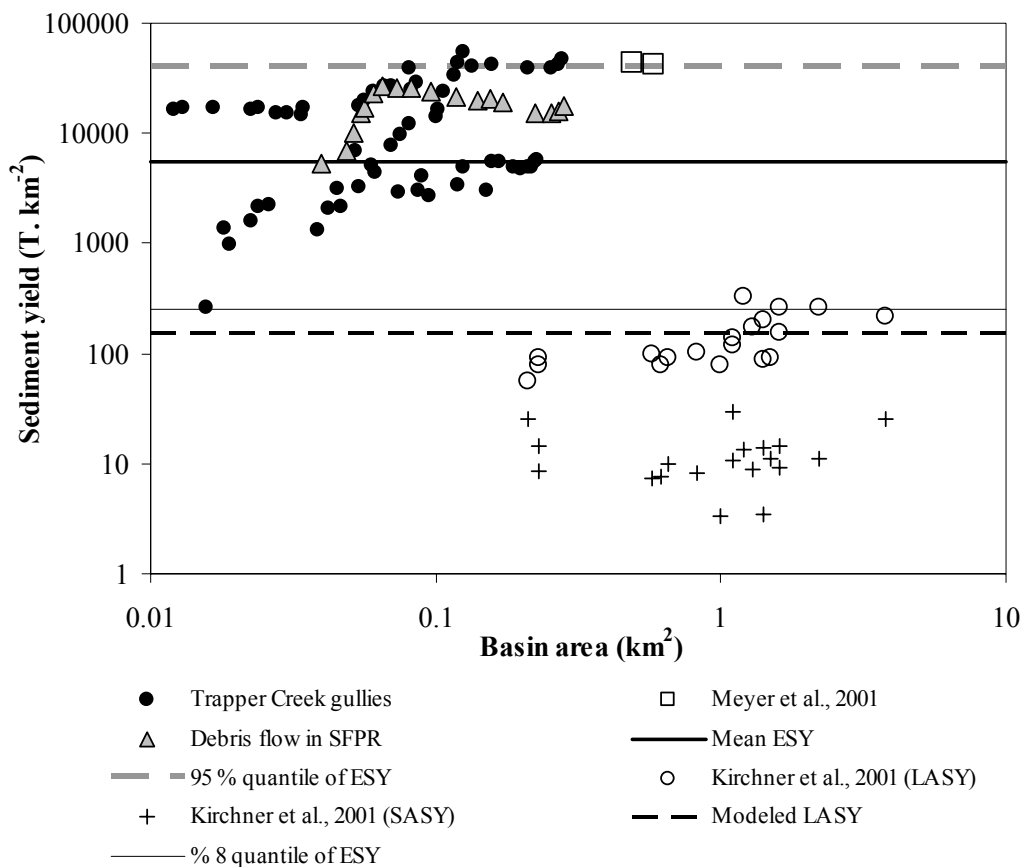
Figure 4-14. Comparisons of the mean event sediment yields (Mean ESY) and long-term annual averages (Modeled LASY) with the observed event and short-term (10 – 28 years) annual average sediment yields (SASY) and the long-term (~ 10,000 years) annual average sediment yields (LASY) obtained using cosmogenic ^{10}Be. In the figure field observations of events sediment yields are between 95% and 8% quantiles of the simulated event sediment yields.

was triggered by the same storm event as the data reported by [*Meyer et al.*, 2001] it did not produce as much sediment (18,000 tons/km^2/year at the outlet). We feel that what this limited data suggest is that episodic erosion due to either landslide induced debris flow or gullying due to flow concentration produces sediment yields in the same order of magnitude and that the sediment yields are mostly limited by soil availability.

Field data reported for event sediment yields are bounded between the 8% and 95% quantiles of the simulated event sediment yields. Most of the observations are between the mean and 95% quantile. We recognize that this comparison is weak because the observations we use are only from recent catastrophic erosion events in the region, but nevertheless Figure 4-14 shows that the model is capable of producing extreme event sediment yields that are observed in the region. The long term average sediment yield the model predicted is 141 tons/km^2/year in 7,000 years. Since the model is not developed to simulate the day-to-day incremental erosion this average only includes the episodic events. The SASY reported by *Kirchner et al.* [2001] did not include any episodic events and has an average value of ~12 tons/km^2/year (average of 19 watersheds). When we add this SASY to the long term averages of episodic events that the model predicts, we find 153 tons/km^2/year for the LASY. Modeled LASY is plotted in figure 4-14 and shows good correspondence with the observed long term averages that range between 55 and 327 tons/km^2/year. No specific calibration was done to produce this match. Among the model parameters only the diffusion constant, wildfire probabilities and sediment transport model parameters are obtained specifically from field data in the study area with the remainder of the parameter values estimated independently from published data

sets pertaining to the Idaho batholith or elsewhere (Table 4-1). We found that on the average episodic sediment delivery of an erosion event is between 35 and up to 560 times greater than the long term averages. When compared to the short-term sediment yields we found that the episodic yields are on the average 450 and up to 7200 times greater. These results suggest that under natural disturbances approximately 92% of the sediment delivery is due to low frequency and high magnitude erosion events.

How do anthropogenic vegetation disturbances caused by forest management occurring in relatively shorter time scales might affect the episodic behavior of sediment yields? In the next section we seek approaches to understand this by designing a paired numerical watershed experiment.

4.3. Timber Harvest

Clearcutting is the easiest and the least expensive timber harvest technique. It is usually preferred by land managers because of its simplicity [*Sidle et al.*, 1985]. Here only clearcutting was modeled because of the uncertainties associated with the other management techniques (e.g., partial cutting, thinning, shelterwood etc.) in terms of their influence on the temporal and spatial variation of root cohesion [*Schmidt et al.*, 2002]. We designed a numerical paired watershed experiment where we compared the effects of clearcutting (anthropogenic) and wildfire (natural) disturbances on sediment yields.

We showed in the previous simulations that under the recent natural disturbance regime and dominant vegetation cover natural fire disturbances along with stochastic climate events alter the soil depths and the magnitude of sediment yields in time. Forest management that starts at a given time provided that the trees are well developed may not

consider the risk of the available sediment in the basin that may erode as a response to

vegetation removal. Severity of erosion following vegetation removal may depend on the

initial condition of colluvium thicknesses in the basin. We have obtained a minimum,

average and a maximum initial condition for spatial soil depths (Figure 4-7) from the

simulation with forest fire recurrence interval of 200 years (P_F=0.005) using the model

parameter values in Table 4-1. The simulation is assumed to represent the natural

variations of soil depths and the sediment yields (Figure 4-11) and the extent of the

erosion dominated valleys (Figure 4-12b) under the current climate and vegetation cover.

The minimum initial soil depth condition is obtained 120 years after the point where the

average soil depth attains the minimum value in Figure 4-7. In the simulations the

average soil depth drops to a minimum value following a wildfire. A 120-year period

(maximum rotation length for the area for healthy forests) is selected to let the trees

regrow before clearcutting starts. The maximum condition is obtained when the average

soil depth in Figure 4-7 reaches to the maximum depth. The initial condition that

represents the average soil depth conditions is obtained in year 5886 in Figure 4-7

between two forest fires after 120 years after the previous fire.

The rotation age for timber harvest is between 80 to 120 years in the Idaho

batholith for healthy and unburned forests [*U.S. Department of Agriculture (USDA)*

Forest Service, 1990]. In the model we used 100 years for rotation length and modeled 3

rotations where all the vegetation is removed for each soil depth initial condition. We

assumed that no wildfires ignite during the management period. For the control case

however we modeled forest fires based on the fire probability of $P_F = 0.005$ during the

comparison period of 300 years. The same random climate events are used in both cases and the experiment is repeated 21 times (for a total of 63 clearcuts or 6300 years) to allow different combinations of climate forcing and forest fire occurrences during 300 years.

We recorded the number of erosion events triggered during the repeated simulations and calculated the average sediment yields for all three model initial conditions both for harvest and natural disturbances (Table 4-5). Figure 4-15 plots the probability distributions of the simulated episodic event sediment yields for both disturbance types.

Our results show that initial sediment availability on hillslopes when forest management is started may greatly influence the erosion rates. We observed a factor of up to 9 increase in both the number of erosion events and sediment yields for harvest and up to 3.7 increase for natural disturbances in Table 4-5. Sediment yield under harvest disturbance is approximately half the sediment yield produced under wildfires for the first initial condition with minimum sediment availability, about the same for the average initial condition and significantly high for the third initial condition with maximum sediment availability (Table 4-5). In fact both sediment yields produced under harvest and natural disturbances on the average produced lower sediment yields in the management time scale of 300 years than the long term averages (153 tons/km^2/yr) (one exception can be the S.Y. for the maximum initial condition under harvest disturbances (Table 4-5).
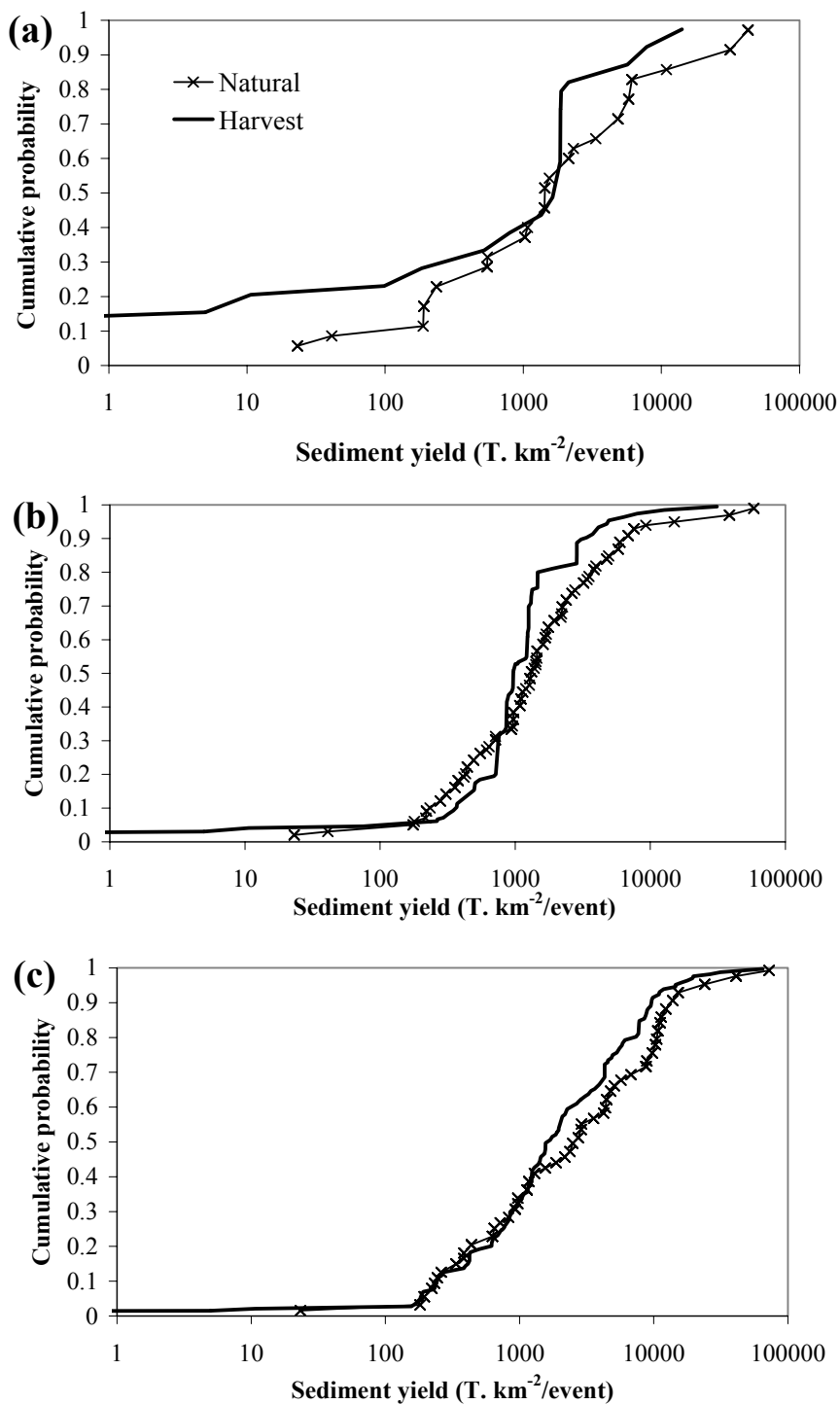
Figure 4-15. Probability distributions of event sediment yields in the numerical paired watershed experiment for different model initial conditions for soil depths in the eroding portions of the watersheds; (a) minimum, (b) average, (c) maximum.

Comparison between the harvest and natural disturbances show that on the average clearcutting doubled the number of erosion events. *Sidle et al.* [1985] reviewed many field observations suggesting that timber harvest may increase the frequency of landsliding even up to orders of magnitude. We see that this increase is mostly because of the rotation length that is half the average return period for wildfires in our simulation. Although the number of events is lower for the case of wildfire disturbances, erosion response to wildfires is relatively more severe for all initial conditions (Figure 4-15). Average event sediment yields plotted in Figure 4-15 are on the average 54% less for harvests. We found that this difference arises from the gully erosion triggered due to fire induced hydrophobicity in the model. For comparison we reported the mean, 5% and 95% quantiles of the simulated event sediment yields under harvest and natural disturbances for the case of average initial condition for soil depths along with the long term simulations of 7,000 years (Table 4-6). It is apparent in the table that all mean, 5% and 95% quantiles reported for natural disturbances during the paired watershed experiment

Table 4-5. Comparison of the Simulated Sediment Yields (S.Y.) and the Number of Erosion Events (N.E.) under Anthropogenic (Harvest) and Natural (Wildfire) Disturbance Regimes for Three Different Initial Conditions of Soil Depths. In the Harvest Simulations, 3 cycles of Forest Clearcutting is Implemented with a Rotation Length of 100 years with 21 Repetition. For the Case of Natural Disturbances Wildfires Are Simulated During the Same Management Period

Initial	Harvest		Natural	
Condition	N. E.	S.Y. (T. km^{-2}/yr)	N. E.	S.Y. (T. km^{-2}/yr)
Minimum	38	26	34	46
Average	194	67	98	74
Maximum	327	235	126	145

Table 4-6. Mean, 5 % and 95 % Quantiles, q of the Simulated Event Sediment Yields under Harvest and Natural Disturbances in 300 Years of Management Period for the Initial Condition with Average Soil Depths, and the Long-Term Simulations of 7,000 years

Statistical parameter	Sediment yield (T km^2/event)		
	Harvest	Natural	Long term
Mean	1,814	3,964	5,363
q=0.05	110	175	164
q=0.95	4,900	15,048	30,960

under the same climate forcing are significantly higher than harvest disturbances. Statistics reported (except q=0.05) for both of the repeated 300 year-long paired watershed experiments are lower than the long term simulation of 7,000 years.

The spatial configuration of soil depths that is produced during long term simulations was not fully reproduced during short term experiments. For example for the case of wildfire runs, erosion response to fires that broke out close to the end of a 300 year management period or to back-to-back fires were not successfully modeled because of a 300 year truncation applied for comparison with harvest cycles. In some cases the model did not even produce any fires during this period. We suggest that comparing sediment yields measured or simulated in relatively short time scales (management time scale) with the long term averages for decision making in forest management may underestimate the consequences of forest management and may not even be a valid criteria especially when not only the magnitude but also the frequency of disturbances is important (i.e., for aquatic habitats).

5. Conclusions

The theory embodied in this paper provide a numerical framework to explore the consequences of different vegetation attributes and vegetation disturbance regimes on the frequency and magnitude of sediment yields and the drainage density of steep forested basins. Comparisons of the simulation results against limited data show good correspondences with the field observations of event sediment yields [*Meyer et al.*, 2001; *Istanbulluoglu et al.*, (Chapter 3)] and long term averages over ~ 10,000 years [*Kirchner et al.*, 2001]. Although our current results are limited to the Idaho batholith conditions, the model can be implemented in areas with similar processes.

In the context of this model forest cover density serves to increase both the tree root cohesion and ground cover density of the understory vegetation both viewed as erosion thresholds. We find that the time between erosion events is controlled by these thresholds. A direct proportionality is found between the time between erosion events and magnitude of event sediment yields in all our experiments. When vegetation is not disturbed by wildfires, sediment delivery is observed to be less frequent but with higher magnitudes for high values of root cohesion (denser forests). An increase in the erosion thresholds tends to decrease drainage density, here examined as the domination of erosion over diffusive infilling.

Forest fires control the timing of sediment delivery. Based on the wildfire return intervals in the area we find that forest fires decrease the mean time between erosion events and lead to more frequent erosion events with smaller magnitudes. The major difference in the episodic behavior of the sediment yields compared to the simulations

with undisturbed forests is the emergence of "Accelerated Erosion Periods" (AEPs) where erosion concentrates during the periods with low erosion thresholds before the recovery of vegetation to pre-disturbed conditions. During the AEPs usually a large erosion event is followed by smaller events that tend to cause a longer tail in the probability distributions of event sediment yields. In the model locations susceptible to landsliding due to the thickening colluvium are evacuated during the AEPs. The episodes of high sediment delivery are then followed by infilling periods that have extended till the next wildfire. In the simulations erosion triggered due to climate events is rare between two wildfires.

We have tested the influence of different sediment availability initial conditions between natural disturbances and regular forest harvesting. Under the same climate forcing and clearcut implementations sediment yields are found to increase as more sediment is available on hillslopes to erode. Based on the model results we suggest that field surveys of sediment thicknesses especially in the convergent hollow axis need to be conducted before the implementation of clearcuts. These surveys may allow mapping the areas with high risks of erosion prior to harvests.

Sediment yields under harvest (clearcutting) and natural (wildfire) disturbances are compared in a numerical paired watershed experiment. We do not find very significant differences in sediment yields between harvest and wildfire disturbances. For both cases the model produce relatively lower average sediment yields and event sediment yields compared to long term averages and event yields (Table 4-5 and 4-6). The major finding is that harvest disturbances may double the number of erosion events

in the area. In contrast to that, the geomorphic response appears to be more severe under wildfire disturbances due to fire related hydrophobicity. Based on the model results we suggest that under harvest disturbances both event sediment yields or yields averaged over a management time period may be less than those produced under a natural disturbance regime.

The response of biologic and aquatic communities to disturbances is strongly related to the duration, intensity and frequency of disturbances [*Reeves et al.*, 1998]. Spatial and temporal variations in the climate and disturbance patterns maintain the spatial heterogeneity and create non-equilibrium habitats of various ages allowing a large number of species to exist [*Pollock*, 1998; *Benda et al.*, 1998]. If forest management increases the frequency of shallow landsliding and debris flow occurrence [*Dietrich et al.*, 2000] then landscapes affected by such disturbances tend to be less heterogeneous than the natural systems. Such landscapes are disturbed more frequently with lesser magnitudes and over larger areas. This anthropogenic disturbance regime results a much simpler range and type of conditions in aquatic systems and thus does not support the most diverse communities [*Reeves et al.*, 1998]. We suggest that when the concern is the amount of sediment episodically delivered to streams (e.g., for engineering design purposes of reservoirs) then the possibility of sediment delivery after wildfires needs to be taken into account. However, if the concern is the disturbances on the aquatic ecosystem and stream habitats then forest management practices should be planned to mimic natural disturbance regimes.

In this paper we modeled the interactions between forest vegetation and vegetation disturbances with the timing and magnitude of sediment yields that disturb aquatic habitats. We feel that this is only one aspect of the problem. The remaining related questions to explore are:

1) How would the aquatic ecosystem evolved to cope with a natural regime of disturbances respond to changes in the disturbance regime?

2) How may we manage forests without causing significant alterations to the biologic and aquatic ecosystems?

Future model developments in forest management require the merging of two research directions. One is continuing to understand the physical basis of hydrologic and geomorphic response and developing state of the art erosion and landscape evolution theories. The second is to develop quantitative theories to the evolution of ecosystems under disturbances.

References

Alberts, E. E., M. A. Weltz and F. Ghidey, Plant growth component, in *USDA - Water Erosion Prediction Project: Hillslope Profile Model Documentation*, Edited by L. J. Lane and M. A. Nearing, NSERL Report No. 2, p. 8.1-8.38, USDA-ARS National Soil Erosion Research Labaratory, West Lafayette, Indiana, 1989.

Arcement, G. J. J., and V. R. Schneider, Guide for selecting Manning's roughness coefficients for natural channels and floodplains, *U.S. Geol. Surv. Report Number RHWA-TS-84-204*, p. 50, U.S. Geol. Surv., 1984.

Arnold, J. G., M. A. Weltz, E. E. Alberts and D. C. Flanagan, Chapter 8: Plant growth component, in *USDA - Water Erosion Prediction Project, National Soil Erosion Research Laboratory*, Report No.10, pp. 8.1-8.41, 1995.

Barret, S., S. Arno, and J. Menakis, Fire episodes in the inland Northwest (1540-1940) based on fire history data, INT-GTR-370, 1997.

Benavides-Solorio, J., and L. H. MacDonald, Post-fire runoff and erosion from simulated rainfall on small plots, Colorado Front Range, *Hydrol. Processes*, 15, 2931-2952, 2001.

Benda, L., and T. Dunne, Stochastic forcing of sediment supply to channel networks from landsliding and debris flow, *Water Resour. Res.*, 33(12), 2849-2863, 1997a.

Benda, L. and T. Dunne, Stochastic forcing of sediment routing and storage in channel networks, *Water Resour. Res.*, 33(12), 2849-2863, 1997b.

Benda, L., D. J. Miller, T. Dunne, and G. H. Reeves, Dynamic landscape systems, in *River Ecology and Management: Lessons from the Pacific Coastal Ecoregion*, edited by R. J. Naiman and R. E. Bilby, pp.261-288, Springer, New York, 1998.

Benda, L. E., and T. W. Cundy, Predicting deposition of debris flows in mountain channels, *Canadian Geotech. J.*, 27, 409-417, 1990.

Benjamin, J. R. and C. A. Cornell, *Probability, Statistics, and Decision for Civil Engineers*, pp. 684, McGraw-Hill, New York, 1970.

Burcar, S., W. W. Miller, S. W. Tyler, and D. W. Johnson, Seasonal preferential flow in two Sierra Nevada soils under forested and meadow cover, *Soil Sci. Soc. Am. J.*, 58, 1555-1561, 1994.

Burroughs, E. R., and B. R. Thomas, Declining root strength in Douglas-fir after felling as a factor in slope stability, *For Serv. Res. Pap. INT-190*, 27 pp. For. and Range Exp. Stn., Ogden, Utah, 1977.

Cannon, S. H., E. R. Bigio, and E. Mine, A process for fire-related debris flow initiation, Cerro Grande fire, New Mexico, *Hydrol. Processes*, 15, 3011-3023, 2001.

Cannon, S. H., P. S. Powers, and W. Z. Savage, Fire-related hyperconcentrated and debris flows on Storm King Mountain, Glenwood Springs, Colorado, *Environ. Geol.*, 35(210-218), 1998.

Chow, V. T., *Open channel hydraulics*, McGraw-Hill, New York, 1959.

Clayton, J. L., and W. F. Megahan, Erosional and chemical denudation rates in the Idaho batholith, *Earth Surf. Processes Landforms*, 11, 389-400, 1986.

Clayton, J. L., and W. F. Megahan, Natural erosion rates and their prediction in the Idaho Batholith, *J. American Water Resour. Assoc.*, 33(3), 1997.

Clayton, J. L., W. F. Megahan and D. Hampton, Soil and bedrock properties: weathering and alteration products and processes in the idaho batholith, *USDA For Serv. Res.*

Pap. INT-237, pp. 35, Intermt. For. and Range Exp. Stn. U.S. Dep. of Agric.,, Ogden, UT, 1979.

Cox, N. J., On the relationship between bedrock lowering and regolith thickness, *Earth Surf. Processes Landforms*, 5, 271-274, 1980.

Crozier, M. J., *Landslides Causes Consequences and Environment*, 252 pp., Croom Helm, London, 1986.

DeBano, L.F., Water repellent soils: a state-of-the art, *For Serv. Gen. Tech. Rep. PSW-46*, 21 pp., Pacific Southwest For. and Range Exp. Station, U.S. Dep. of Agric., Berkeley, Ca, 1981.

Dietrich, W. E., D. Bellugi, and R. R. d. Asua, Validation of the shallow landslide model, SHALSTAB, for forest management, in *Land Use and Watersheds: Human Influence on Hydrology and Geomorphology in Urban and Forest Areas*, edited by M. S. Wigmosta and S. J. Burges, AGU, pp. 195-227, Washington, DC, 2000.

Dietrich, W. E., and T. Dunne, The Channel Head, in *Channel Network Hydrology*, edited by K. Beven and M. J. Kirkby, pp. 175-219, John Wiley, New York, 1993.

Dietrich, W. E., R. Reiss, M.-L. Hsu, and D. R. Montgomery, A process-based model for colluvial soil depth and shallow landsliding using digital elevation data, *Hydrol. Processes*, 9, 383-400, 1995.

Doerr, S. H. and A. D. Thomas, The role of soil moisture in controlling water repellency: new evidence from forest soils in Portugal, *J. of Hydrol.*, 231-232, 134-147, 2000.

Eagleson, P. S., Climate, soil and vegetation: 2. the distribution of annual precipitation derived from observed storm sequences, *Water Resour. Res.*, 14(5), 713-721, 1978.

Engman, E. T., Roughness coefficients for routing surface runoff, *J Irrig. and Drain. Engrg*, 112(1), 39-53, 1986.

Foster, G. R., L. J. Nearing, and J. D. Nowlin, A model to estimate sediment yields from field-sized areas: selection of parameter values, in *CREAMS-A Field Scale Model for Chemicals, Runoff and Erosion from Agricultural Management Systems*, Vol. II, User Manual, Ch.2, pp.193-281, 1980.

Freeman, G. E., W. J. Rahmeyer and R. R. Copelan, Determination of resistance due to shrubs and woody vegetation, *US Army Corps of Engineers, Report ERDC/CHL TR-00-25*, pp. 62, Washington DC, 2000.

Garde, R. J., and K. G. R. Raju, *Mechanics of sediment transportation and alluvial stream problems*, 2 nd. Edition, 618 pp., John Wiley, New York, 1985.

Govers, G., Evaluation of transporting capacity formulae for overland flow, in *Overland flow hydraulics and erosion mechanics*, edited by A. J. Parsons, and A. D. Abrahams, pp. 243-273, Chapman, New York, 1992.

Gray, D. H., and W. F. Megahan, Forest vegetation removal and slope stability in the Idaho Batholith., *For. Serv. Res. Pap. INT-271*, 23 pp., Intermt. Res. Stn., For. Serv., U.S. Dep. of Agric., Ogden, Utah, 1981.

Gregory, K. J., Drainage networks and climate, in *Geomorphology and Climate*, edited by E. Derbyshire, pp. 289-315, John Wiley, New York, 1976.

Hammond, C., D. Hall, S. Miller and P. Swetik, Level I Stability Analysis (LISA) Documentation for Version 2.0, *For. Serv. Res. Pap. General Technical Report INT-285*, 190 pp., Intermt. For. and Range.Exp. Stn., For. Serv., U.S. Dep. of Agric., Ogden, Utah , 1992.

Hampton, D., W.F. Megahan and J.L. Clayton. 1974. Soil and rock properties research in the Idaho batholith, Howard Univ., Dept. Civ. Engng., pp. 126, Washington, DC.

Heimsath, A. M., W. E. Dietrich, K. Nishlizumi and R. C. Finkel, The soil production function and landscape equilibrium, *Nature*, 388(24), 358-361. 1997.

Heimsath, A., W. E. Dietrich, K. Nishiizumi and R. C. Finkel, Cosmogenic nucliedes, topography, and the spatial variation of soil depth, *Geomorphol.*, 27, 151-172. 1999.

Heimsath, A., J. Chappell, W. E. Dietrich, K. Nishiizumi and R. C. Finkel, Soil production on a retreating escarpment in southern Australia, *Geol.*, 28, 787-790. 2000.

Heimsath, A., W. E. Dietrich, K. Nishiizumi and R. C. Finkel, Stochastic processes of soil production and transport: erosion rates, topographic variation and cosmogenic nuclides in the oregon cost range, *Earth Surf. Processes Landforms*, 26, 531-552. 2001.

Huggins, L. F. and J. R. Burney, Surface runoff, storage and routing, in *Hydrologic Modeling of Small Watersheds*, Edited by C. T. Haan, ASAE, pp.169-225, 1982.

Hutchinson, M. F., Stochastic Space-Time Weather Models from Ground-Based Data, *Agricultural and Forest Meteorology*, 73, 237-264. 1995.

Iida, T., A stochastic hydro-geomorghological model for shallow landsliding due to rainstorm, *Catena*, 34, 293-313. 1999.

Inbar M., M. Tamir and L. Wittenberg, Runoff and erosion processes after a forest fire in Mount Carmel, a Mediterranean area, *Geomorphol.*, 24, 1998.

Jan, C. D. and H. W. Shen, Review dynamic modeling of debris flows, in *Recent Developments in Debris Flows*, edited by A. Armanini and M. Michiue, pp. 93-116, Springer-Verlag, New York, 1997.

Jaramillo, D. F., L. W. Dekker, C. J. Ritsema and J. M. H. Hendrickx, Occurrence of soil water repellency in arid and humid climates, *J. Hydrol.*, 231-232, 105-111. 2000.

Johnson, A. C., D. N. Swanston and K. E. McGee, Landslide initiation, runout and deposition within clearcuts and old-growth forests of alaska, *Journal of the American Water Resources Association*, 36, 1, 17-30, 2000.

Julien, P. Y. and D. B. Simons, Sediment transport capacity of overland flow, *Transactions of the ASAE*, 28, 3, 755-762. 1985.

Karsian, E. A., *A 6800-year vegetation and fire history in the Bitterroot Range, Montana*, Master's Thesis, University of Montana, Bozeman, 1995.

Kidd, W. J. J., Probable return periods of rainstorms in central Idaho, *U.S. Dept. Ag. For. Serv. Res. Note INT-28*, pp. 8, Intermt, For. and Range Exp. Stn., U.S. Dept. of Agric., Ogden, Utah. 1964.

Kirchner, J. W., R. C. Finkel, C. S. Riebe, D. E. Granger, J. L. Clayton, J. G. King and W. F. Megahan, Mountain erosion over 10 yr, 10 k.y., and 10 m.y. time scales, *Geol.*, 29, 7, 591-594. 2001.

Lancaster, S.T., S.K. Hayes, and G.E. Grant, Modeling sediment and wood storage and dynamics in small mountainous watersheds, *Geomorphic Processes and Riverine Habitat*, edited by J.M. Dorava, D.R. Montgomery, B.B. Palcsak, and F.A. Fitzpatrick, pp. 85-102, American Geophysical Union, Washington, 2001.

Megahan, W. F., Erosion processes on steep granitic road fills in central idaho, *Soil Sci. Soc. of Am. J.*, 42, 2, 350-357, 1978.

Megahan, W. F., Hydrologic effects of clearcutting and wildfire on steep granitic slopes in Idaho, *Water Resour. Res.*, 19, 3, 811-819, 1983.

Megahan, W. F., An overview of erosion and sedimentation processes on granitic soils, in *Decomposed Granitic Soils*, pp., 11-30, 1992.

Megahan, W. F., N. F. Day and T. M. Bliss, Landslide occurrence in the western and central northern rocky mountain physiographic province in idaho, in *Fifth North American For. Soils Conference*, edited by C. T. Youngberg, pp.116-139, Colo. State Univ., Fort Collins, CO, 1978.

Megahan, W. F. and W. J. Kidd, Effect of logging roads on sediment production rates in the Idaho Batholith, *USDA For. Serv. Res. Pap. INT-123, pp. 14,* Intermt. For. and Range.Exp. Stn., For. Serv., U.S. Dept. of Agric., Ogden, Utah, 1972.

Megahan, W. F. and D. C. Molitor, Erosional effects of wildfire and logging in Idaho, in *Watershed management symposium*, ASCE Irrig. and Drain. Div., pp. 423-444, Logan, UT, 1975.

Megahan, W. F., K. A. Seyedbagheri and P. C. Dodson, Long-term erosion on granitic roadcuts based on exposed tree roots, *Earth Surf. Processes Landforms*, 8, 19-28, 1983.

Meyer, G. A., J. L. Pierce, S. H. Wood and A. J. T. Jull, Fire, storms and erosional events in the Idaho batholith, *Hydrol. Processes*, 15, 3025-3038, 2001.

Moglen, G. E., E. A. B. Eltahir and R. L. Bras, On the sensitivity of drainage density to climate change, *Water Resour. Res.*, 34, 855-862, 1998.

Montgomery, D. R., Road Surface Drainage, Channel Initiation, and Slope Instability, *Water Resour. Res.*, 30(6), 1925-1932. 1994.

Montgomery, D. R., W. E. Dietrich, and J. T. Heffner, Piezometric response in shallow bedrock at CB1: Implications for runoff generation and landsliding, *Water Resour. Res.*, 38(12), 1274, doi:10.1029/2002WR001429, 2002.

Montgomery, D. R. and W. E. Dietrich, A physically based model for the topographic control on shallow landsliding, *Water Resour. Res.*, 30(4), 1153-1171. 1994.

Montgomery, D. R., K. M. Schmidt, H. M. Greenberg and W. E. Dietrich, Forest clearing and regional landsliding, *Geol.*, 28(4), 311-314. 2000.

Moore, I. D., G. J. Burch and P. J. Wallbrink, Preferential flow and hydraulic conductivity of forest soils, *Soil Sci. Am. J*, 50, 876-881. 1986.

Naiman, R. J., K. L. Fetcherston, S. J. McKay and J. Chen, Riparian forests, in *River Ecology and Management: Lessons from the Pacific Coastal Ecoregion*, Edited by R. J. Naiman and R. E. Bilby, pp. 289-323, Springer-Verlag, New York, 1998.

Niemann, J. D., N. M. Gasparini, G. E. Tucker and R. L. Bras, A quantitative evaluation of Playfair's law and its use in testing long-term stream erosion models, *Earth Surf. Processes Landforms*, 26, 1317-1332, 2001.

Pack, R. T., D. G. Tarboton and C. N. Goodwin, Terrain stability mapping with SINMAP, technical description and users guide for version 1.00, *Report Number 4114-0*, Terratech Consulting Ltd., Salmon Arm, B.C., Canada (report and software available from http://www.engineering.usu.edu/dtarb/), 1998.

Pollock, M. M., Biodiversity, in *River Ecology and Management: Lessons from the Pacific Coastal Ecoregion*, edited by R. J. Naiman and R. E. Bilby, pp.430-452, New York, 1998.

Prosser, I. P. and W. E. Dietrich, Field experiments on erosion by overland flow and their implication for a digital terrain model of channel initiation, *Water Resour. Res.*, 31(11), 2867-2876, 1995.

Prosser, I. P. and M. Soufi, Controls on gully formation following forest clearing in a humid temperature environment, *Water Resour. Res.*, 34(12), 3661-3671, 1998.

Prosser, I. P. and L. Williams, The effect of wildfire on runoff and erosion in native Eucalyptus forest, *Hydrol. Processes*, 12, 251-265, 1998.

Ree, W. O., F. L. Wimberley and F. R. Crow, Manning's n and the overland flow equation, *Transaction of the ASAE*, 20(1), 89-95, 1977.

Reeves, G. H., P. A. Bisson and J. M. Dambacher, Fish communities, in *River Ecology and Management: Lessons from the Pacific Coastal Ecoregion*, Edited by R. J. Naiman and R. E. Bilby, pp. 200-234, Springer-Verlag, New York, 1998.

Riebe, C. S., J. W. Kirchner, D. E. Granger and R. C. Finkel, Minimal climatic control on erosion rates in the Sierra Nevada, California, *Geol.*, 29, 447-450, 2001.

Schaake, J. C., V. I. Koren, Q.-Y. Duan, K. Mitchell and F. Chen, Simple water balance model for estimating runoff at different spatial and temporal scales, *J. Geophys. Res.*, 101(D3), 7461-7475, 1996.

Schmidt, K. M., D. R. Montgomery, S. Schaub, J. J. Roering, J. D. Stock and W. E. Dietrich, The variability of root cohesion a an influence on shallow landslide susceptibility in the Oregon cost Range, *Canadian Geotech. J.*, 38(5), 995-1024. 2002.

Selby, M. J., *Hillslope Materials and Processes*, Oxford University Press Inc., 451 pp., N.Y., 1993.

Shakesby, R. A., S. H. Doerr and R. P. D. Walsh, The erosional impact of soil hydrophobicity: current problems and future research directions, *J. of Hydrol.*, 231-232, 178-191. 2000.

Sidle, R. C., A theoretical model of the effects of timber harvesting on slope stability," *Water Resour. Res.*, 28(7), 1897-1910. 1992.

Sidle, R. C., A conceptual model of changes in root cohesion in response to Vegetation Management, *J. Environ. Qual.*, 20, 43-52. 1991.

Sidle, R. C., A. J. Pearce and C. L. O'Loughlin, *Hillslope stability and land use*, Water Resources Monograph 11th. Edition, pp. 140 ,American Geophysical Union, 1985.

Smith, R. E., D. C. Goodrich, D. A. Woolhiser and C. L. Unkrich, Kineros - a KINematic Runoff and EROsion Model, in *Computer Models of Watershed Hydrology*, Edited by V. P. Singh, pp.697-732, Water Resources Publications, 1995.

Strahler, A. N., Quantitative geomorphology of drainage basins and channel networks, in *Handbook of applied hydrology*, Edited by V. T. Chow, pp. 4-39-4-76, McGraw-Hill, New York, 1964.

Tarboton, D. G., A new method for the determination of flow directions and contributing areas in grid digital elevation models, *Water Resour. Res.*, 33(2), 309-319, 1997.

Tucker, G. E. and R. L. Bras, Hillslope processes, drainage density and landscape morphology, *Water Resour. Res.*, 34(10), 2751-2764, 1998.

Tucker, G. E. and R. L. Bras, Dynamics of vegetation and runoff erosion, *Part-I of final technical report submitted to U.S. Army Corps of Engineers Construction Engineering Research Labaratory*, Department of Civil and Environmental Engineering, MIT, 1999.

Tucker, G. E. and R. L. Bras, A stochastic approach to modeling drainage basin evolution, *Water Resour. Res.*, 36(7), 1953-1964, 2000.

Tucker, G. E. and R. Slingerland, Drainage basin responses to climate change, *Water Resour. Res.*, 33(8), 2031-2047, 1997.

U.S. Department of Agriculture (USDA) Forest Service, Land and resource management plan for the Boise national forest, USDA For. Serv., Intermt region, 1990.

Walsh, R. P. D., C. d. O. Coelho, A. Elmes, A. J. D. Ferreira, A. J. B. Goncalves, R. A. Shakesby, J. L. Ternan and A. G. Williams, Rainfall simulation plot experiments as a tool in overland flow and soil erosion assessment, north central portugal, *GeoOkoDynamic*, 19, 139-152, 1998.

Welch, E. B., J. M. Jacoby and C. W. May, Stream quality, in *River Ecology and Management: Lessons from the Pacific Coastal Ecoregion*, edited by R. J. Naiman and R. E. Bilby, pp. 69-94, New York, 1998.

Wells, W. G., The effects of fire on the generation of debris flows in southern California, in *Debris Flows/Avalanches, Process, Recognititon, and Mitigation*, edited by J. E. Costa and G. F. Wieczorek, pp. 105-114, GSA Reviews in Engineering Geology VII, 1987.

Whipple, K. X. and G. E. Tucker, Dynamics of the stream-power river incision model: Implications for height limits of mountain ranges, landscape response timescales, and research needs, *J. Geophys. Res.*, 104(B8), 17,661-17,674. 1999.

Willgoose, G., R. L. Bras and I. Rodriguez-Iturbe, A coupled channel network growth and hillslope evolution model 1. theory, *Water Resour. Res.*, 27(7), 1671-1684, 1991.

Willgoose, G. R., *A physically based channel network and catchment evolution model*, Ph.D. Thesis, M.I.T., Cambridge, MA, 464 pp. 1989.

Wolman, M.G., and J.P. Miller, Magnitude and frequency of forces in geomorphic processes, *J. Geol.*, 68, 54-74, 1960.

Wu, W. and R. C. Sidle, A distributed slope stability model for steep forested watersheds, *Water Resour. Res.*, 31(8), 2097-2110, 1995.

Yu, B., Theoretical justification of SCS method for runoff estimation, *J Irrig. and Drain. Engrg*, 124(6), 306-309, 1998.

Ziemer, R. R. and T. E. Lisle, Hydrology, in *River Ecology and Management: Lessons from the Pacific Coastal Ecoregion*, edited by R. J. Naiman and R. E. Bilby, pp. 43-68 Springer-Verlag, New York, 1998.

CHAPTER 5

SUMMARY, CONCLUSIONS, AND RECOMMENTATIONS

Chapters 2 to 4 report the main scientific results of this dissertation. Here I summarize and emphasize the important conclusions and recommend avenues for future research.

1. Summary and Conclusions

The major objective of the study described in this dissertation was to 1) quantify the influence of natural (wildfires) and anthropogenic (forest harvest) disturbances on the frequency and magnitude of sediment yields in managed forests, 2) show how forest management may alter the sediment delivery regime of steep soil-mantled mountainous basins.

The specific study areas selected for this study were Trapper and Robert E. Lee (REL) Creeks within the North Fork of the Boise River in southwestern Idaho (see Figure 2-2). Valleys are typically narrow and V shaped in the study watershed with an average slope of approximately 40% and up to 98%. Colluvium is grussy, clay-poor, shows little or no cohesion and is subject to runoff erosion and mass wasting especially following vegetation disturbances [*Gray and Megahan*, 1981; *Meyer et al.*, 2001]. Average precipitation is approximately 1000 mm with 60% to 70% in the form of snow. Localized high intensity rainstorms of short duration are common during summer. At other times of the year low intensity storms with longer durations occur, often in conjunction with snowmelt.

Trapper Creek was intensely burned by a wildfire in 1994 and extreme gullying was initiated by a convective summer storm in 1995, possibly due to water repellent conditions of the surface soil. The gullies generated by this storm are probably ephemeral channels, but resulted in considerable erosion. REL Creek was partially burned to a light to moderate degree. Although REL Creek is adjacent to Trapper Creek intense gullying did not occur in REL Creek, presumably due to either higher infiltration capacity from less water repellency or lower localized rainfall intensities, or a combination of both. These two neighboring watersheds gave us the opportunity to compare the effects of wildfires on the spatial extent and the magnitude of soil erosion.

Substantial amounts of sediment can be transported from hillslopes to streams due to channel incision [*Dietrich and Dunne*, 1993]. We conducted field work in the summer of 2000 and determined channel head locations, median sediment sizes right above the channel heads and local slopes in the two study watersheds, to study and document the possible influences of wildfires on the extent of the channel network and to understand the mechanics of channel initiation. In order to estimate the volume of eroded material from the gullies we measured the gully cross-sections spaced at intervals on the average of 20 to 30 m. Slope is an important variable in sediment transport [*Nearing et al.*, 1997]. In the field slope measurements were taken at each measurement location over a length of 10 to 20 m.

Montgomery and Dietrich [1988, 1989, 1992, 1994] found inverse relationships between the source area and local slope at channel heads where channel initiation was due to overland flow erosion, landsliding and seepage erosion. Following Montgomery

and Dietrich's work, several other researchers have sought to find an inverse relationship between area and slope at channel heads in their data sets. Some data sets revealed such inverse relationships [*Vandekerckhove et al.*, 1998, 2000; *Prosser and Abernety*, 1996] but some did not [*Prosser and Soufi*, 1998; *Desmet and Govers*, 1997]. However one common observation in all data sets was that they show significant scatter in the relationship between area and slope. For example for a given slope the Tennessee Valley study area data set of *Montgomery and Dietrich* [1992] in Marin county California shows a factor of 8 variation in the contributing area sizes required to support a channel head. *Montgomery and Dietrich* [1992, 1994] discussed possible causes of this variability and its importance in the development of valleys.

Chapter 2 of this dissertation described a physically based probabilistic approach to channel initiation. First a deterministic channel initiation threshold for overland flow shear stress is written as a function of runoff rate, r, additional roughness due to non-transportable obstructions and vegetation, n_a and median sediment size, d_{50}. The analytic form of the theory is organized in the form of the topographic threshold given by Montgomery and Dietrich as $aS^\alpha \geq C$ (r; n_a; d_{50}). Then spatially homogenous probability distributions are assumed for r, n_a and d_{50} to derive a probability distribution for C to characterize the inherent variability of the area-slope threshold observed at channel head locations in the field (Figure 2-1). The probability of channel initiation (PCI) at a given location is described as the probability of the channel initiation threshold being less than or equal to the aS^α where a and S are calculated from the topography. In chapter 2 we first compare the observed aS^α at channel head locations with the calculated channel

initiation threshold, C for each location using the d_{50} values observed in the field and assuming constant r and n_a to see the contribution of d_{50} to the spatial variability of the channel head locations. Second we compare the derived probability distributions for C with the probability distributions of the observed aS^{α}. We also illustrate the PCI theory on slope-area plots. In chapter 2 it is reported that:

(1) Channels may incise in different topographic locations dominated by different sediment transport mechanisms over the long term depending on the spatial and temporal variability of climate and land cover. Thus the observed relationship between drainage area to support a channel head and local slope can not be attributed to the functional form of channel initiation function, but is instead related to where the channel heads happen to be at any point in time on the landform that has evolved in response to long term average processes.

(2) The measured variability of sediment grain size is related to and accounts for a significant portion of the variability in channel initiation threshold observed in the field.

(3) A probability distribution of slope-area dependent channel initiation threshold matches the same form of the slope-area distribution of channel heads observed in the field.

(4) Erosion risk can be visualized by mapping the PCI using DEMs.

(5) PCI maps reveal the probabilities of flow transport in overland and channeled states and contribute to understanding the effects of geomorphic changes to the hydrologic response.

Sediment transport equations are often derived based on the assumption that the sediment transport capacity can be determined by a dominant variable such as shear stress, discharge and slope, stream power or flow velocity [*Tayfur*, 2002]. Recent developments in the numerical modeling of landscape evolution revealed that the functional form of erosion and sediment transport equations have important geomorphic implications on for example hillslope morphology, drainage density and concavity of river basins [*Willgoose et al.*, 1991; *Tucker and Bras*, 1998]. The sediment transport equations are derived using data from rivers and experimental flume studies. We know of no studies that examines the theoretical foundations of these equations for naturally eroded, self-formed gullies on steep, soil-mantled hillslopes. In chapter 3 we first theoretically adapted a general dimensionless sediment transport capacity equation that predicts sediment transport as a function of dimensionless shear stress [e.g., *Parker and Klingeman*, 1982] to incising gullies. We physically related flow shear stress and flow width to contributing area, slope, steady-state runoff rate and parameters that describe the roughness and shape of eroding channels. We calibrated the parameters of the dimensionless sediment transport function, an empirical constant κ and a shear stress exponent p for the case of recent gully erosion using field data from Trapper Creek. The main conclusions from chapter 3 can be summarized as:

(1) The field data suggested that under high shear stresses p=3 in the sediment transport function $Q_s \sim \tau^p$.

(2) A shear stress exponent of p=3 in the model corresponds to exponents M=2.1 and N=2.25 in the sediment transport function $Q_s \sim A^M S^N$ that also fits the data.

(3) When the sediment size and roughness conditions in the gullies were spatially

homogenous 80% of the spatial variability of the sediment transport rates was

represented by the model whereas only 44% of the variability in sediment transport

rates was described when heterogeneities in the roughness conditions are observed

(4) The concavity index θ_c=(M-1)/N, obtained from the sediment transport equation

for transport limited catchments agreed well with the observed profile concavity of

the gullies developed in Trapper Creek.

Chapter 4 developed a physically based numerical model of hillslope erosion to

model the episodic behavior of mountain erosion and to explore the influence of forest

vegetation and natural (wildfires) and anthropogenic (forest harvest) vegetation

disturbances on erosion rates. In the model soil development is modeled by bedrock

weathering and divergence of diffusive sediment transport. Soil is removed by gully

erosion, shallow landsliding and debris flow generation. The climate forcing is

characterized by selecting random climate events from annual maximum probability

distributions. Forest fires are modeled randomly based on the probability of wildfire

events in the study region. Wildfires are assumed to kill all the overstory and the

understory vegetation which then regrows with time. Based on the numerical experiments

we concluded that:

(1) Model results showed good correspondence with the field observations of event

sediment yields from gully erosion and debris flows both in Trapper Creek and in

several other geomorphically similar watersheds in the Idaho batholith. The long

term average erosion rate predicted by the model was within the range of the long

term average erosion rates (~ 10,000 years) reported for several Idaho catchments with similar sizes.

(2) Forest vegetation was shown to act as an erosion threshold and control the time between erosion events.

(3) Episodic sediment delivery events were modeled to be less frequent but with higher event magnitudes as forest vegetation density increased in undisturbed forests.

(4) An increase in forest cover decreased the extent of erosion dominated valleys.

(5) Forest fires decreased the time between erosion events and lead to more frequent erosion with smaller event magnitudes.

(6) With a simulated regime including forest fires, erosion was found to be concentrated to the periods with low erosion thresholds "Accelerated Erosion Period" (AEP) during vegetation recovery. During the AEPs the amount of erosion modeled was larger than the event sediment yields under undisturbed forest cover conditions.

(7) The initial sediment availability on hillslopes when forest management was simulated significantly influenced the erosion rates.

(8) In a numerical paired watershed experiment forest cleacutting was shown to cause a 2-fold increase in the number of erosion events in the Idaho batholith. In contrast to that geomorphic response appeared to be more severe under wildfire disturbances.

A common perspective in fluvial geomorphology is that in rivers most of the sediment is carried by moderate intensity flood events which recur much more frequently

than low frequency and high magnitude catastrophes [*Wolman and Miller*, 1960].

Modeling results presented in chapter 4 along with some published field observations in

the Idaho batholith [*Kirchner et al.*, 2001; *Meyer et al.*, 2001] and modeling experiments

conducted in Oregon Cost Range by *Benda and Dunne* [1997a, 1997b] however suggest

that sediment yield in mountain basins is dominated by rare and brief catastrophic erosion

events. These recent results should not be taken to fully contradict with the previous

perspective suggested by Wolman and Miller on the importance of moderate intensity

floods on sediment transport. One possible explanation is that the results presented in

chapter 4 are for basin sizes up to 10 km^2 however in Wolman and Miller's paper basin

sizes used were in the range of 25 to 350000 km^2. One might expect that as basin size

increases the number of sources for sediment supply would also increase. Each source

creates a sediment pulse independently due to the spatial and temporal variability in

storm sizes and sediment availability on hillslopes. Sediment introduced to the river from

different upland sources accumulate downstream but the dominance of individual pulses

attenuates because of different timing of sediment delivery to the network, sediment

storage on fans and in the river channel and long travel times from the sediment sources

to the watershed outlet. This may lead to the dominance of higher frequency and lower

magnitude sediment transport events in the annual sediment yields of the large basin.

Although this argument seems to be plausible and was also shown in the simulation

experiments of *Benda and Dunne* [1997b], *Kirchner et al.* [2001] also reports some

limited data for large river basins in Idaho that suggest the same episodic behavior in

sediment fluxes as was observed in small watersheds. *Kirchner et al.* [2001] attributed

this observation to high spatial and temporal correlations in catastrophic wild fire and extreme precipitation events. Flow and sediment transport data used by Wolman and Miller was limited to several decades. Kirchner and others' data that the model was tested against reports averages of annual sediment yields both measured over decadal time periods and long term averages up to 10 million years obtained using cocmogenic [10]Be. It may be arguable that rare catastrophes were not represented in the data used by *Wolman and Miller* [1960]. I believe that more field data and modeling studies are required for more exact conclusions.

The model developed in chapter 4 can be used as a research tool to test hypothesis on the controls of forest vegetation and forest management practices on sediment yields, developing field research programs and as a decision support tool for forest management. In the latter use field observations of soil thickness and root cohesion on hillslopes would be needed in order to provide reasonable initial conditions to the model. Soil depths can be mapped in the field and the model can be used to match the observed soil depths using relevant model parameter values for the area of interest. Once the initial condition for spatially variable soil depths is obtained the model can be used to consider different clearcut scenarios. Modeling of other forest management practices such as partial and shelter wood cutting and thinning would require estimation of the impacts these practices have on root cohesion and additional roughness. This was not pursued here because we do not field observations to quantify the effect of these other practices.

The research presented in chapter 4 has uncertainty due to imperfect knowledge and understanding of the processes and their parameters in the field. The uncertainties

identified can serve to motivate additional field research to identify key parameters and better understand key processes where better quantified understanding is required. Based on the understanding of the model sensitivities developed while doing this research critical processes that should be better quantified, include soil creep (diffusion) rates, root cohesion and additional roughness due to vegetation and how these grow and decay. The terrain curvature is also critical as a determinant of hollow infilling rate motivating the need for high-quality digital elevation data.

2. Recommendations

Simulation experiments presented in chapter 4 showed that vegetation imposes controls on the timing and magnitude of erosion events. The influence of vegetation on geomorphology will open avenues for interdisciplinary future research both for short term and long term geomorphic processes. In this dissertation we have started with assuming spatially uniform forest vegetation growth and vegetation disturbances only due to wildfires and forest harvest. This assumption ignores the controls of hillslope soil moisture, form, aspect and soil characteristics on vegetation growth and the effect of floods on vegetation disturbance. In the model all the hollows in a watershed where there is enough soil accumulation are destabilized upon loosing root cohesion and collectively produce slope failures and gullying following vegetation disturbances. Assuming spatially variable vegetation growth would not dramatically change the model results because wildfires would reset forest vegetation each time they occur. Recent field observations however show that in undisturbed forests spatial variation in forest vegetation species and age can trigger local slope failures [*Schmidt et al.*, 2002].

Therefore I feel that future research on spatial vegetation growth and its implications on erosion rates would be more important for forests that are not disturbed with fires.

I believe that extensive process-based field observations are needed in the long term to understand the spatial and temporal variability of vegetation on hillslopes and to better understand and formulate its influence on sediment transport, erosion, soil evolution and runoff production. Research on the spatial growth patterns of vegetation would also have important implications for understanding biodiversity and nutrient cycles in watersheds.

In order to improve the current vegetation theory presented in chapter 4, the first step would be to calibrate the root cohesion and surface roughness model parameters using vegetation observations in different locations on the landscape with different aspects and moisture conditions.

Some questions on the influence of vegetation on the formation of drainage basins important for future research are:

(1) How do vegetation and vegetation disturbances such as fires and floods control the drainage basin relief, hillslope and channel profiles and drainage density?

(2) How does vegetation respond to climate change and what is the effect on erosion rates and landscape morphology?

In the model climate forcing is assumed to be stationary with independent climate events each year. This assumption ignores possible cycles, clustering and autocorrelation of climate events. In the theory climate forcing is used to calculate overland flow discharge that is used in modeling erosion and the relative wetness parameter required for

the factor of safety analysis for shallow landslide initiation. Climate researchers have identified a number of short and long term climate cycles, some associated with ocean teleconnections such as El Nino, Southern Oscillation. The model presented in chapter 4 is capable of accepting modified climate inputs to reflect these climate changes or cycles and future research is recommended to address the impacts of climate cycles or changes on the findings. In particular, if used for management the impact of predicted climate changes could be assessed.

In discussing climate variability or climate change effects the question of dependence between vegetation type and forest fire occurrence may be important. At present the model does not relate vegetation characteristics to soil moisture and climate, so the consequences of significant oscillations in a climate regime can not be modeled. This again leads me to recommend research in vegetation dynamics related to climate variability and changes.

In all three major chapters in this dissertation we used digital elevation model grid cells as model elements. I think that the biggest challenge in computer modeling of geomorphic processes is the representation of continuous topographic surfaces using discrete connected elements. Three widely used strategies for terrain discretization are regular grids, triangulated irregular networks (TINs) and contour elements [*Tucker et al.*, 2001b]. In the last decade regular grids [e.g., *Willgoose et al.*, 1991] and TINs [e.g., *Tucker et al.*, 2001a] have mostly been preferred over contour elements [*Moore et al.*, 1988] for the modeling of geomorphic processes. In numerical modeling, model elements usually have a constant resolution. The constant resolution introduces biases to the

predictions of topographic attributes such as drainage area, local slope and curvature. One can expect that sediment yields, timing of erosion events and evolution of the topography will also be biased due to the selected resolution. This doesn't mean that one needs to use finer model element resolutions instead resolution should be selected relevant to the topographic texture. I suggest that new methods needs to be developed; 1) to spatially vary the resolution of the model elements based on the texture of the topography for modeling erosion and runoff generation (when element elevations are assumed constant); 2) to adapt the model element resolution parallel to landscape evolution (e.g., adding and deleting nodes of a TIN network as channels extent or contract) in models of landscape evolution. I believe that a better representation of the topography will gain more importance when the interactions between geomorphology and soil moisture, vegetation, biologic activities etc., are of interest.

In the last decade there have been considerable efforts to parameterize the slope dependent sediment transport laws and the topographic controls on soil evolution [e.g., *Dietrich et al.*, 1986; *Reneau and Dietrich*, 1991; *Heimsath et al.*, 1997, 2001]. However no process based sediment transport laws are parameterized for sheetwash, gullying, landsliding and debris flows from field observations [*Dietrich et al.*, 2001]. Our attempt in chapter 3 can be regarded as an initial step for parameterizing such transport laws for upland gully erosion. However controlled field experiments are needed to understand the influence of hillslope shape, drainage area, slope, sediment size and vegetation on both fluvial sediment transport and erosion and debris flow behavior in upland areas.

The gully erosion observations we presented in chapter 3 are for the case of a catastrophic erosion event where all the sediment is mobilized and the gully eroded to bedrock in most of the cross-sections. Therefore we assumed equal mobility in sediment transport modeling [*Parker et al.*, 1982]. Recent observations in rivers showed that transport rates of coarser size fractions can be orders of magnitude smaller than finer fractions due to size selective partial transport of fine sediments [*Wilcock and McArdell*, 1997; *Wilcock*, 1998]. A similar phenomenon can be justified in field experiments with eroding rills where size selective sediment entrainment in rills cause roughening of the eroding surface as erosion progresses [*Govers*, 1992; *Nearing et al.*, 1997, 1999]. *Megahan* [1974] reported that surface armoring in the first year following soil disturbances in the Idaho batholith due to surface wash contribute to the reduction of erosion rates before vegetation regrowth. I suggest that process-based field experiments are needed to understand the mechanism of size selective transport of sediment on hillslopes and the interactions between erosion and flow hydraulics. Such observations may contribute to our understanding of some important geomorphology problems such as the downstream fining phenomenon observed in some basins, gravel- to sand-bed transitions [*Gasparini et al.*, 1999] and the hillslope form [*Band*, 1990] and on the transport and deposition of fine sediments and nutrients that alter the water quality and habitat conditions for fish and invertebrates [*Welch et al.*, 1998].

References

Band, L. E., Grain size catenas and hillslope evolution, *Catena Supplement*, 17, 167-176, 1990.

Benda, L., and T. Dunne, Stochastic forcing of sediment supply to channel networks from landsliding and debris flow, *Water Resour. Res.*, 33(12), 2849-2863. 1997a.

Benda, L., and T. Dunne, Stochastic forcing of sediment routing and storage in channel networks, *Water Resour. Res.*, 33(12), 2849-2863. 1997b.

Desmet, P. J. J., and G. Govers, Two-dimensional modelling of the within-field variation in rill and gully geometry and location related to topography, *Catena*, 29, 283-306, 1997.

Dietrich, W. E., D. Bellugi, A. M. Heimsath, J. J. Roering, L. S. Sklar and J. D. Stock, Geomorphic transport laws for predicting landscape form and dynamics, in *A MARGINS Education and Planning Workshop Developing a Community Sediment Model*, available at; http://instaar.colorado.edu/deltaforce/workshop/csm.html. 2001.

Dietrich, W. E., and T. Dunne, The channel head, in *Channel Network Hydrology*, edited by K. Beven and M. J. Kirkby, pp.175-219, John Wiley, 1993.

Dietrich, W. E., C. J. Wilson and S. L. Reneau, Hollows, colluvium, and landslides in soil-mantled landscapes, in *Hillslope Processes*, edited by A. D. Abrahams, pp.361-388, Allen & Unwin, Boston, 1986.

Gasparini, N. M., G. E. Tucker and R. L. Bras, Downstream fining through size selective transport, *Geol.*, 27(12), 1079-1082, 1999.

Govers, G., Relationship between discharge, velocity and flow area for rills eroding loose, non-layered material, *Earth Surf. Processes and Landforms*, 17, 515-528, 1992.

Gray, D. H., and W. F. Megahan, Forest vegetation removal and slope stability in the Idaho Batholith., *For. Serv. Res. Pap. INT-271*, 23 pp., Intermt. Res. Stn., For. Serv., U.S. Dep. of Agric., Ogden, Utah, 1981.

Heimsath, A., W. E. Dietrich, K. Nishiizumi, and R. C. Finkel, Stochastic processes of soil production and transport: erosion rates, topographic variation and cosmogenic nuclides in the oregon cost range, *Earth Surf. Processes and Landforms*, 26, 531-552, 2001.

Heimsath, A. M., W. E. Dietrich, K. Nishlizumi and R. C. Finkel, The soil production function and landscape equilibrium, *Nature*, 388(24), 358-361, 1997.

Kirchner, J. W., R. C. Finkel, C. S. Riebe, D. E. Granger, J. L. Clayton, J. G. King and W. F. Megahan, Mountain erosion over 10 yr, 10 k.y., and 10 m.y. time scales, *Geol.*, 29(7), 591-594, 2001.

Megahan, W. F., Erosion over time on severely disturbed granitic soils: A model, *USDA For. Serv. Res. Pap. INT-156*, 14 pp., Intermt. For. and Range.Exp. Stn., Ogden, Utah, 1974.

Meyer, G. A., J. L. Pierce, S. H. Wood, and A. J. T. Jull, Fire, storms and erosional events in the Idaho batholith, *Hydrol. Processes*, 15, 3025-3038, 2001.

Montgomery, D. R., and W. E. Dietrich, Where do channels begin, *Nature*, 336, 232-234. 1988.

Montgomery, D. R., and W. E. Dietrich, Source areas, drainage density and channel initiation, *Water Resour. Res.*, 25(8), 1907-1918, 1989.

Montgomery, D. R., and W. E. Dietrich, Channel initiation and the problem of landscape scale, *Science*, 255, 826-830, 1992.

Montgomery, D. R., and W. E. Dietrich, Landscape dissection and drainage area-slope thresholds, in *Process Models and Theoretical Geomorphology*, edited by M. J. Kirkby, pp., 221-246, John Wiley, New York, 1994.

Moore, I., E. M. O'Loughlin, and G. J. Burch, A contour based topographic model for hydrological and ecological applications, *Earth Surf. Processes and Landforms*, l3, 305-320, 1988.

Nearing, M. A., L. D. Norton, D. A. Bulgakov, G. A. Larinov, L. T. West, and K. M. Dontsova, Hydraulics and erosion in eroding rills, *Water Resour. Res.,* 33(4), 865-876, 1997.

Nearing, M. A., J. R. Simanton, L. D. Norton, S. J. Bulygin, and J. Stone, Soil erosion by surface water flow on a stony, semiarid hillslope, *Earth Surf. Processes Landforms*, 24, 677-686, 1999.

Parker, G., P. C. Klingeman, and D. G. McLean, Bedload and size distribution in paved gravel-bed streams, *ASCE, J. of Hydaul. Div.*, 108, 1757-1760, 1982.

Parker, G., and P C Klingeman, On why gravel bed streams are paved, *Water Resour. Res.*, 18(5), 11409-1423, 1982.

Prosser, I. P., and B. Abernety, Predicting the topographic limits to a gully network using a digital terrain model and process thresholds, *Water Resour. Res.*, 33(7), 2289-2298, 1996.

Prosser, I. P., and M. Soufi, Controls on Gully Formation Following Forest Clearing in a Humid Temperature Environment, *Water Resour. Research*, 34(12), 3661-3671, 1998.

Reneau, S. L., and W. E. Dietrich, Erosion rates in the southern Oregon coast range, Evidence for an equilibrium between hillslope erosion and sediment yield, *Earth Surf. Processes and Landforms*, 16, 307-322, 1991.

Schmidt, K. M., D. R. Montgomery, S. Schaub, J. J. Roering, J. D. Stock, and W. E. Dietrich, The variability of root cohesion a an influence on shallow landslide susceptibility in the Oregon cost Range, *Canadian Geotech. J.*, 38(5), 995-1024. 2002.

Tayfur, G., Applicability of sediment transport capacity models for nonsteady state erosion from steep slopes, *J. Hydr. Engrg.*, 7, 3, 252-258, 2002.

Tucker, G. E., and R. L. Bras, Hillslope processes, drainage density and landscape morphology, *Water Resour. Res.*, 34(10), 2751-2764, 1998.

Tucker, G. E., S. T. Lancaster, N. M. Gasparini, and R. L. Bras, The Channel-Hillslope Integrated Landscape Development Model (CHILD), in *Landscape Erosion and Sedimentation Modeling*, edited by R. S. Harmon and W. W. Doe, Kluwer Press, 2001a.

Tucker, G. E., S. T. Lancaster, N. M. Gasparini, R. L. Bras, and S. M. Rybarczyk, An object oriented framework for distributed hydrologic and geomorphic modeling using triangular irregular networks, *Computers and Geosciences*, 27(8), 959-973, 2001b.

Vandekerckhove, L., J. Poesen, D. O. Wijdenes, and T. d. Figueiredo, Topographic thresholds for ephemeral gully initiation in intensely cultivated areas of the Mediterranean, *Catena*, 33, 271-292, 1998.

Vandekerckhove, L., J. Poesen, D. O. Wijdenes, J. Nachtergaele, C. Kosmas, M. J. Roxo and T. d. Figueired, Thresholds for gully initiation and sedimentation in Mediterranean Europe, *Earth Surf. Procsses and Landforms*, 25, 1201-1220, 2000.

Welch, E. B., J. M. Jacoby, and C. W. May, Stream quality, in *River Ecology and Management: Lessons from the Pacific Coastal Ecoregion*, edited by R. J. Naiman and R. E. Bilby, pp. 69-94, Springer-Verlag, New York, 1998.

Wilcock, P. R., Two-fraction model of initial sediment motion in gravel-bed rivers, *Science*, 280, 410-412, 1998.

Wilcock, P. R., and B. W. McArdell, Partial transport of a sand/gravel sediment, *Water Resour. Res.*, 33(1), 235-245, 1997.

Willgoose, G., R. L. Bras and I. Rodriguez-Iturbe, A coupled channel network growth and hillslope evolution model 1. theory, *Water Resour. Res.*, 27(7), 1671-1684, 1991.

Wolman, M.G., and J.P. Miller, Magnitude and frequency of forces in geomorphic processes, *J. Geol.*, 68, 54-74, 1960.

APPENDIXES

Appendix A

This appendix describes derivations of some of the model components used in the sediment transport capacity calculations in Chapter 3

A1. Derivation of the Shape Constant C for Trapezoidal, Triangular and Parabolic Channels;

The shape constant in equation (10) is given here for trapezoidal, triangular and parabolic channels based on the width to depth ratio z_1 and sideslope ratio z_2 (for triangular and trapezoidal channels only). We recognize that for a fixed channel z_1 changes with discharge (and depth), nevertheless it is treated here as a constant parameterization of the form of an eroding channel where there is some degree of adjustment of cross sectional form to discharge. Equation (10) gives,

$$C = \frac{A_f^{0.5}}{R}. \tag{A1}$$

Writing A_f and R as a function of z_1 and z_2 we obtain C_s for trapezoidal, triangular and parabolic channel geometries from (A1) respectively;

$$C_{trap} = \frac{(z_1 - z_2)^{0.5}}{(z_1 - 2z_2) + 2(z_2^2 + 1)^{0.5}} \tag{A2}$$

$$C_{tri} = \frac{z_2^{0.5}}{2(z_2^2 + 1)^{0.5}} \tag{A3}$$

$$C_{prb} = \frac{\sqrt{1.5}z_1^{1.5}}{1.5z_1^2 + 4}. \tag{A4}$$

A2.   Derivation of the Effective Shear Stress Proportional to Q and S

It is commonly assumed in sediment transport mechanics that both the Manning's roughness coefficient and hydraulic radius are the summation of those of grains and bedforms [*Simons and Senturk*, 1977]. Here we assumed; 1) bedforms resistance is negligible during gully incisions and 2) non-transportable obstacles and gully shape irregularities impose additional resistance to the flow similar to bedforms. Manning's equation for open channel flow gives

$$V = \frac{R^{2/3} S^{1/2}}{n} \qquad (A5)$$

where n is the Manning's roughness coefficient. The total shear stress at the channel bed is,

$$\tau = \rho_w g R S \qquad (A6)$$

Manning's roughness is comprised of a grain and additional roughness components,

$$n = n_{gc} + n_{ac}. \qquad (A7)$$

Now given an average flow velocity in the channel the grain component of hydraulic radius is obtained as [*Laursen*, 1958],

$$R_{gc} = (n_{gc} \frac{V}{S^{0.5}})^{1.5} \qquad (A8)$$

from (A5) with only the grain roughness considered. This is then assumed to give the

fraction of the shear stress acting on grains in (A6) as,

$$\tau = \rho_w g R_{gc} S \qquad \text{(A9)}$$

Substituting (A5) into (A8), R_{gc} is written as a function of R,

$$R_{gc} = R(\frac{n_{gc}}{n})^{1.5}. \qquad \text{(A10)}$$

(A10) predicts grain hydraulic radius as a fraction of the total hydraulic radius.

Observations in rivers have revealed an inverse relationship between Manning's

roughness coefficient and discharge at a given station. Because as flow depth increases

roughness elements become relatively less effective in retarding the flow [*Dingman*,

1984]. Here we implemented an empirical relationship for n based on discharge [*Leopold

et al.*, 1964; *Knighton*, 1998],

$$n = k_n Q^{-m_n} \qquad \text{(A11)}$$

where k_n and m_n are empirical parameters. (A11) when substituted into (A10) predicts an

increase in $(n_{gc}/n)^{1.5}$ with discharge which suggests that as discharge increases the fraction

of the grain hydraulic radius would increase. Now equation (12) is substituted into

equation (10). The result and equation (11) is substituted into equation (A10) to get R_{gc}.

R_{gc} is substituted into equation (A9) to finally arrive at

$$\tau_f = \rho_w g k_n^{-1.13} C_s^{0.75} n_{gc}^{1.5} Q^{0.375+1.13m_n} S^{0.8125} \; .$$

(A12)

A3. Derivation of the Flow Width
In an Eroding Channel Proportional to Q and S

Given the assumption of a constant width to depth ratio of the flow in an eroding channel, the flow cross section area can be described by W_f, z_1 and z_2 for different channel geometries. The flow cross section areas of trapezoidal, triangular and parabolic channels are obtained as,

$$A_{f,trap} = \frac{W_f^2}{z_1} - \frac{W_f^2 z_2}{z_1^2}$$

(A13)

$$A_{f,tri} = \frac{W_f^2}{4z_2}$$

(A14)

$$A_{f,prb} = \frac{2W_f^2}{3z_1} \; .$$

(A15)

Equating (12) to A_f described by channel geometry above and solving for W_f we obtained the flow width as a function of Q and S,

$$W_f = k_s k_n^{0.375} C^{-0.25} Q^{0.375(1-m_n)} S^{-0.1875}$$

(A16)

where, k_s is another dimensionless shape constant which is; $z_1/(z_1 - z_2)^{0.5}$ for trapezoidal channels, $2z_2^{0.5}$ for triangular channels and $(1.5z_1)^{0.5}$ for parabolic channels.

A4. Non-Dimensional Form of
   The Govers Equation

An empirical sediment transport equation was proposed by *Govers* [1992] using 434 data points collected from a 6 m long and 0.117 m wide non-recirculating flume. In the experiments the slopes ranged from 1.7% to 21% and five well-sorted quartz materials with median grain sizes ranging from 0.058 to 1.098 mm were used as sediment. The equation Govers fitted is,

$$\log T_c = 2.457 \log(\frac{\tau - \tau_c}{d^{0.33}}) - 4.348 \tag{A17}$$

where, T_c is the sediment transport capacity in kgm^{-1}s^{-1}. Rearranging this equation the following expression for the unit sediment discharge, q_s (m^3/s/m) is obtained

$$q_s = \frac{10^{-4.348}}{\rho_s d^{0.811}} \tau^{2.457} (1 - \frac{\tau_c}{\tau})^{2.457} . \tag{A18}$$

This equation is of similar form to equation (3) as can be seen by substituting (4a), (4b) and (4c) into (3) and solving for q_s,

$$q_s = \frac{\kappa \sqrt{g(s-1)d^3}}{[\rho_w g(s-1)d]^p} \tau^p (1 - \frac{\tau_c}{\tau})^p . \tag{A19}$$

Equation (A19) is another expression of the generic sediment transport equation that was expressed in dimensionless form in equation (3). Since equations (A18) and (A19) are in the same form (A19) can be calibrated to (A18). The exponent p is equated to 2.457 and κ is obtained by equating the first terms in (B2) and (B3) and solving for κ,

$$\kappa_G = 10^{-4.348}\,\rho_s^{-1}\,\rho_w^{2.457}\,g^{1.957}\,(s-1)^{1.957}\,d^{0.146} \qquad (A20)$$

The subscript G in κ_G indicates Govers coefficient κ. This equation can be simplified to

$\kappa_G = 34.70(s-1)^{1.957}d^{0.146}$ by substituting ρ_s=2650 kgm^{-3}, ρ_w=1000 kgm^{-3} and g=9.81 ms^{-2}. The calibrated κ and p allow one to write the Govers equation in the form of (3)

$$q_{s*} = \kappa_G(1-\frac{\tau_{*c}}{\tau_*})^{2.457}\,\tau_*^{2.457}. \qquad (A21)$$

Figure 3-2 plots this equation to compare with the field observations.

References

Dingman, S. L., *Fluvial Hydrology*, 383 pp., Freeman, San Francisco, 1984.

Govers, G., Evaluation of transporting capacity formulae for overland flow, in *Overland flow hydraulics and erosion mechanics*, edited by A. J. Parsons, and A. D. Abrahams, pp. 243-273, Chapman & Hall, New York, 1992.

Knighton, D., *Fluvial Forms and Processes*, 383 pp., Arnold, London, 1998.

Laursen, E. M., The total sediment load of streams, *J. Hydraul. Div.*, 84, 1-6, 1958.

Leopold, L. B., M. G. Wolman, and J. P. Miller, *Fluvial processes in geomorphology*, 522 pp., Freeman, San Francisco, 1964.

Simons, D. B., and F. Senturk, *Sediment Transport Technology*, 807 pp., Water Resour. Pub., Fort Collins, 1977.

Appendix B

Dear Erkan,
You have my permission to use these papers in your dissertation. If you
need this faxed with original signature let me know.

Best Regards,
Charlie

_____

Charlie Luce
Research Hydrologist
USDA Forest Service
316 E. Myrtle St. Boise, ID 83702
(208) 373-4382
cluce@fs.fed.us
http://www.fs.fed.us/rm/boise/

_____

Erkan Istanbulluogl To: Charlie Luce/RMRS/USDAFS <cluce@fs.fed.us>
u cc:
<slccr@cc.usu Subject: permission request
.edu>

08/26/2002
08:28 AM

Dear Charlie:

This e-mail is to request permission to include in my dissertation complete
copies of the following papers in which you appear as a coauthor:

Istanbulluoglu, E., D. G. Tarboton, R. T. Pack and C. Luce, A
probabilistic approach for channel initiation, Water Resources Research (in press).

Istanbulluoglu, E., D. G. Tarboton, R. T. Pack and C. Luce, A sediment
transport model for incising gullies on steep topography, Water Resources Research (submitted
manuscript).

Istanbulluoglu, E., D. G. Tarboton, R. T. Pack and C. Luce, Modeling of the interactions between
forest vegetation, disturbances and sediment yields. To be submitted to Water Resources
Research.

Thanks for your help.

Erkan

CURRICILUM VITAE

Erkan Istanbulluoglu

(January 2003)

Postdoctoral Associate, Massachusetts Institute of Technology, Department of Civil and Environmental Engineering. MIT Room 48-114, Cambridge MA, 02139.

Phone: 617-253-5450
Email: erkan@mit.edu

Education:

Ph.D., Civil Engineering, Utah State University, Logan, Utah, 2002.
    Concentrations: Hydrology, fluvial geomorphology, modeling hillslope processes.
    Dissertation Title; Quantification of Stream Sediment Inputs
                from Steep Forested Mountains. Advisor: David G. Tarboton.

M.S., Agricultural Engineering**,** Uludag University, Turkey, 1998.
    Concentrations: Hydrology, irrigation engineering, environmental management in
          irrigated agriculture.
B.S., Agricultural Engineering, Uludag University, Turkey, 1996.

Areas of Interest:

    Hydrology
    Fluvial geomorphology, modeling hillslope processes.
    Landscape evolution

Experience:

Postdoctoral Associate, Massachusetts Institute of Technology, present.
Graduate Research Assistant, Utah State University, Utah Water Research Laboratory, Logan UT, from 1999 to 2002.
Graduate Research Assistant, Uludag University College of Agriculture, Bursa Turkey, from 1996 to 1999.
Work Study, Rheinischen Friedrich-Wilhelms-Universität Bonn, Bonn Germany, 1995.

Teaching experience:

Teaching Assistant in Hydrology, Hydraulics and Water Resources Systems Planning, Uludag University, Turkey.

Publications

Refereed Papers:

Istanbulluoglu, E., D. G. Tarboton, R. T. Pack and C. Luce, 2002. A Probabilistic Approach for Channel Initiation. *Water Resources Research* 38(12), doi:10.1029/2001WR000782.

Istanbulluoglu, E., D. G. Tarboton, R. T. Pack and C. Luce. A Sediment Transport Model for Incising Gullies on Steep Topography, submitted to *Water Resources Research*, (in press).

Istanbulluoglu, E. 2000. Theoretical Justification of SCS Method for Runoff Estimation (Discussion). Journal of Irrigation and Drainage Eng. 126(1), 74-75.

Conference Proceedings & Posters:

Istanbulluoglu, E., D. G. Tarboton, R. T. Pack and C. Luce, 2001. A Probabilistic Approach for Channel Initiation. In: Ramirez, J. A. (ed.), Proceedings of the 21th Annual American Geophysical Union Hydrology Days, p. 134-145.

Istanbulluoglu, E., D. G. Tarboton, R. T. Pack, 2001. Quantifying the Exposure of Streams to Sediment Inputs using Probabilistic Methods. Poster presented at the Geomorphology section of the AGU spring meeting. 29 May-2 June, Boston, MA.

Istanbulluoglu, E., D. G. Tarboton and R. T. Pack, (2001), "A Sediment Transport Model for Incising Gullies Based On Upland Topographic Controls," Eos Trans. AGU 82(47) Fall Meet. Suppl., Poster presented at AGU fall meeting.

Istanbulluoglu E., H. Degirmenci, and S. Yazgan, 1998. A Mathematical Simulation Model Approach in Pre-Seasonal Irrigation Planning. 13th International Congress on Agricultural Engineering, Vol. 1, Rabat-MOROCCO,.

Istanbulluoglu E., A.O. Demir and H. Degirmenci, 1998. Rainfall-Runoff relations of Bursa-Mahmudiye Watershed. Uludag University College of Agriculture Publications, V;13 (in Turkish with an English abstract).

Istanbulluoglu E., A. Korukcu, and E. Karas, 1998. Rainfall-Runoff Modeling using SCS-CN Method in Kurukavak Watershed. 2nd. National Hydrology Congress, 22-24 June 1998, Istanbul Technical University, Istanbul-Turkey (in Turkish with an English abstract).

Degirmenci, H., S. Yazgan, and E. Istanbulluoglu, 1998. Monitoring and Evaluation Indicators Based on Environmental Problems in Irrigation Management. Kripton Curi International Symposium on Environmental Management of Mediterranean Sea, 18-20 June 1998, Antalya-Turkey.

Degirmenci, H., S. Yazgan, A.O. Demir and E. Istanbulluoglu, 1997. Evaluating the Water Delivery Performance of Bursa-Mustafakemalpasa Irrigation System. 6th. National Congress on Agricultural Engineering, 5-8 June 1997, Bursa-Turkey (in Turkish with an English abstract).